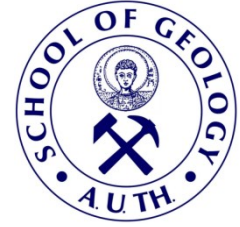




ARISTOTLE UNIVERSITY OF
THESSALONIKI
DEPARTMENT OF GEOLOGY
Laboratory of Engineering Geology and
Hydrogeology



Research Project (Code 97824)

Groundwater depletion. Are **Eco**-friendly Energy Recharge
Dams a solution?

REPORT OF WORK PACKAGE 5 / (WP5/D5-4)



Groundwater **Re** **De** **P** **L** **E** **T** **I** **O** **N**

PRINCIPAL INVESTIGATOR:

KAZAKIS NERANTZIS

Dr. HYDROGEOLOGIST

Funding: Hellenic Foundation for Research

& Innovation H.F.R.I.



February 2024

Table of Contents

1	Introduction.....	3
2	Software - Modeling	3
2.1	Case Study Areas	5
2.1.1	Campania region	5
2.1.2	Eastern Thermaikos Gulf and Anthemountas basin.....	7
2.1.3	Mouriki basin	11
2.1.4	Marathonas basin	13
2.2	ArcSWAT	15
2.2.1	SWAT Project Setup.....	16
2.2.2	Calibration/Validation.....	25
2.2.3	ArcSWAT Results	27
2.3	Dams Optimization	36
2.4	Groundwater simulation.....	55
2.4.1	SWI2 - Seawater Intrusion Package Simulation.....	63
2.4.2	Nitrate simulation.....	69
2.5	Conclusions of simulation.....	72
3	Thematic maps	73
3.1	Anthemountas basin.....	73
3.2	Mouriki basin	77
3.3	Marathonas basin	79
4	Publications.....	84
4.1	Conferences.....	84
4.1.1	Online Youth Water Congress: “Emerging water challenges since COVID-19”	84
4.1.2	16 th International Congress of the Geological Society of Greece.....	84
4.1.3	6th Edition of FLOWPATH.....	84
4.1.4	12 th World Congress on Water Resources and Environment (EWRA 2023)	84
4.2	Book Chapter	85

4.2.1	Handbook of Hydrosystem Restoration.....	85
4.3	International Journals.....	85
4.3.1	Science of the Total Environment.....	85
4.3.2	Remote Sensing	85
4.3.3	Journal of Environmental Management.....	86
4.3.4	Water.....	86
5	Conclusions.....	87
6	References.....	88

1 Introduction

Within this report are presented the results of the simulation and software applications, the corresponding thematic maps, as well as the list of the publication of the project until the submitted period of February 2024.

2 Software - Modeling

Within this chapter included the application of the produced codes and software for dam operation and application of managed aquifer recharge. Additionally includes the simulation of the aquifers for the determination of groundwater depletion. More specifically, this deliverable serves as a comprehensive repository of insights garnered from the extensive application of the optimization algorithm across a multitude of study areas. In addition to providing a thorough analysis of these study areas, we have endeavored to broaden the scope of our investigation by extending our methodology to encompass an in-depth examination of an existing small hydroelectric project. This expanded approach not only deepens our understanding of the algorithm's efficacy but also sheds light on its practical applicability in real-world scenarios. Parallel to the execution of the algorithm within the designated study areas, a series of meticulously designed computational experiments were conducted. These experiments were instrumental in not only refining the optimization method but also in fine-tuning its parameters to ensure optimal performance across diverse environments. To bolster the reliability and versatility of our approach, a sophisticated random number generation machine was developed, underscoring our commitment to robustness and adaptability in algorithmic design. Within the heart of our research lies the reservoir optimization algorithm, a powerful tool wielded to maximize energy production efficiency across a spectrum of reservoirs, both existing and prospective. While this algorithm yielded promising results in most instances, its application encountered significant challenges when confronted with the complexities inherent in larger basins. The formidable computational demands, coupled with the intricate decision space characterized by strong convexity, posed formidable obstacles, often resulting in program crashes and operational inefficiencies. In response to these challenges, we

embarked on a quest for alternative solutions, seeking to overcome the limitations inherent in optimizing large basins. One such breakthrough involved harnessing the capabilities of the modelMuse software, which proved to be powerful in optimizing underground aquifers. This strategic pivot not only yielded superior performance compared to previous attempts utilizing FlopY but also laid the groundwork for more efficient and effective optimization strategies in similar contexts.

For this reason, we used the modelMuse software to solve the groundwater flow which achieved a much better performance than FlopY. Splitting the optimization pier into two parts is possible according to the model as the objective functions have the same kind of response. Therefore, they constitute a linear combination which can be optimized by the individual study of the objective functions. The modelMuse was also chosen because is an open access software.

2.1 Case Study Areas

2.1.1 Campania region

The Upper Volturno and Calore basin, located in the picturesque Campania region on the Tyrrhenian side of the Southern Apennines in Italy, encompass a sprawling landscape spanning approximately 5,613 square kilometers. The terrain is characterized by a diverse range of altitudes, stretching from as low as 16 meters to towering peaks reaching 2,118 meters. With a moderate mean annual temperature of 16.4 °C and a generous average annual rainfall of 1,245 millimeters, the climate sets the stage for a rich tapestry of ecological diversity. Geologically, the Upper Volturno-Calore basin is a mosaic of formations, comprising dolomites, limestones, sandstones, clay-marl flysch, and pyroclastic fall deposits, as depicted in **Figure 2.1**. These geological features not only contribute to the region's natural beauty but also play a crucial role in shaping its hydrological dynamics. The primary aquifer in the area is predominantly hosted within alluvial formations, boasting an average thickness of approximately 80 meters. Elevation gradients vary significantly, ranging from 15.5 meters to 2,102 meters. Such diverse topography creates a unique hydrological landscape, ripe for exploration and analysis. Human activities within the basin are as diverse as its natural features. In the lowlands, agricultural and livestock endeavors flourish, while the mountainous regions are characterized by mixed forests and pastures. Vineyards, cereals, vegetables, and orchards dominate the agricultural scene, painting a vibrant mosaic of rural life.

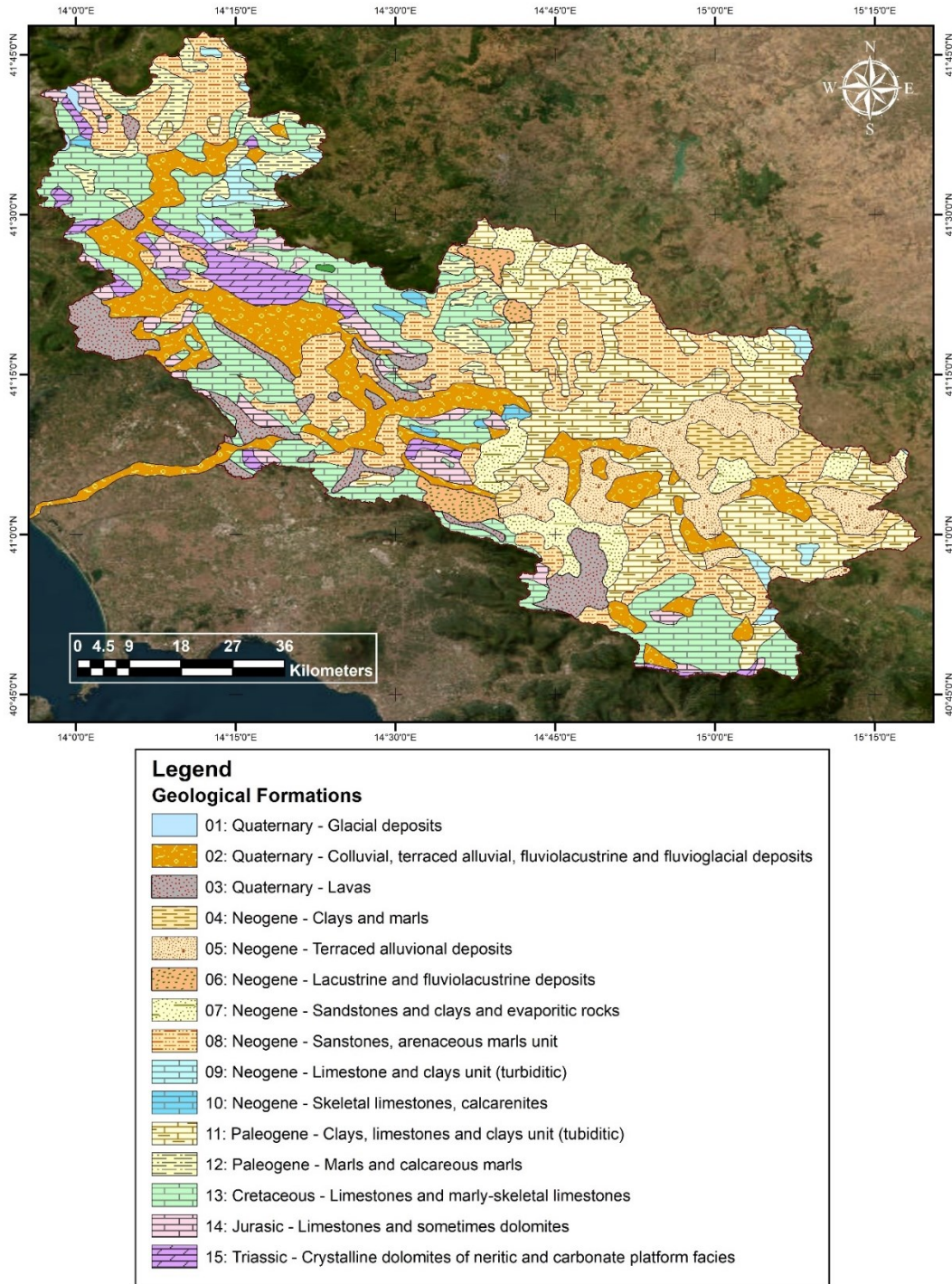


Figure 2.1 Geological map for Upper Volturno-Calore basin.

2.1.2 Eastern Thermaikos Gulf and Anthemountas basin

The Eastern Thermaikos Gulf, located in the northern region of Greece, is a captivating landscape teeming with natural beauty and cultural heritage. Spanning an expansive area of 932.7 square kilometers, the basin offers a tapestry of diverse ecosystems and geological formations, with altitudes ranging from the tranquil coastal zones at sea level to the majestic heights of Mount Hortiatis soaring 1199 meters above sea level, as illustrated in Figure 2.2. The climate of the region mirrors the quintessential Mediterranean archetype, characterized by semi-arid conditions typified by dry summers and wet winters. With mean annual temperature hovering around 15.1°C and annual precipitation averaging at 575 millimeters, the rhythm of the seasons shapes the ebb and flow of life within this vibrant ecosystem. The geological map of the site is shown in Figure 2.3, is a testament to the intricate interplay of earth's forces over millennia. The basin hosts a complex aquifer system, comprising various aquifer types. These include a porous aquifer nestled within Quaternary and Neogene sediments, a karst aquifer nestled in the basin's southern-central expanse, and fractured rock aquifers dotting the mountainous terrain. The mean thickness of the alluvial aquifer is 100 m. In terms of economic activity, agriculture reigns supreme as the primary livelihood of the area's inhabitants, sustaining communities through generations with its bounty. However, the allure of the region has not gone unnoticed, with tourism witnessing a steady uptick in recent years, particularly during the balmy summer months. The fertile soils of the region nurture a diverse array of crops, including verdant vegetables, luscious olives, succulent wine grapes, golden corn, and hearty cereals, as depicted in Figure 2.4. Yet, amidst the abundance, the basin grapples with the challenges of sustainable water management. The burgeoning demands of both domestic consumption and agricultural irrigation are met largely through a network of boreholes tapping into the porous aquifers. However, rampant overexploitation has led to alarming groundwater depletion, underscoring the urgent need for holistic water resource management strategies. In essence, the Eastern Thermaikos Gulf and the Anthemountas basin encapsulate the rich

tapestry of Greece's natural and cultural heritage, beckoning explorers, scientists, and stewards alike to safeguard and cherish this precious corner of the world.

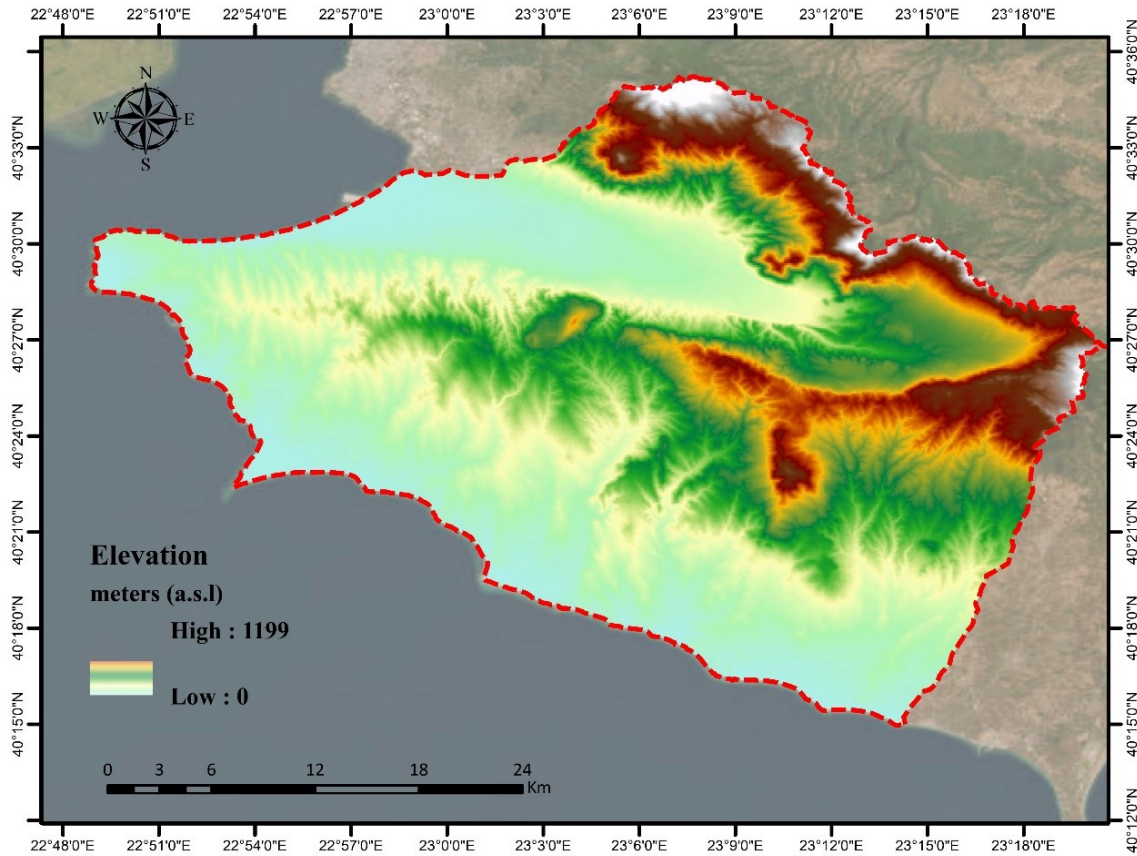
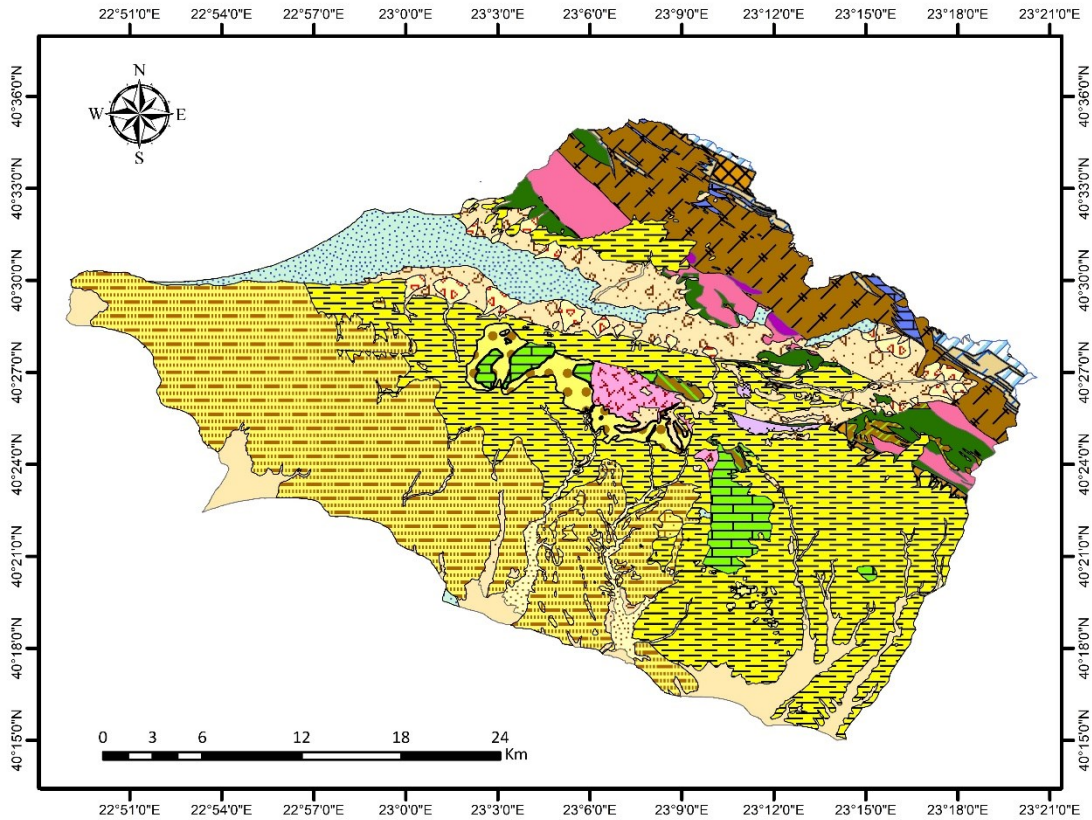


Figure 2.2 Spatial distribution of elevation in Eastern Thermaikos Gulf.



Legend

Geology


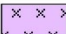
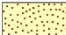


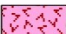


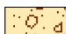



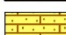











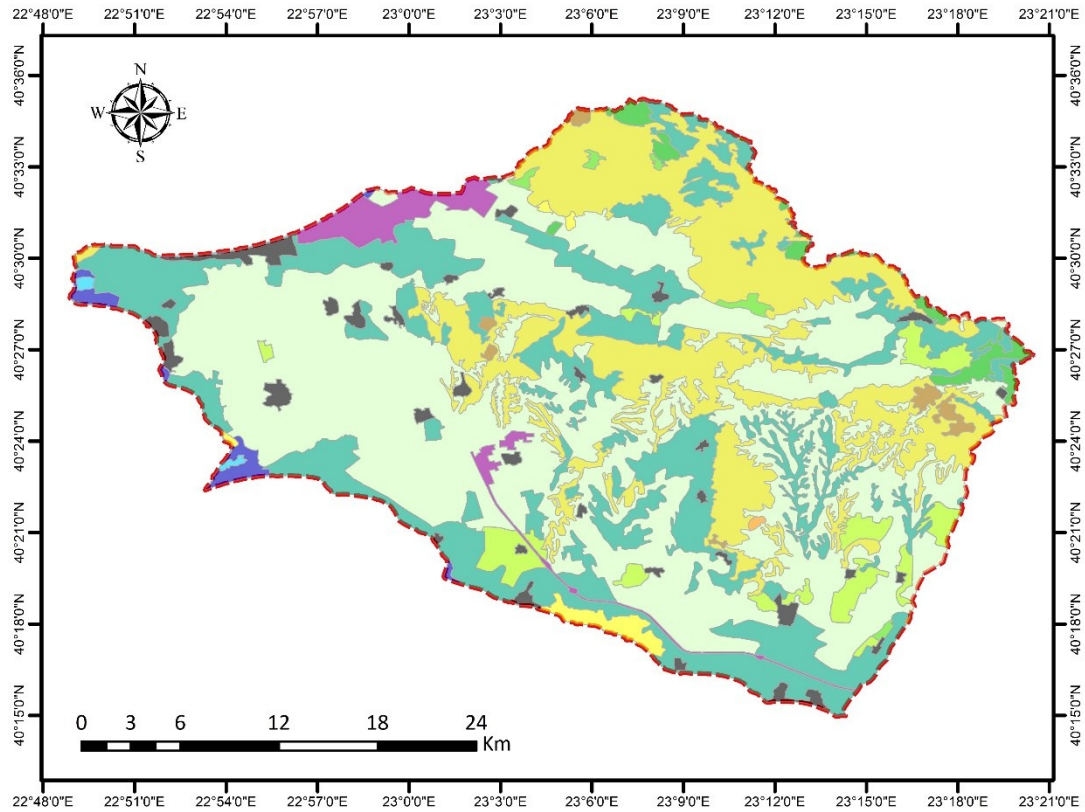
 Holocene: Alluvial deposits	 Mesozoic: Epidote - actinolite schist
 Holocene: Lower stage of lowest terrace system	 Mesozoic: Gabbro
 Holocene: Valley deposits	 Mesozoic: Granodiorite
 Pleistocene: Fans	 Mesozoic: Limestones
 Pleistocene: Terrace systems	 Mesozoic: Phyllites (Svoula group)
 Neogene: Basic conglomerate series	 Mesozoic: Pyroxenites
 Neogene: Fresh water Limestones	 Mesozoic: Quartzites (Svoula group)
 Neogene: Red clay series	 Mesozoic: Shales
 Neogene: Sandstone - marl series	 Mesozoic: Ultramafic rocks
 Neogene: Travertine limestones	 Mesozoic: Leucocratic gneiss
 Mesozoic: Clay-Schists	 Mesozoic: Limestones recrystallized
 Mesozoic: Diorite (complex of Yerakini)	 Paleozoic: Two-mica gneiss (Vertiskos formation)

Figure 2.3 Geological map for Eastern Thermaikos Gulf.



Legend

LandUse

Artificial surfaces

- Urban fabric
- Industrial, commercial and transport units
- Mine and construction sites
- Artificial, non-agricultural vegetated sites

Agricultural areas

- Arable land
- Permanent crops
- Pastures
- Heterogenous agricultural areas

Forests and semi natural areas

- Forests
- Scrub and heraceous vegetation associations
- Open spaces with little or no vegetation

Wetlands and water bodies

- Inland wetlands
- Maritime wetlands
- Inland waters
- Marine waters

Figure 2.4 Spatial distribution of land use dominance in Eastern Thermaikos Gulf.

2.1.3 Mouriki basin

Mouriki basin is located in the northern part of Kozani Prefecture in northern central Greece, the Mouriki basin emerges as a verdant oasis amidst the rugged terrain, as depicted in Figure 2.5 . This inland basin spans an expansive surface area of 110 square kilometers, offering a sanctuary for both natural wonders and human endeavors. The climate of the region mirrors the classic Mediterranean semi-arid archetype, characterized by mild winters and moderate rainfall during the summer months. With an average annual air temperature of 11.2°C and precipitation averaging at 636 millimeters, the rhythm of the season's shapes life within this vibrant ecosystem, fostering a delicate balance between aridity and abundance. Geologically, the study area's foundation is an intricate mosaic of formations, as illustrated in Figure 2.5. The primary aquifer system, vital for sustaining life in the region, is ensconced within alluvial deposits, boasting a mean thickness of 60 meters and covering an expansive area of 30.5 square kilometers. Groundwater, following the contours of the local terrain, meanders towards the lowlands in a gentle SSW to NNE trajectory, replenishing vital ecosystems along its path. With a mean altitude of 874.5 meters above sea level and a modest slope inclination averaging at 26.1%, as depicted in Figure 2.6, the study area's topography creates a rich tapestry of diverse landscapes, from rugged peaks to tranquil valleys. Human activities within the basin are as varied as its natural features. Livestock rearing and agriculture stand as pillars of the local economy, sustaining communities with their bounty. Corn, cereal crops, fruit trees, vegetables, and legumes flourish in the fertile soils, painting a vibrant mosaic of rural life. The mountainous reaches of the basin are cloaked in a tapestry of mixed and coniferous forest vegetation, adding to the region's natural allure. In essence, the Mouriki basin embodies the timeless harmony between nature and human endeavor, offering a haven of ecological diversity and cultural richness amidst the rugged beauty of northern Greece.

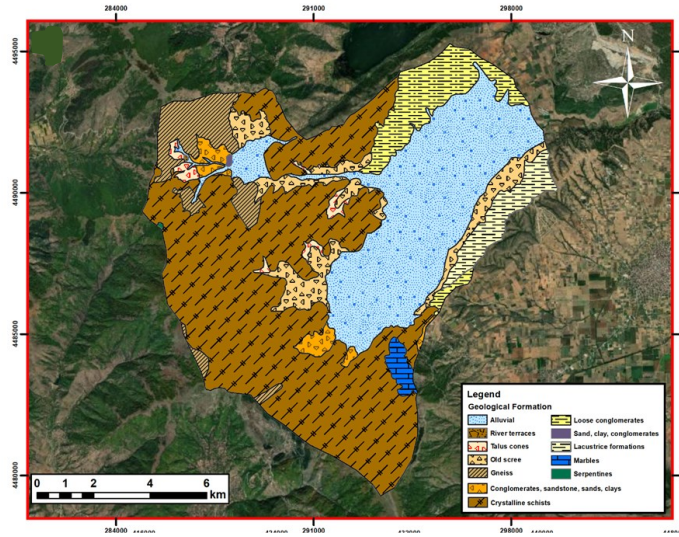


Figure 2.5 Geological map for Mouriki basin.

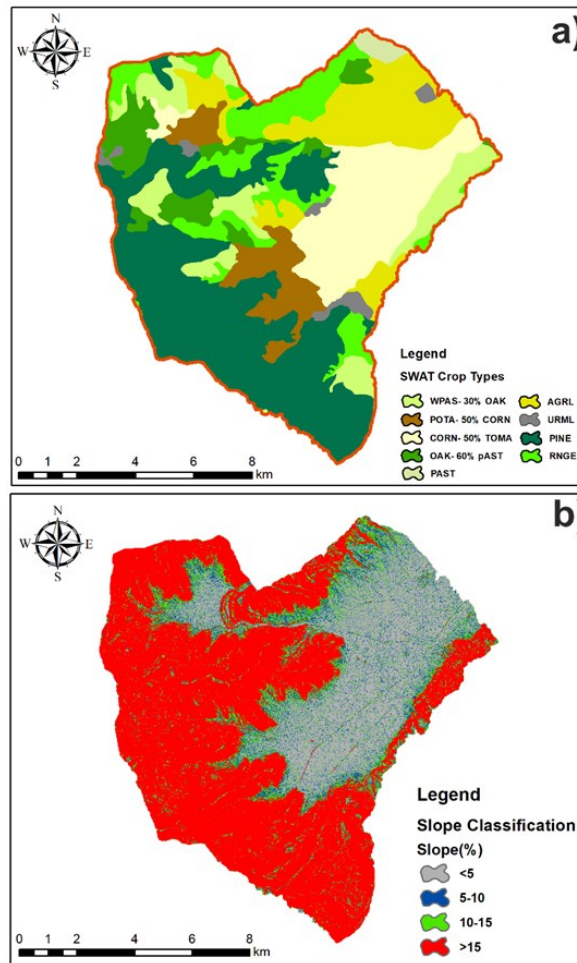


Figure 2.6 Land use (a) and slope classes (b) in Mouriki basin.

2.1.4 Marathonas basin

Situated in the eastern reaches of Attica, southern Greece, the plain of Marathonas emerges as a tranquil expanse of natural beauty and cultural heritage. Encompassing a sprawling area of 182.6 square kilometers, this basin offers a captivating blend of diverse landscapes and ecological habitats. The elevation within the basin varies dramatically, ranging from sea level to towering peaks reaching 1407 meters. The central portion of the plain is characterized by gentle slopes and flat terrain, while its peripheries transition into semi-mountainous and mountainous terrain, particularly in proximity to the majestic massif of Parnitha, as depicted in Figure 2.7. The basin is graced with the presence of numerous environmental protection zones, including the renowned national park of Parnitha and the mountain range of Penteli, which envelop the basin of Marathon. These protected areas serve as vital sanctuaries for biodiversity and natural ecosystems, enhancing the region's ecological resilience and cultural significance. In terms of climate, the basin experiences a Mediterranean climate with average annual air temperatures hovering around 15.7°C and precipitation averaging at 477.4 millimeters during the period from 2011 to 2020. Classified within the Attic-Cycladic zone of the Aegean, the region boasts a rich geological heritage, with formations ranging from alluvial deposits to marbles-limestones, schists, and serpentines. Intensive erosion phenomena and small-scale soil movements characterize the area, driven by the erosive nature of these formations. Hydrologically, the basin hosts a porous aquifer along its coastal areas, complemented by karstic aquifers underlying areas dominated by marble formations. Groundwater resources are primarily utilized for domestic purposes and irrigation, particularly in the sub-urban coastal zone, where extensive agricultural activities thrive. However, both aquifers face the challenge of intense pumping, exacerbated by extended irrigation periods, notably in areas adorned with greenhouses. The landscape of the plain of Marathonas is a tapestry of urban areas, verdant forests comprising pine, mixed forest, and sclerophyllous vegetation, shrublands, oak forests, pastures, cultivated fields, and wetlands, as depicted in Figure 8. Spatial and temporal variations in the extent of these landscapes have been observed in recent years, accentuated by the devastating wildfires that ravaged a significant portion of the vegetation in 2009. In essence, the plain of Marathonas stands as a testament to the delicate interplay

between human activities and natural forces, offering a sanctuary of ecological diversity and cultural heritage amidst the picturesque landscapes of southern Greece.

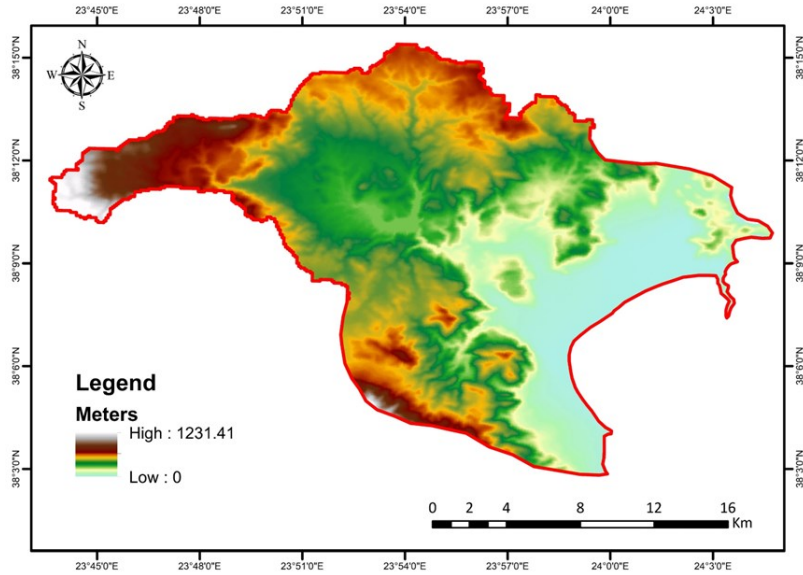


Figure 2.7 Spatial distribution of elevation in Marathonas basin.

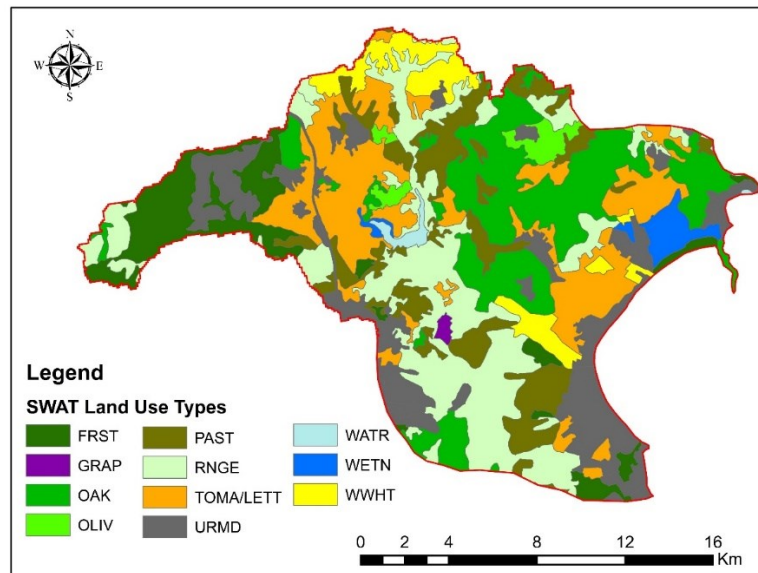


Figure 2.8 Spatial distribution of land use dominance in Marathonas basin.

2.2 ArcSWAT

The Soil and Water Assessment Tool (SWAT) numerical model is a hydrological model created by the Agricultural Research Service, U.S. Department of Agriculture (USDA). The model aims to calculate the effect on the hydrology of land use changes, different types of soils and slopes, as well as the climate of the area in terms of water quantity and quality. Regarding the quantitative analysis of the model, this lies in the calculation of the effect of the above on the drainage of the basin, on the steric transport, and the infiltration into the groundwater. In the last years, SWAT applicability was greatly increased thanks to the possibility of using a growing number of available global and regional datasets, making SWAT utilization much easier than before (Abbaspour et al., 2019). The model's main advantage is that it can simulate both long periods and large watersheds in a short period. It allows the user to choose the time step in days or months depending on the accuracy sought in his calculations.

The SWAT model considers climatic information, specifically precipitation and maximum and minimum values of temperature, for the determination of the main processes involved in the hydrological cycle. Morphology, soil infiltration degree, vegetation type, and agricultural practices are also considered in the evaluation since they can greatly affect the overall groundwater balance.

During the SWAT processing, the analyzed basin is divided into multiple sub-basins, further subdivided into hydrologic response units (HRUs) according to the land use type, slope range, and soil units. The main step of the model consists of the creation of the HRUs, referring to all those portions of a territory characterized by unique land-use, morphological, and soil attributes combination (Neitsch et al., 2000). Subbasin division offers the designer more accurate distribution of features by having more control points in the basin. Thus, each hydrological response unit consists of three distinct components, a land use, a land type, and a land slope.

2.2.1 SWAT Project Setup

A basic application of a superficial simulation model requires detailed hydro-meteorological data along with geospatial data such as: elevation, land cover, soil, water quality, groundwater level measurements, and meteorological data. In this study, only the quantitative water simulation analysis is provided. The SWAT model was applied to assess the current and future water balance changes and groundwater recharge in the Anthemountas, Mouriki, Marathonas and Campania basins.

The elevation is the most crucial conditioning factor for the modeling setup. In the present study, a digital elevation model (DEM) with a high-resolution cell of 10×10 m was utilized for the determination of the main basin features. Soil is controlled by land cover, topography, geomorphology, climate conditions, and the parent rock. Thus, is classified using multiple approaches because of its complexity and diversity (Costantini and Dazzi, 2013; Schismenos et al., 2022). Soil information was obtained by integrating three datasets: the Digital Soil World Map (DSMW FAO 2007; scale 1:5 million), the Land Systems of Campania (Sistemi di terre delle Campania), and the World Soil Information Service (WOSIS) dataset. In this study, land cover maps such as the Italian Land Cover map (Carta utilizzo agricolo dei suoli; CUAS of 2009) and the CORINE land cover classes for the year 2018 were used. The collected data was ratified by satellite images and previously published research studies. Precipitation values along with minimum and maximum values of temperature in daily recording steps were collected in meteorological stations. Hydrological impacts of climate change on a catchment are typically assessed using climate projections based on different climate change scenarios as a result of human climate forcing with projections of future greenhouse gas (GHG) emissions. Regional climates, consistent with global changes, are created by downscaling the results of a global climate model (GCM) using either statistical or dynamic (regional climate model - RCM) methods. The ArcSWAT implementation initially obtained meteorological data from stations for the period 2000-2020 according to data availability. Additionally, climate data were obtained from the Coordinated Regional Climate Downscaling Experiment (CORDEX) considering the Representative Concentration Pathway (RCP) 4.5 and the climate model REMO 2009 (Jacob et al., 2012) for the period 2000-2040. The Hargreaves method was used to calculate potential evapotranspiration (PET).

Primary and secondary data were jointly used in the SWAT simulation. Within the process used data from fieldwork to reconnaissance survey to obtain a general understanding of the hydrogeological features of the study areas, such as geological mapping and the collection of meteorological data from the stations. During the process, data were also collected from online free-access sources (Table 2.1) and relevant literature.

Table 2.1 List of database sources.

Raw Data	Extension	Format	Reference
Soil Classification	World	Shapefile	http://www.fao.org/geonetwork/srv/en/metadata.show?id=14116
Digital Elevation Model (DEM)	World	Raster	https://asterweb.jpl.nasa.gov/gdem.asp
Historical climatic data	World	Database	https://www.ncei.noaa.gov/cdo-web/
Land Use classification	Europe	Shapefile	https://land.copernicus.eu/pan-european/corine-land-cover
Climate Projections	World	Database	https://esgf-data.dkrz.de/search/esgf-dkrz/
Monthly data of ET	World	Raster	https://earthdata.nasa.gov/

Data from two meteorological stations (Aristotelis and Kozani) were used for Mouriki basin and one station (Makedonia airport) for Anthemountas basin. In Marathonas basin the nearby station had less data and thus, the Climate Forecast System Reanalysis (CFSR) model was used. The CFSR was designed and executed as a global, high-resolution, coupled atmosphere-ocean-land surface-sea ice system to provide the best estimate of the state of these coupled domains over this 31-year period. Nine meteorological stations (Alife, Bagnoli Iripino, Benevento, Sorgenti Grassano, Trevico, Colle Sannita, Forli del Sannio, Isernia, Fornelli) were used for SWAT simulation in Campania basin.

2.2.1.1 Eastern Thermaikos Gulf and Anthemountas basin

The Anthemountas basin was divided into 233 sub-basins retaining a maximum of 500 HRU (Figure 2.27). The maximum of 500 HRU was set to reduce the model's spatial requirements and computational time in accordance with Busico et al. (2020). The analysis showed that the land use of Anthemountas basin was mainly agricultural. Over 50% of the basin is cultivated with crops including wheat, corn, olives, and vegetables (mainly lettuce and carrot), while urban settlements account for 6% of the basin's surface area and are mainly located along the coast (Figure 2.9). Two soil categories were identified in

Anthemountas basin following the DSMW classification: i) Chromic Luvisols in the central and eastern parts of the basin ii) Calcaric Regosols with a clay-loam texture and a K_s of 4.2 mm/h that occur in the western part of the site and near the coastal zone. Additionally, the sub-basins of the studied dams (4 and 5) which are part of the Eastern Thermaikos Gulf site were simulated to provide the data for the dam optimization (Figure 2.10 and Figure 2.11). One soil category was identified in both basins. The main part of the basins is covered by oak and wheat. The elevation in the basin of dam 4 varies between 139 and 256 meters and from 94 to 212 in the basin of dam 5. The SWAT model run in these sub-basins followed the same simulation steps and parameters for the calibration/validation as in Anthemountas basin.

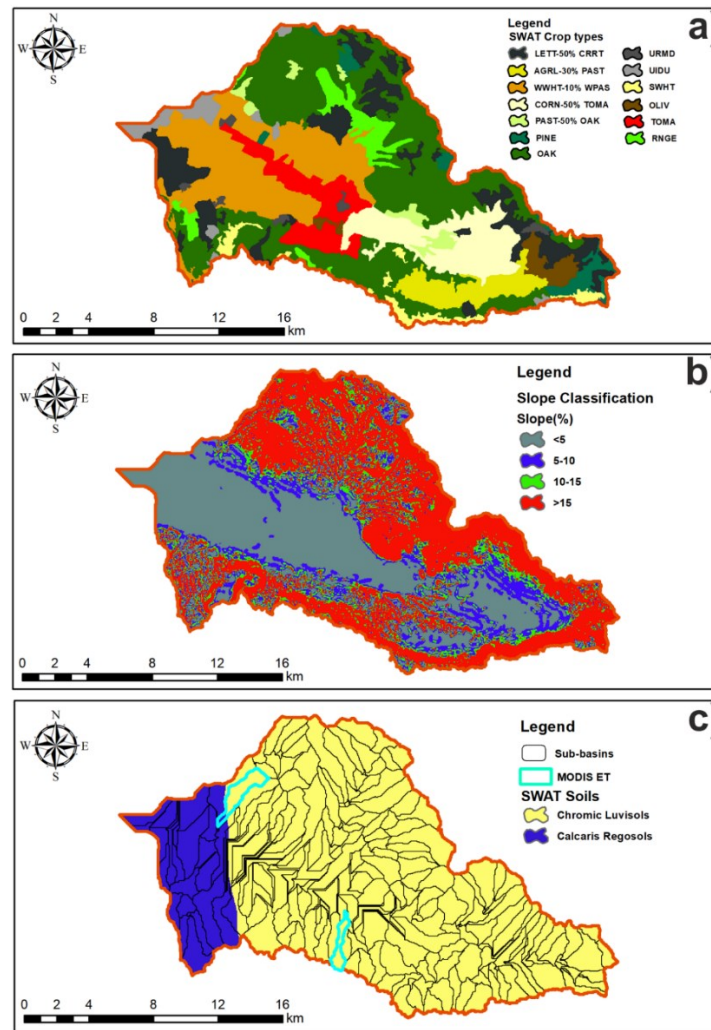


Figure 2.9 SWAT model setup for the Anthemountas basin containing the main watershed informations, land use dominance (a), slope classes (b), soil (c).

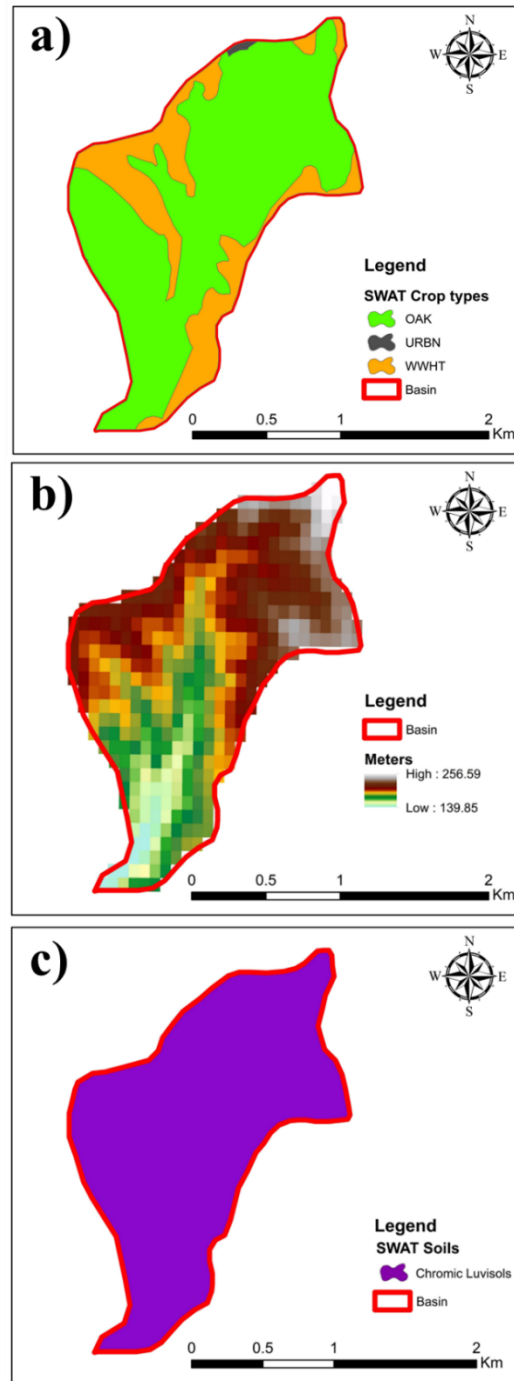


Figure 2.10 SWAT model setup for the basin of dam 4 in Eastern Thermaikos Gulf containing the main watershed informations, land use dominance (a), elevation (b), soil (c).

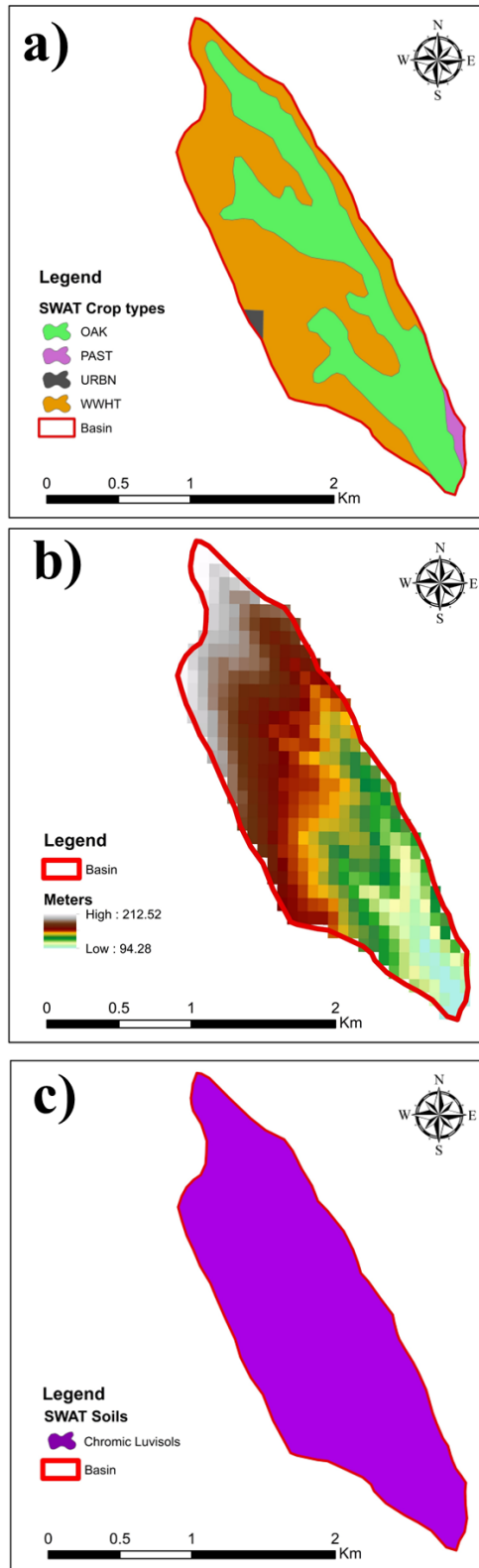


Figure 2.11 SWAT model setup for the basin of dam 5 in Eastern Thermaikos Gulf containing the main watershed informations, land use dominance (a), elevation (b), soil (c).

2.2.1.2 Mouriki basin

Mouriki basin was divided into 149 sub-basins and a total of 500 HRU. The area is mainly agricultural (Figure 2.12), dominated by wheat and vegetable crops (mainly tomatoes and potatoes) that cover 70% of the territory. Urban settlements account for less than 2% of the site's surface and the remaining areas are covered by dense pine and oak forests. The slope classification varies from <5 to >15 %. One soil category was identified in Mouriki basin following the DSMW classification: i) Calcaric Regosols with a clay-loam texture.

2.2.1.3 Marathonas basin

Marathonas basin was divided into 93 sub-basins and a total of 500 HRU. The elevation varies between 1223 and 3.6 m (Figure 2.13). According to the DSWM, the basin is characterized by Chromic Luvisols and Calcaric Regosols. The area is mainly agricultural, dominated by vegetable crops and the upper part of the basin covered by forests.

2.2.1.4 Campania basin

The morphology in the basin is characterized from flat to steep, thus a great variety of elevations is distinguished in the region (Figure 2.32). The classification of soil types in the study area is shown in Figure 2.14. The main part of the basin is covered by Cambisols with a sandy loam texture. The presence of vegetation, crops, pasture, industrial and residential areas have different impacts on groundwater balance. The basin is covered by agricultural areas and vegetation to the most extent. The Campania basin is covered mainly by forests (FRST 31%) and wheat crops (WWHT 24%) (Figure 2.16).

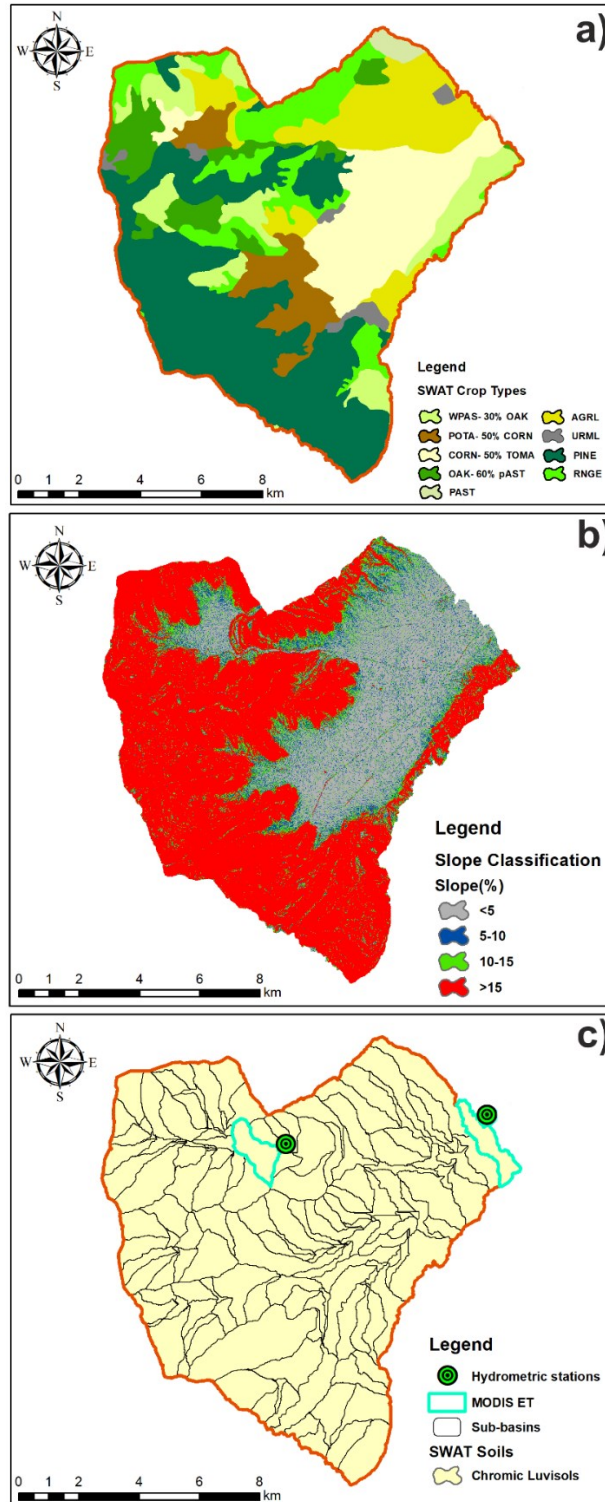


Figure 2.12 SWAT model setup for the Mouriki basin containing the main watershed informations, land use dominance (a), slope classes (b), soil (c).

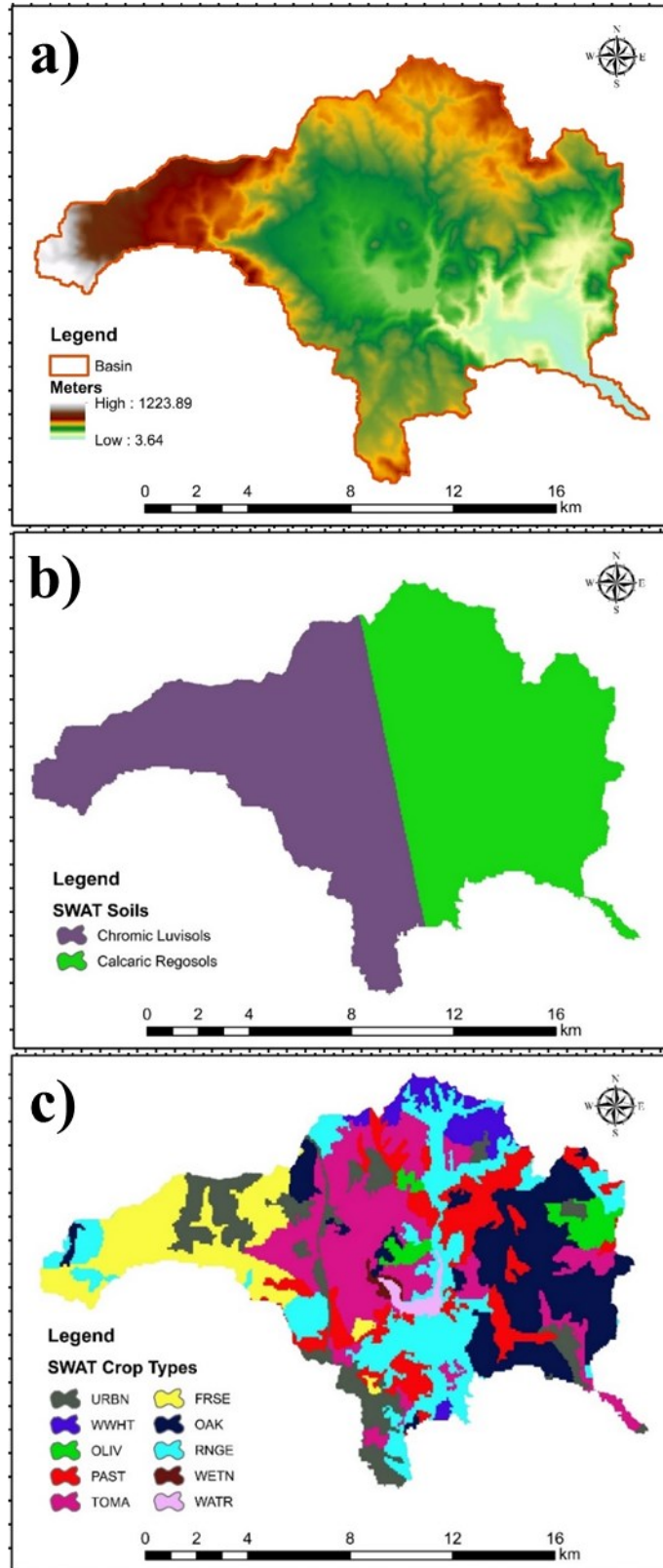


Figure 2.13 SWAT model setup for the Marathonas basin containing the main watershed informations, elevation (a), soil (b) and land use dominance (c).

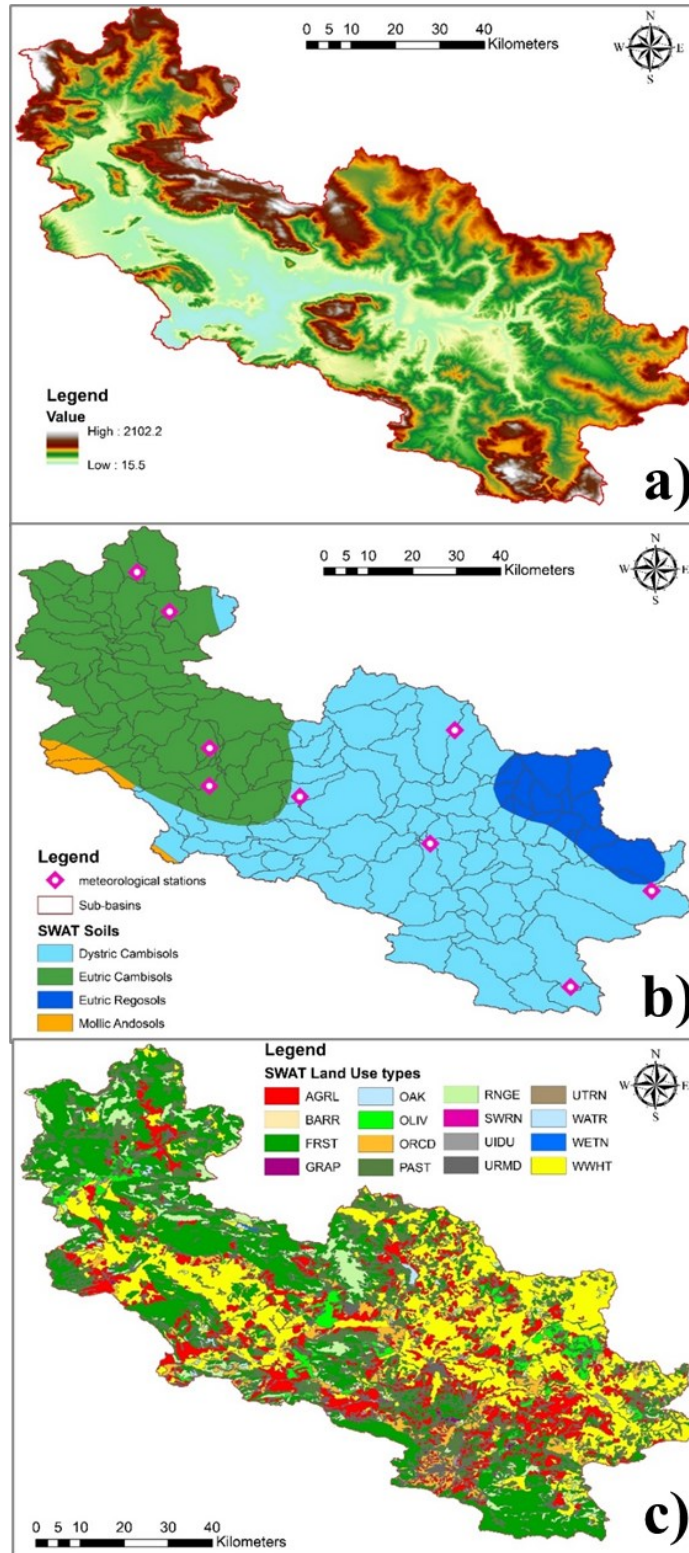


Figure 2.14 SWAT model setup for the Upper Volturno-Calore basin containing the main watershed information, elevation (a), soil (b), and land use dominance (c).

2.2.2 Calibration/Validation

The assessment of groundwater recharge variations and their relationship with other hydrological parameters requires various hydrological and hydrogeological data. Calibration/Validation was applied via SWAT-CUP software by adjusting manually parameters and ranges iteratively between autocalibration runs. Parameter sensitivity analysis helps focus the calibration and uncertainty analysis and is used to provide statistics for goodness-of-fit. The user interaction or manual component of the SWAT-CUP calibration forces the user to obtain a better understanding of the overall hydrologic processes (e.g., baseflow ratios, crop yields) and of parameter sensitivity. The parameters used in SWAT-CUP and their sensitivity analysis results are provided in the following tables (Table 2.2, Table 2.3, Table 2.4, Table 2.5).

A double calibration/validation (CV) procedure using streamflow data and MODIS ET was conducted for Mouriki and Campania basin, whereas only ET values were used in Anthemountas and Marathonas basin due to the complete lack of hydrometric data for these sites.

Data on daily river discharge and monthly ET values were used for the model calibration/validation (CV) in Mouriki basin. Discharge data was obtained from two hydrometric monitoring stations (Galatia and Variko) located within Mouriki basin for the period November 2004 to September 2007 and one hydrometric station (Amorosi) in Campania basin.

Monthly ET values for 2000-2014 were sourced from the MODIS dataset and used in the model implementation. The MOD16A2 Version 6 Total ET product (including potential and real ET) is an 8-day composite dataset produced at 500 x 500 m pixel resolution. The data was downloaded using the AppEARS interface and the MYD16A3GF model (Running et al. 2019). Specifically, the algorithm used in the MOD16 products is based on the Penman-Monteith equation, which includes inputs of daily meteorological data along with MODIS remotely sensed data products such as vegetation property dynamics, albedo and land cover (Mu et al. 2011). The ET data was extracted using the average spatial values of internal sub-basins within the study areas. The historical climate data and future projections for the entire period of 1976-2040 focused on simulations performed by the GCM/RCM combination, entitled MPI-M-MPI-ESM-LR/MPI-CSC-

REMO2009, and here called REMO, made available by the World Climate Research Programme's CORDEX initiative (www.euro-cordex.net).

Table 2.2 SWAT main used parameters for the study areas adjusted during calibration and their sensitivity statistics.

Parameter Name	Description	Method*
DEP_IMP.hru	Depth to impervious layer in the soil profile (mm)	Replace
CN2.mgt	SCS curve number for moisture condition	Relative
ESCO.hru	Soil evaporation compensation factor	Replace
RCHRG_DP.gw	Deep aquifer percolation factor	Replace
GW_REVAP.gw	Groundwater "revamp" coefficient	Replace
ALPHA_BF.gw	Baseflow alpha factor for groundwater	Replace
CH_K2.rte	Effective hydraulic conductivity of channel	Replace
GWQMN.gw	Threshold water depth in the shallow aquifer for base flow	Replace
GW_DELAY.gw	Delay time for aquifer recharge	Replace

*Relative: parameter value is replaced by a given value or absolute change; Replace: parameter value is multiplied by the given value or relative change ([Abbaspour et al., 2007](#)).

Table 2.3 Sensitivity analysis results and calibrated parameters for Mouriki and Anthemountas basins.

Mouriki Basin - SUFI 2					Anthemountas Basin - Trial and error	
Parameters	Final value	Min.	Max.	P-value	Parameters	Fitted value
V_ALPHA_BF.gw	0.12	0.00	1.00	0.000	ALPHA_BF.gw	-
V_CH_K2.rte	11.38	5.00	130.00	0.000	CH_K2.rte	-
V_DEP_IMP.hru	2340.50	500.0	5000.0	0.000	DEP_IMP.hru	-
		0	0			
R_CN2.mgt	0.08	-0.20	0.20	0.150	CN2.mgt	-
V_RCHRG_DP.gw	0.63	0.20	1.00	0.280	RCHRG_DP.gw	0.30
V_GW_DELAY.gw	110.00	1.00	450.00	0.350	GW_DELAY.gw	-
V_GWQMN.gw	1417.00	500.0	1500.0	0.390	GWQMN.gw	750.00
		0	0			

R_ESCO.hru	0.68	0.50	1.00	0.430	ESCO.hru	0.99
V_GW_REVAP.g	0.17	0.00	0.20	0.790	GW_REVAP.g	0.12
w					w	

Table 2.4 Sensitivity analysis results and calibrated parameters for the Campania basin.

Parameter Name	Fitted Value	Min value	Max value
R_CN2.mgt	-0.1732	-0.2	0.2
V_GWQMN.gw	1179.5	500	2000
V_DEP_IMP.hru	3507.5	3500	6000
V_ESCO.hru	0.809	0	1
V_RCHRG_DP.gw	0.1565	0	0.5
V_GW_REVAP.gw	0.15194	0.02	0.2

Table 2.5 Sensitivity analysis results and calibrated parameters for the Marathonas basin.

Parameter Name	Fitted Value	Min value	Max value
R_CN2.mgt	-0.1816	-0.2	0.2
V_GWQMN.gw	1023.2	500	2000
V_DEP_IMP.hru	3441.1	3500	6000
V_ESCO.hru	0.927	0	1
V_RCHRG_DP.gw	0.1883	0	0.5
V_GW_REVAP.gw	0.16197	0.02	0.2

2.2.3 ArcSWAT Results

For the period 2000-2019, total ET was estimated to account for 72% of the entire hydrological balance in Anthemountas basin, while recharge to the shallow aquifer and surface runoff accounted for 12% and 16%, respectively (Figure 2.15). Mean annual recharge to the shallow aquifer was calculated as $17.9 \times 10^6 \text{ m}^3$, while runoff was $28.1 \times 10^6 \text{ m}^3$. The runoff/recharge ratio appears stable for 2000-2019 thus confirming the strong relationship between the two parameters. According to the predicted RCP 4.5 scenario, greater variation will characterize the years 2020-2040 and the average annual recharge will decrease by 30%. The climate scenario predicts severe drought conditions due to low precipitation and high ET rates which will negatively affect both recharge and runoff values. Runoff value is predicted to reduce by 30% but remain consistently higher than recharge values.

The total average annual ET in Mouriki basin was calculated as accounting for 75% of the hydrological balance, while recharge and runoff account for 16% and 9%, respectively. Mean annual recharge for the period 2000-2019 was calculated to be $12.4 \times 10^6 \text{ m}^3$ while runoff was much lower with an average value of $3.00 \times 10^6 \text{ m}^3$ per year. A high inverse

correlation between recharge and ET was estimated. The simulation for 2020-2040 under the RCP 4.5 scenario (Figure 2.15) did not predict significant differences in the average percentages of the examined parameters. The relation between recharge and ET remained constant in the predicted scenario. The total amount of infiltration is not predicted to decrease significantly but is predicted to experience annual variations in the future.

The total average annual ET in Marathonas basin accounted for 67% of the hydrological balance, while recharge and runoff account for 11% and 22%, respectively. The mean annual recharge for the period 2000-2019 was calculated to be $1.28 \times 10^7 \text{ m}^3$ while the runoff average value was calculated as $2.73 \times 10^7 \text{ m}^3$ per year. The simulation for 2020-2040 under the RCP 4.5 scenario (Figure 2.16 Figure 2.15) predicts significant differences in the average percentages of the runoff and recharge parameters. The mean annual recharge to shallow aquifer was calculated as $1.32 \times 10^{15} \text{ m}^3$, while runoff was $1.96 \times 10^{14} \text{ m}^3$ in Campania basin. According to Figure 2.16, the lower values of infiltration appeared during the years 2006-2008 in the actual period with an additional increase in ET. On the other hand, in the future scenario, the precipitation shows significant changes with a direct influence on infiltration. The lower runoff values appeared in the years 2032, 2036, and 2038. A high probability of water stress is expected during the period 2031-2034.

For the investigation of the spatial distribution of possible changes in future infiltration and runoff values in the basin, the RCP 4.5 scenario was used for the period 2020-2040. To identify the most sensitive sub-basins in the study area, a 5-year average infiltration and runoff value was calculated for each sub-basin for four stress periods (2021-2025, 2026-2030, 2031-2035, 2036-2040). Each sub-basin was classified as “Low Recharge” and “High Recharge”. The red colour indicates that the mean value of the parameter in the sub-basin is lower than the mean value of the same parameter during the whole period 2021-2040, whereas the opposite condition is presented in green colour. Significant changes in the spatial distribution of recharge and runoff parameters were identified in each stress period.

The higher recharged areas of Mouriki basin are concentrated near the basin’s outlet where the morphology is flat. Consequently, all the mountainous areas are characterized by steeper reliefs and higher runoff. No significant changes over time were identified during the four stress periods (Figure 2.17). However, one exception is predicted to occur

in the years 2026-2030 where a 10% increase is observed in the areas of “High recharge”. A different situation is observed in the Anthemountas basin. The first three stress periods showed stable classification, with the central part of the basin classified as “High recharge” (Figure 2.17). For the last stress period of 2026-2030, the entire basin is predicted to show an average recharge of under 40 mm. The lower recharge occurs in 2021-2025 for Campania basin. An increase in the parameter appeared in the region with the higher elevation for the period 2026-2030. In the stress period 2031-2035, “High Recharge” is observed throughout the Campania basin (Figure 2.18). In Marathonas basin “Low Recharge” is observed during the first two stress periods while an increase in recharge is mentioned in the periods of 2031-2040 (Figure 2.18). The surface run off that obtained from the simulations is shown in **Figure 2.19**, **Figure 2.20**, **Figure 2.21**, **Figure 2.22**, **Figure 2.23**, **Figure 2.24**, **Figure 2.25** and **Figure 2.26**.

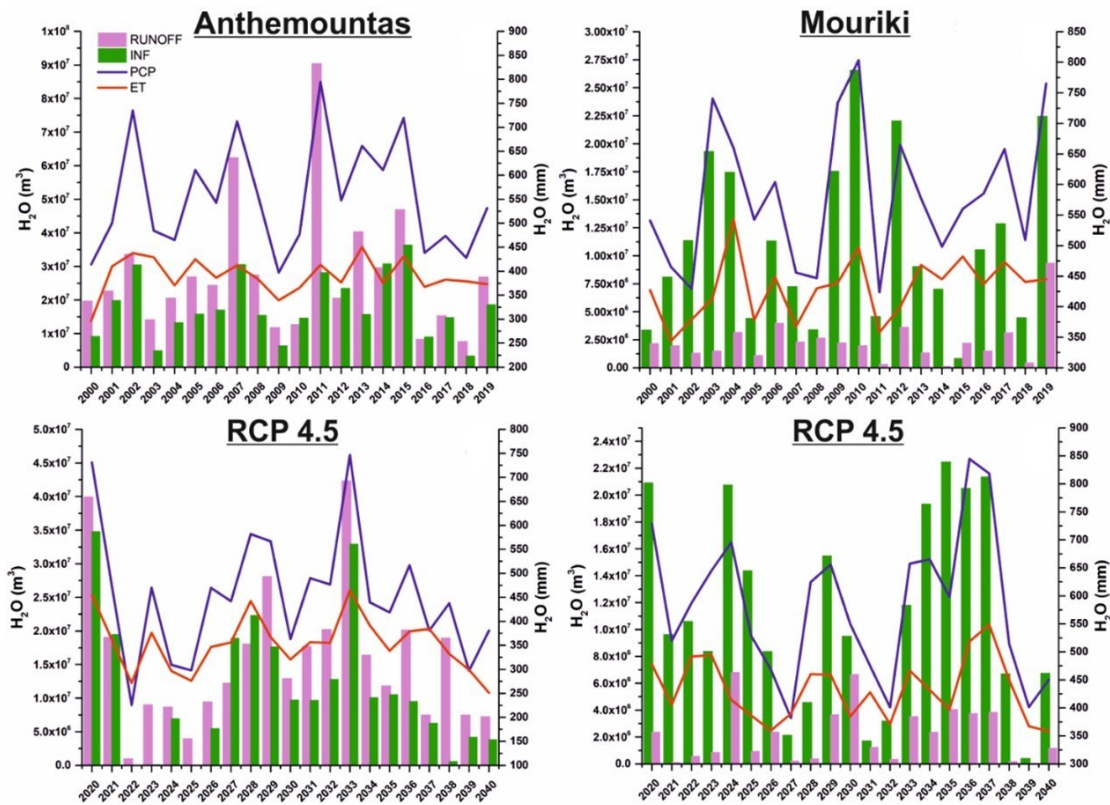


Figure 2.15 Water balance representation for the Anthemountas and Mouriki basins considering the actual scenario and the predicted future scenario.

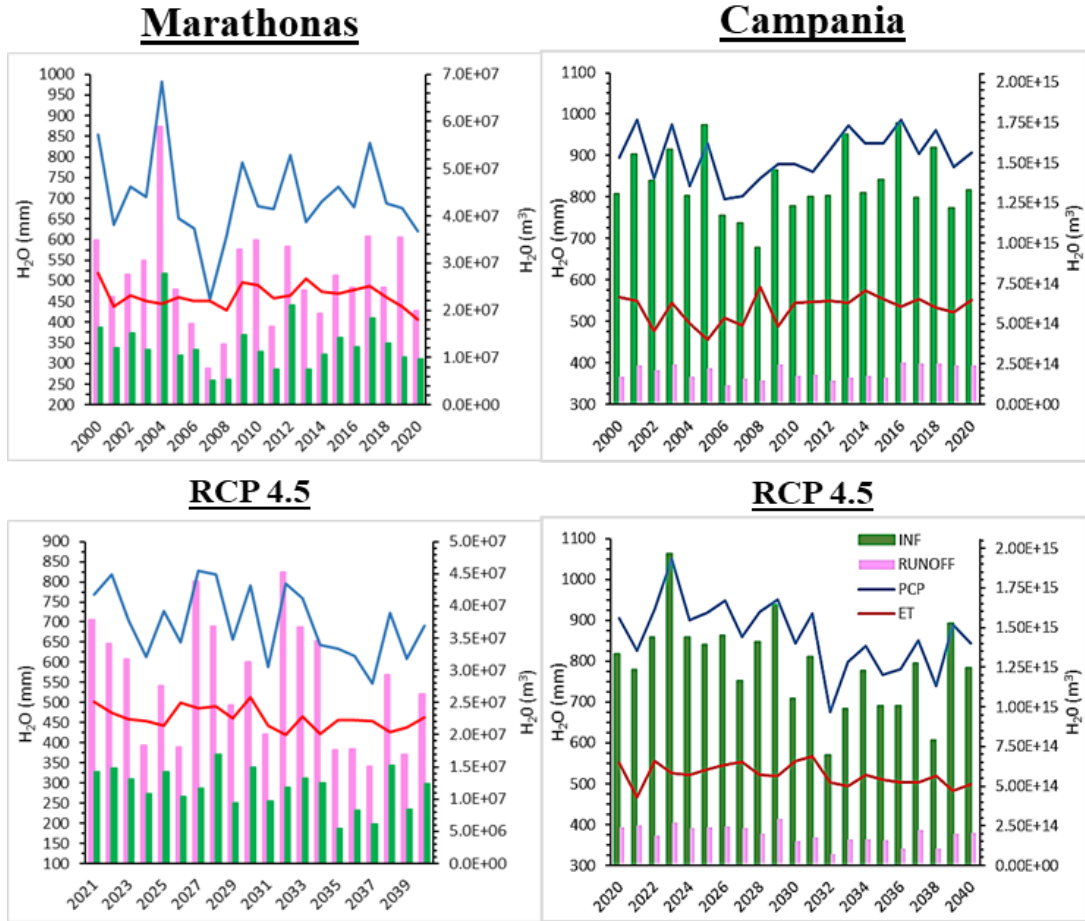


Figure 2.16 Water balance representation for the Campania and Marathonas basins considering the actual scenario and the predicted future scenario.

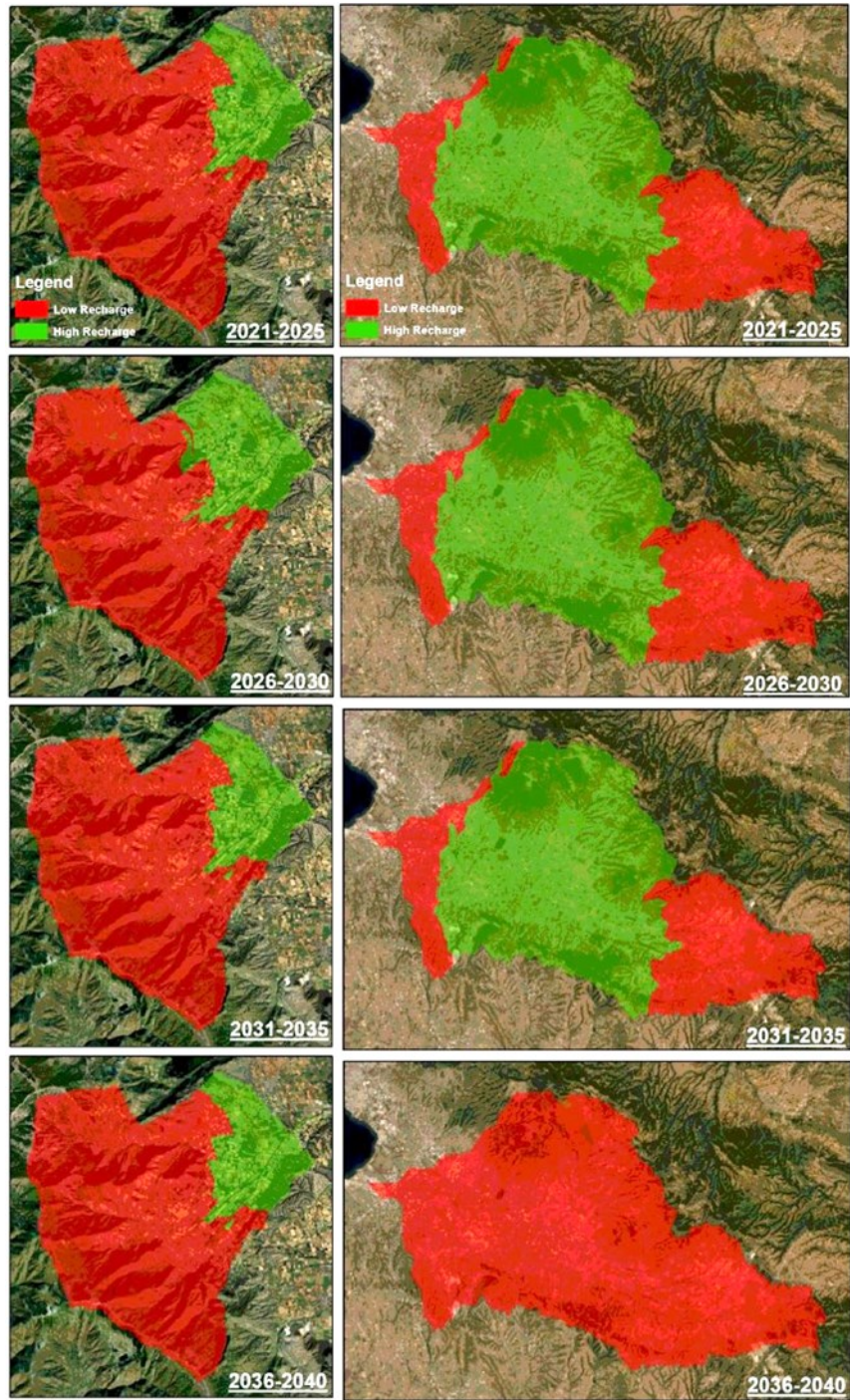


Figure 2.17 Spatial distribution of “High” and “Low” recharge areas in Mouriki (left) and Anthemountas (right) basins.

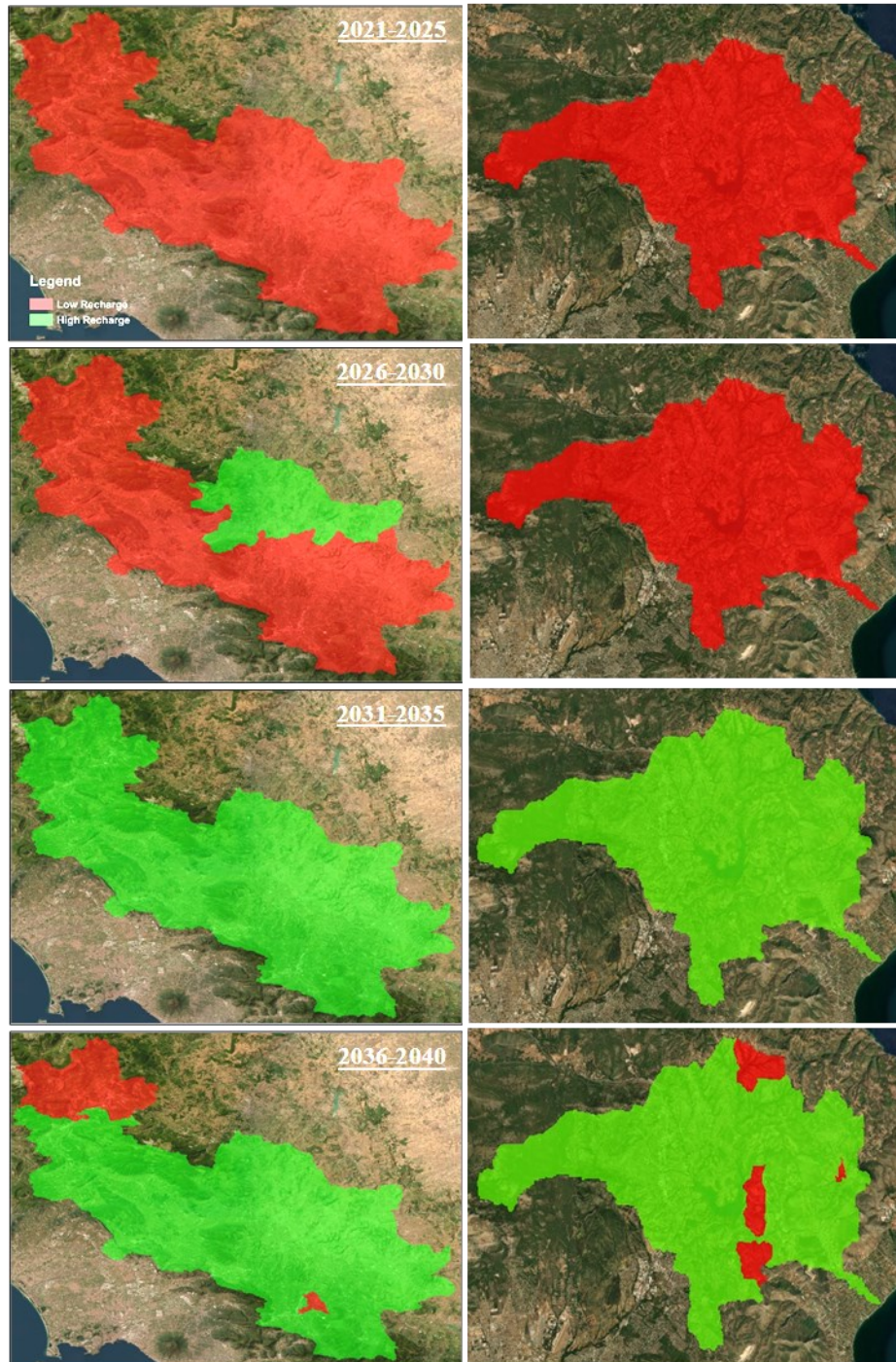


Figure 2.18 Spatial distribution of “High” and “Low” recharge areas in Campania (left) and Marathonas (right) basins.

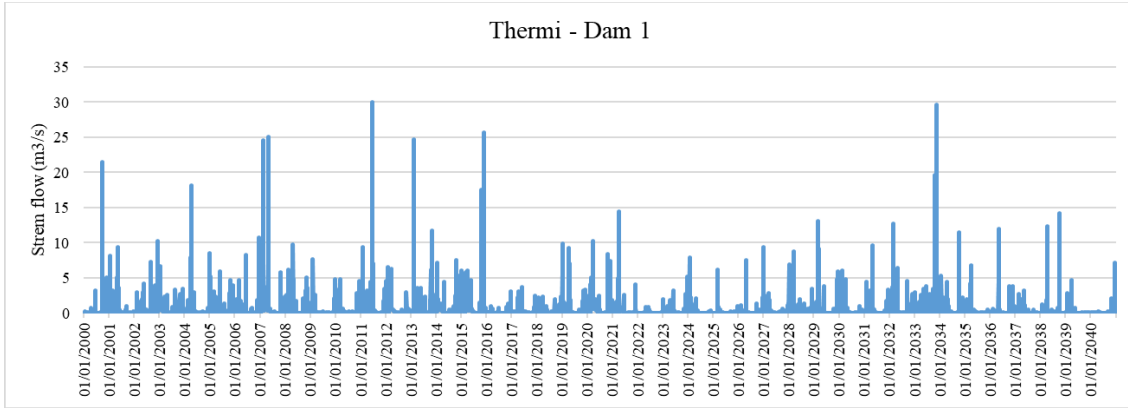


Figure 2.19 Inflow to DAM 1 (Eastern Thermaikos Gulf).

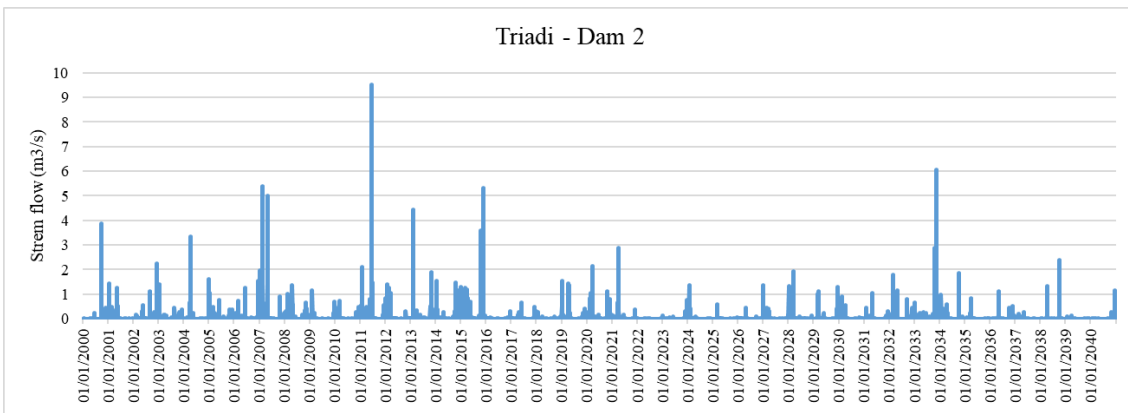


Figure 2.20 Inflow to DAM 2 (Eastern Thermaikos Gulf).

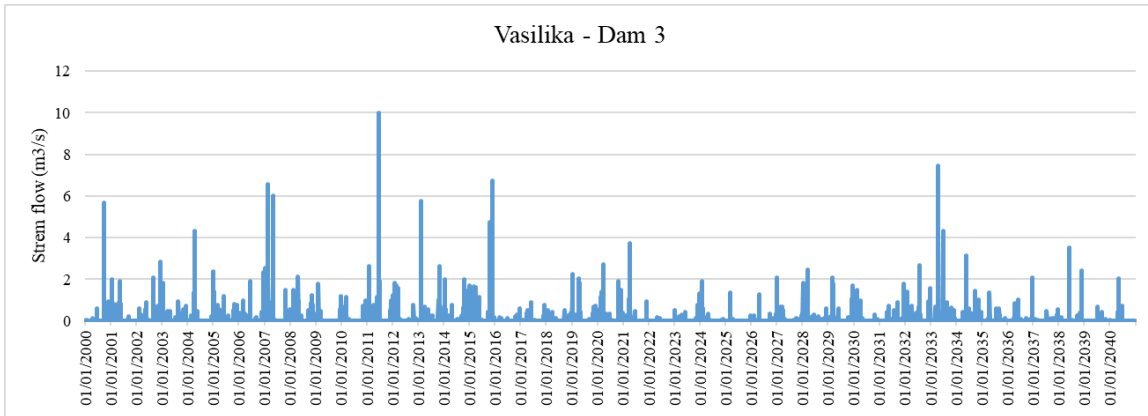


Figure 2.21 Inflow to DAM 3 (Eastern Thermaikos Gulf).

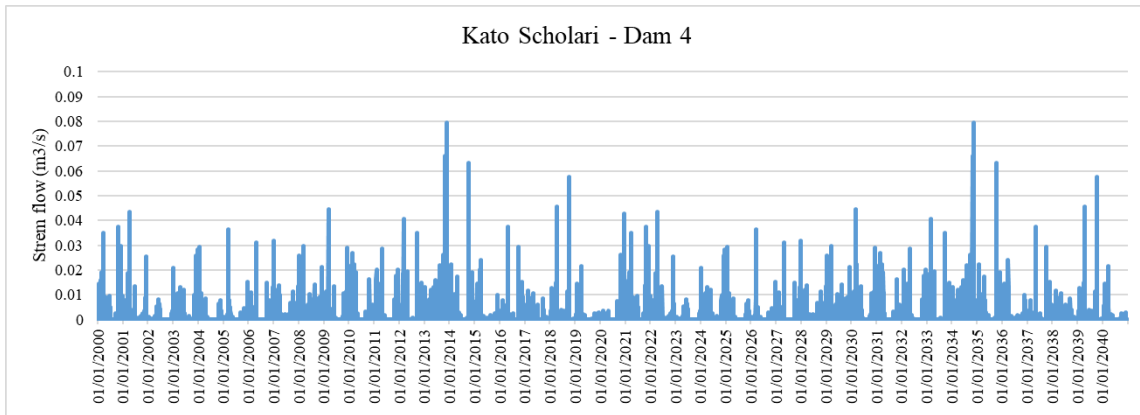


Figure 2.22 Inflow to DAM 4 (Eastern Thermaikos Gulf).

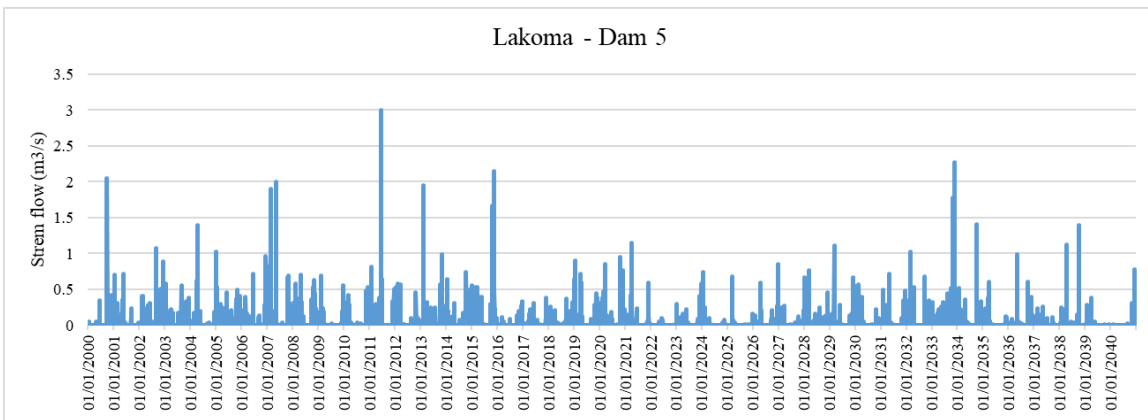


Figure 2.23 Inflow to DAM 5 (Eastern Thermaikos Gulf).

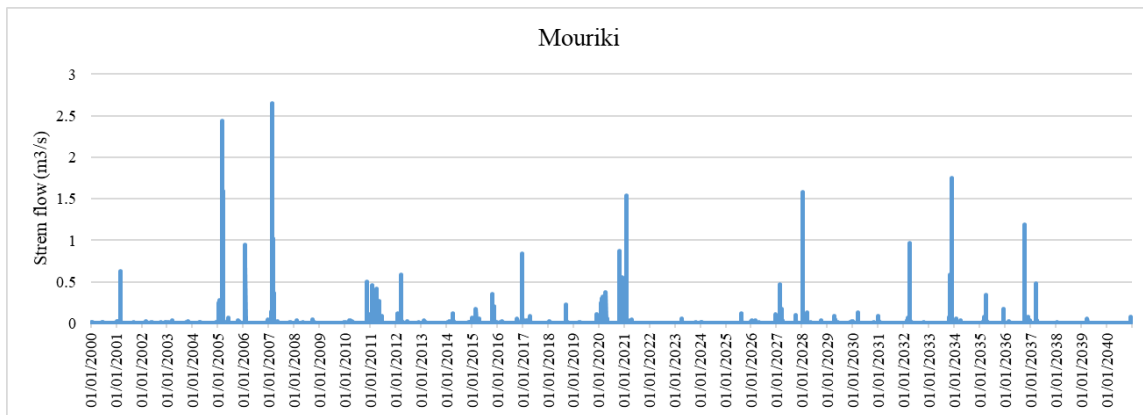


Figure 2.24 Inflow to Mouriki dam.

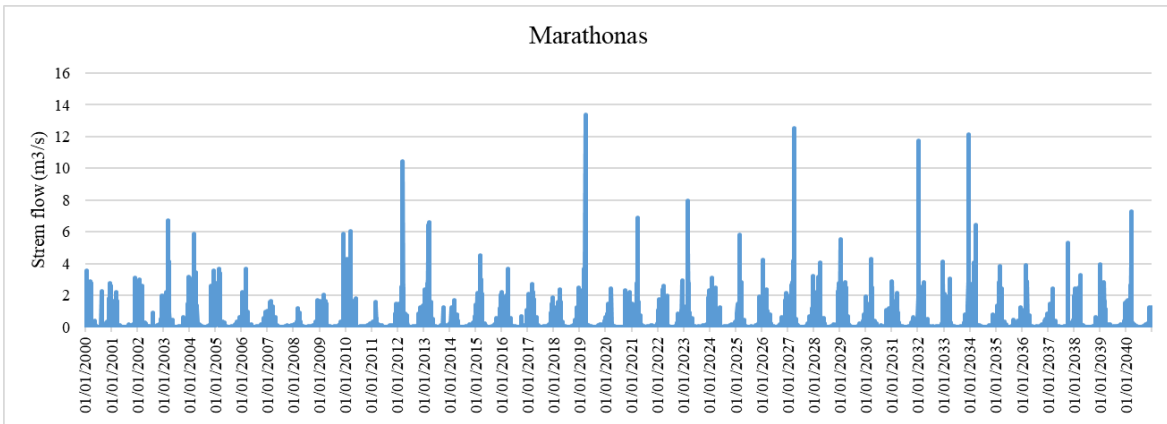


Figure 2.25 Inflow to Marathonas basin dam.

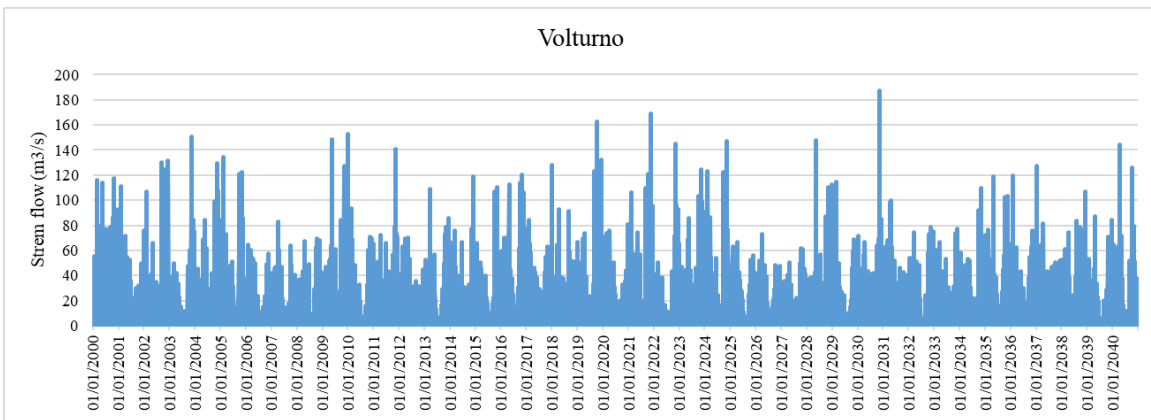
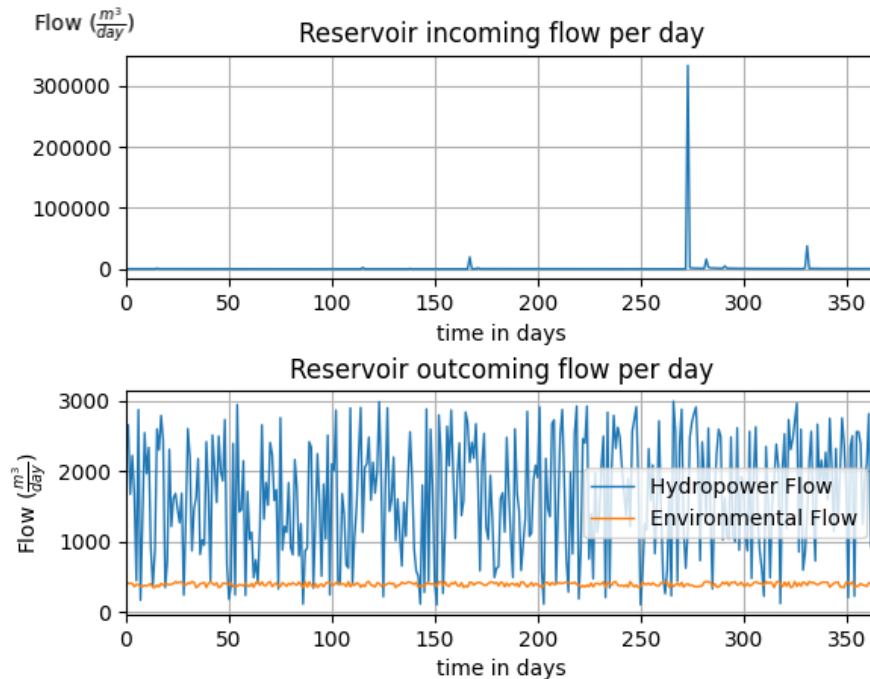


Figure 2.26 Inflow to Campania dam.

2.3 Dams Optimization

The locations of the Eastern Thermaikos Gulf and Anthemountas basin dams are shown in Figure 2.27, for the Mouriki basin in Figure 2.28, for the Marathon basin in Figure 2.29 and the dam for the Campania region in Figure 2.30. Of the above dams studied, only the Dam of the Campania region is an existing hydroelectric plant. The rest of the reservoirs have an agricultural, irrigation or anti-flood function. The purpose of running the algorithm on these reservoirs is to explore the possibility of converting them into hydroelectric ones. Given the inflow from the ArcSwat model as well as the snow model the inflow diagrams for the eight reservoirs, in the aforementioned study areas as well as for hydropower generation, current reservoir volume and ecological flow are presented in the following figures. In Figure 2.31 are shown the location of the dams in the Eastern Thermaikos Gulf and Anthemountas basin, while the graphs of the other dams operation are show in Figure



2.32,

Figure 2.33 Charts of Eastern Thermaikos Gulf and Anthemountas basin Dam 2.

, Figure 2.34, Figure 2.35 and Figure 2.36. In the figures are presented the mean daily values for the simulation period (2020-2040). The simulation of dam operation provided the output water for MAR application for the period 2020-2040.

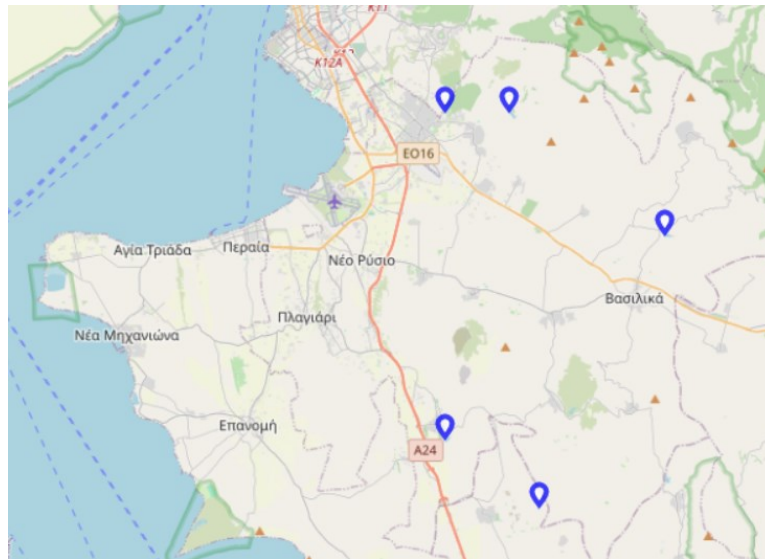


Figure 2.27 The locations of the Dams in Eastern Thermaikos Gulf and Anthemountas basin.

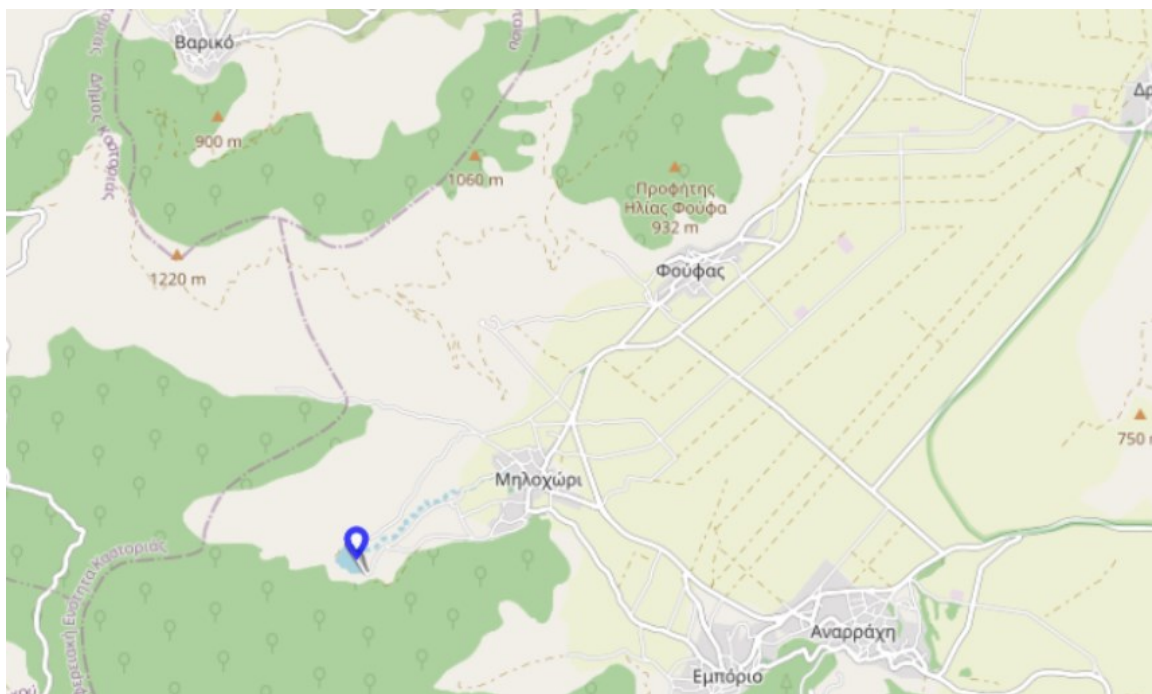


Figure 2.28 The locations of the Dam in Mouriki basin.

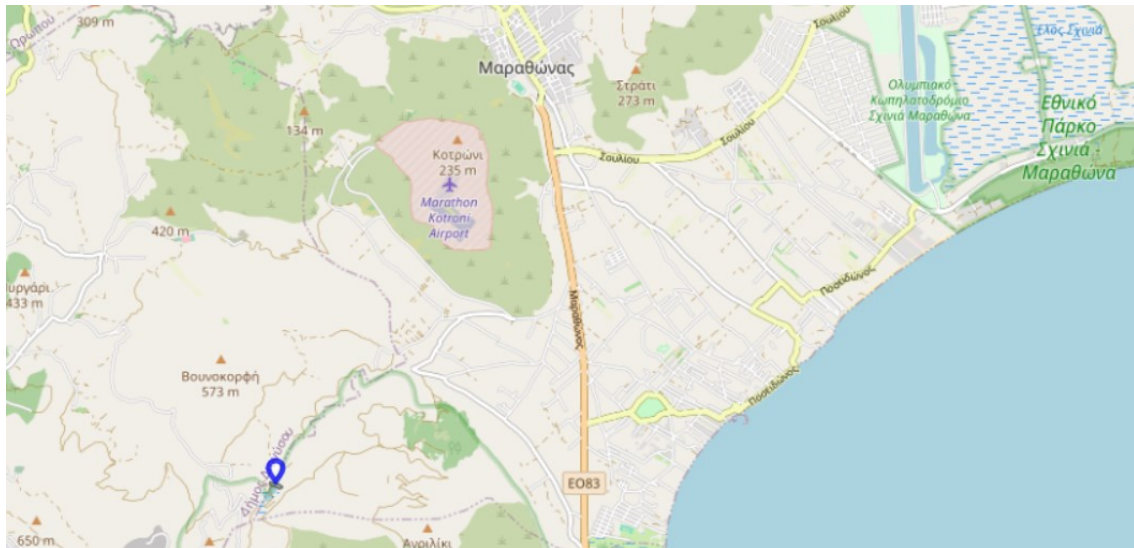


Figure 2.29 The locations of the Dam in Marathonas's basin.

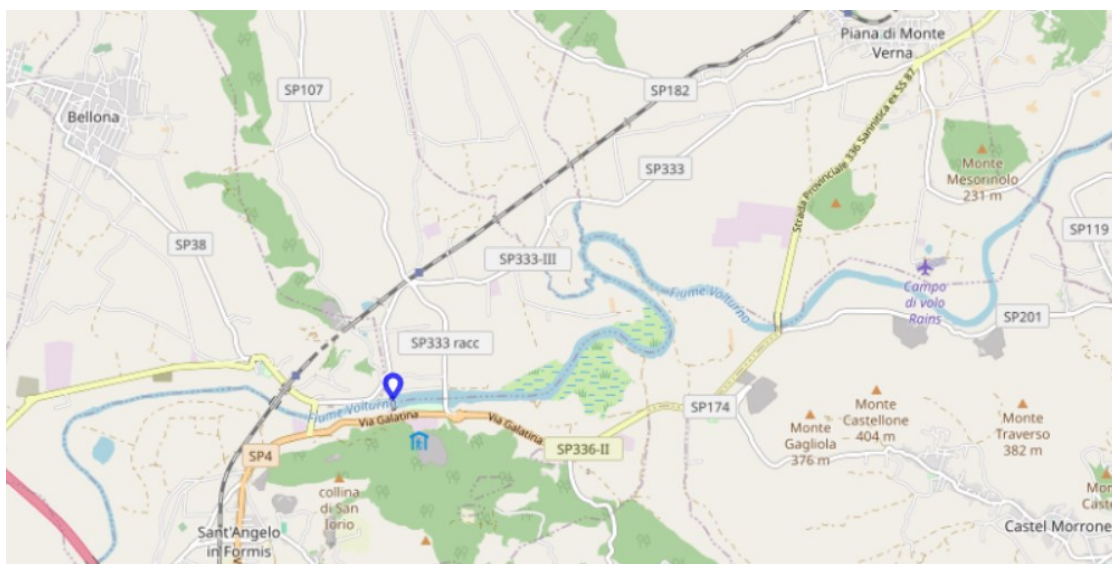


Figure 2.30 Dam in Campania's basin.

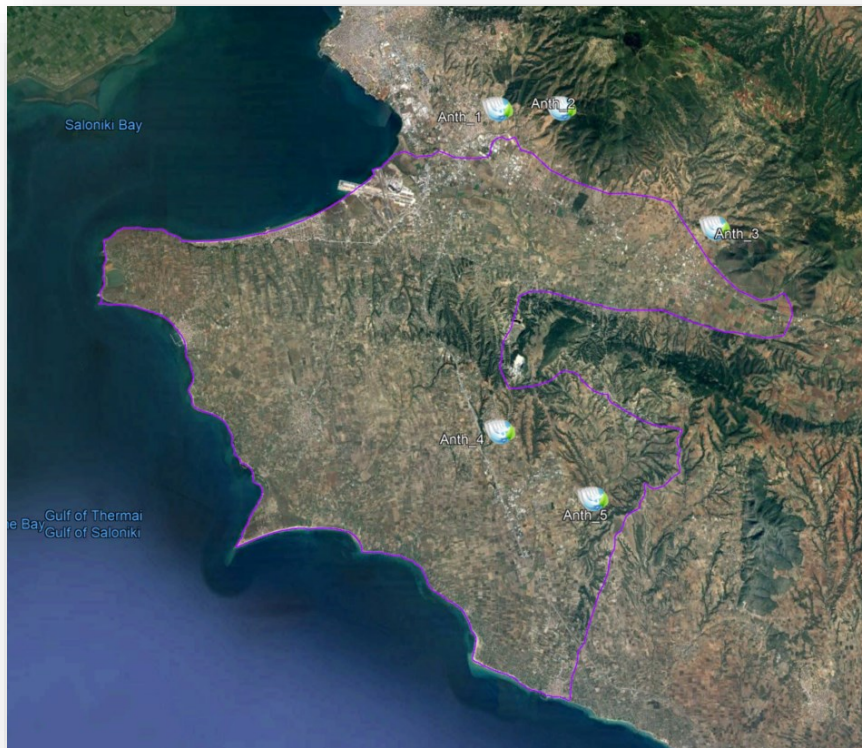


Figure 2.31 Dams in Eastern Thermaikos Gulf and Anthemountas basin.

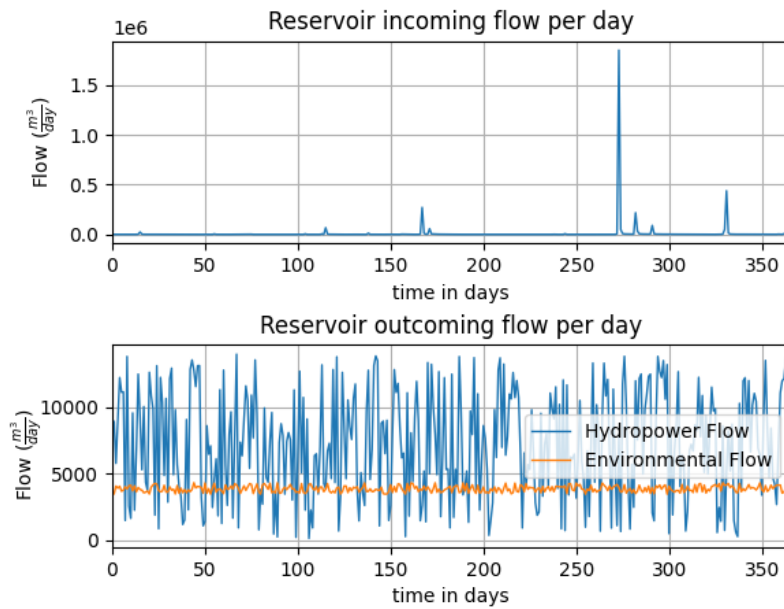


Figure 2.32 Charts of Eastern Thermaikos Gulf and Anthemountas basin Dam 1.

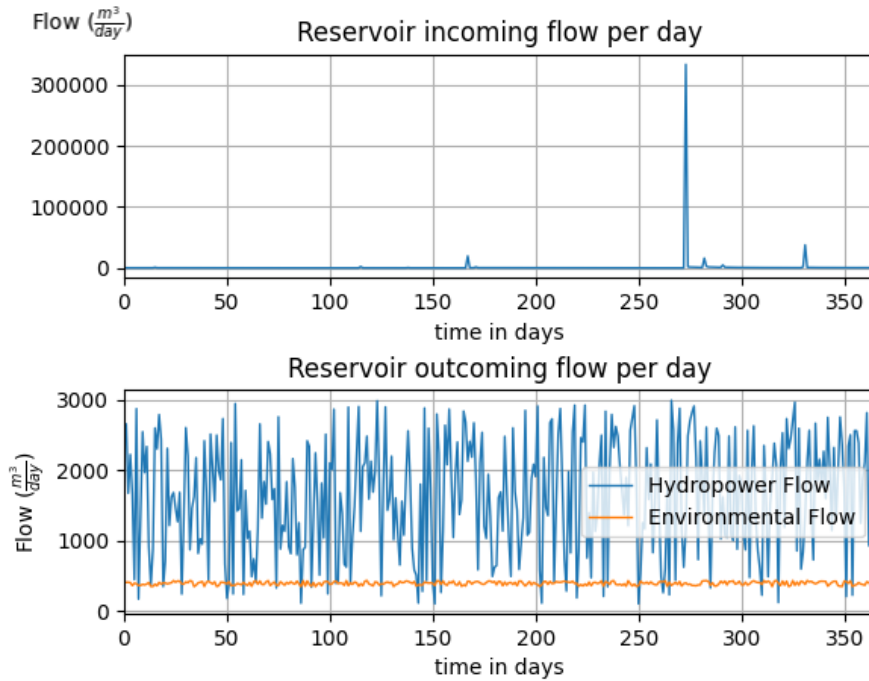


Figure 2.33 Charts of Eastern Thermaikos Gulf and Anthemountas basin Dam 2.

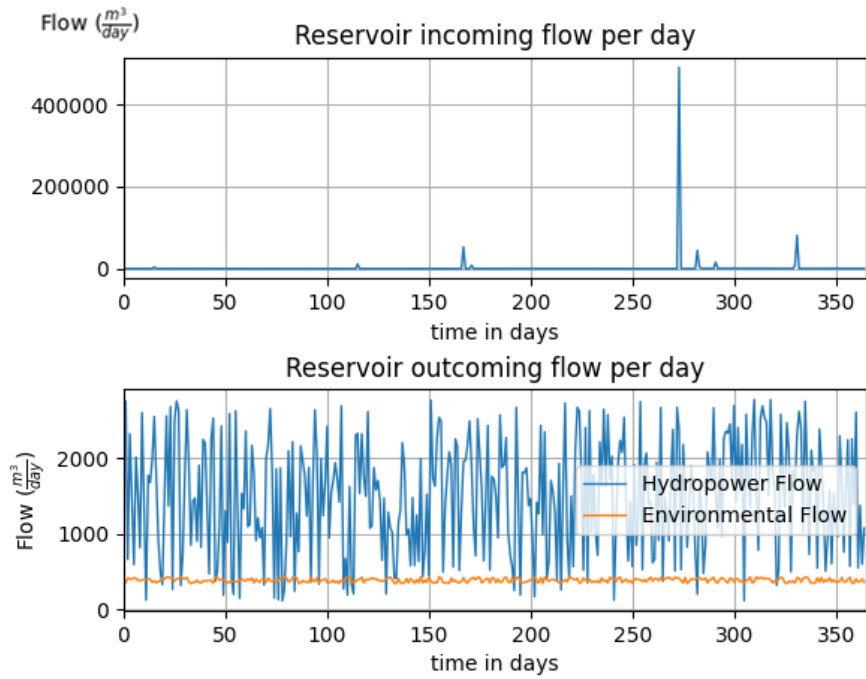


Figure 2.34 Charts of Eastern Thermaikos Gulf and Anthemountas basin Dam 3.

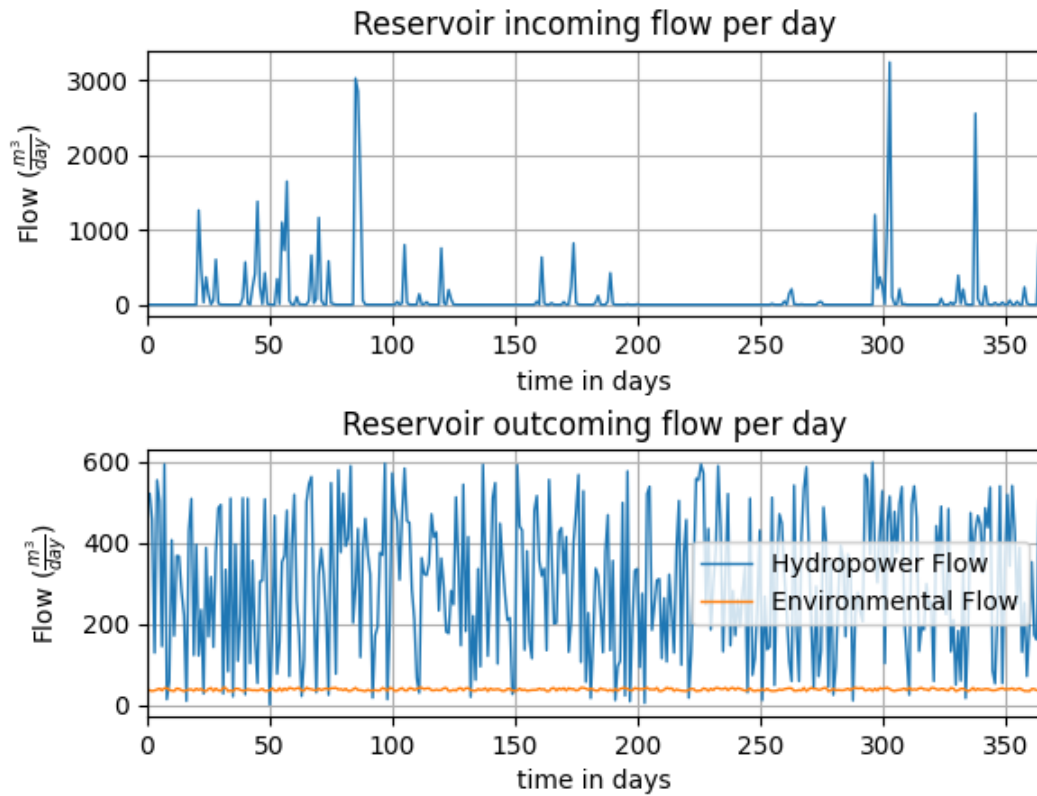


Figure 2.35 Charts of Eastern Thermaikos Gulf and Anthemountas basin Dam 4.

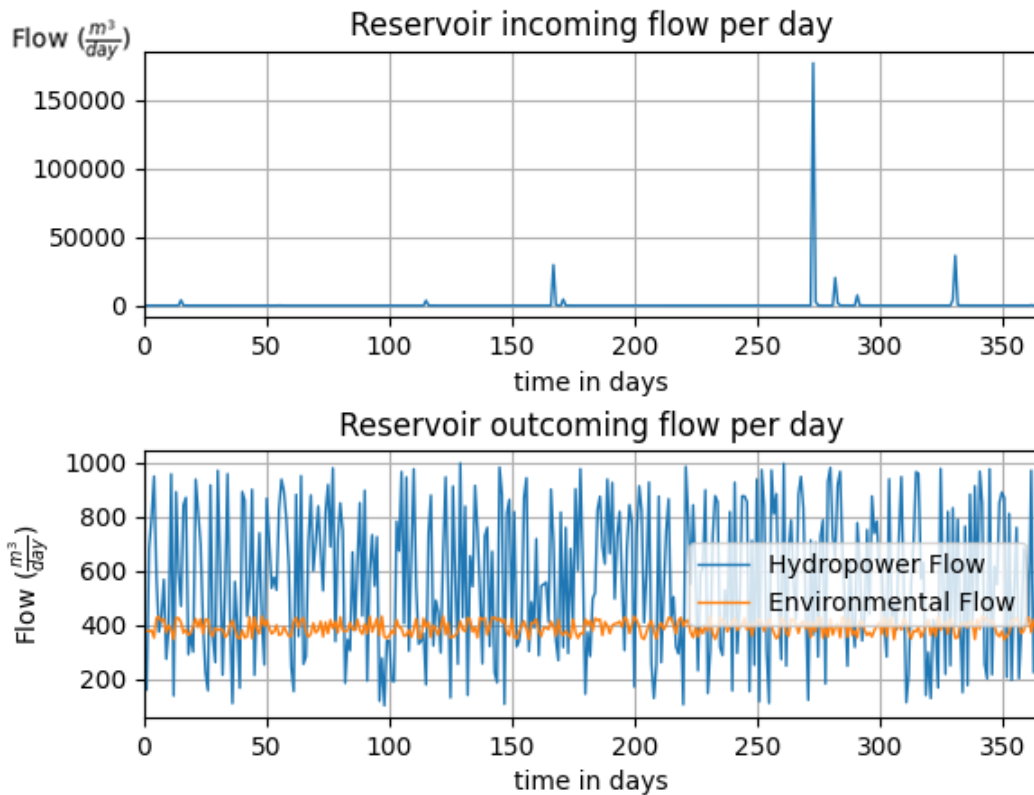


Figure 2.36 Charts of Eastern Thermaikos Gulf and Anthemountas basin Dam 5.

In Figure 2.37 is shown the location of the Dam in Mouriki basin, while in Figure 2.38 is shown the graphs of the dam operation. The Dam in Marathonas basin is shown in Figure 2.39, while the graph of the dam operation is shown in Figure 2.40. In Figure 2.41 is shown the dam in Campania, while the dam operation graph is shown in Figure 2.43.



Figure 2.37 Dam of Mouriki basin.

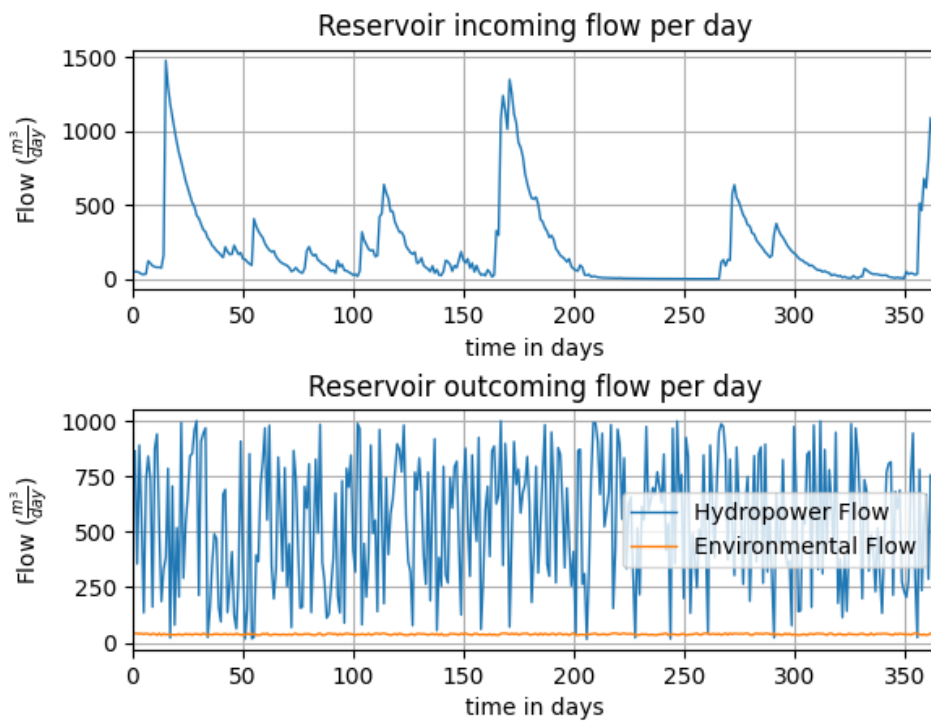


Figure 2.38 Charts of Mouriki Dam.

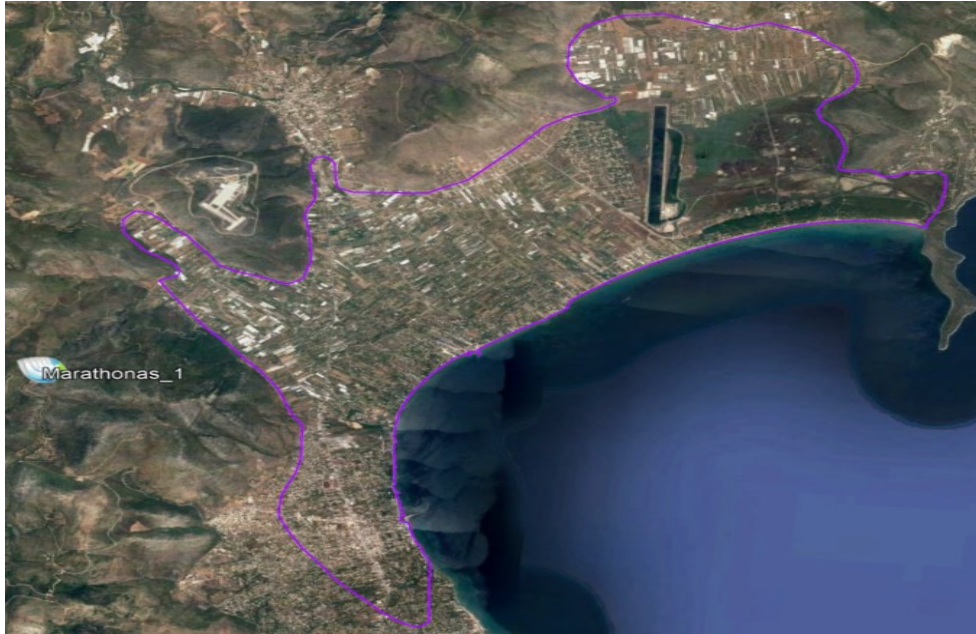


Figure 2.39 Dam of Marathonas.

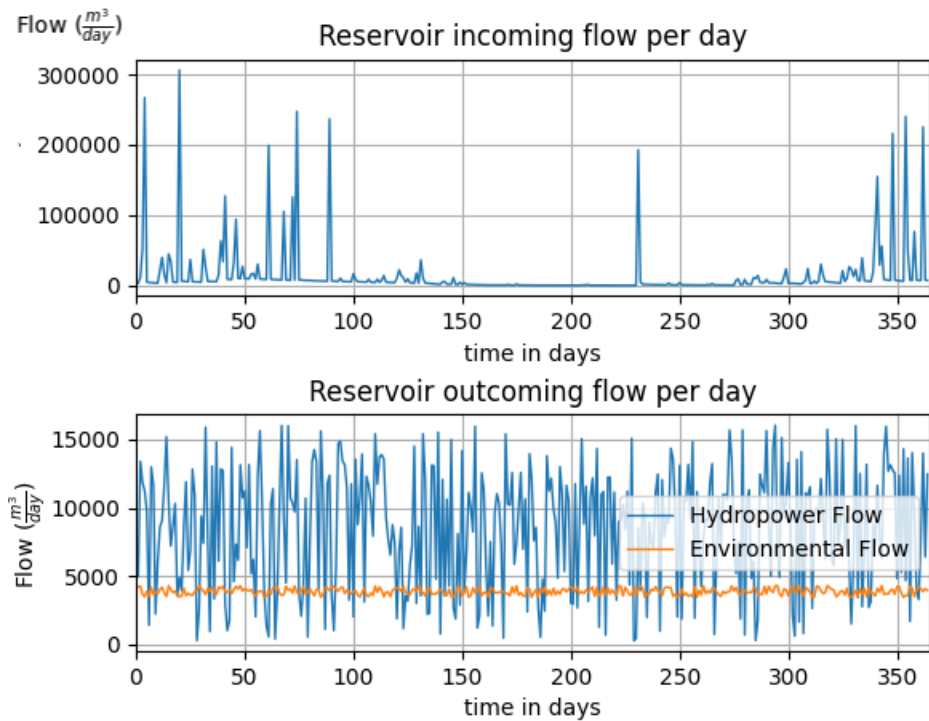


Figure 2.40 Charts of Marathonas Dam.

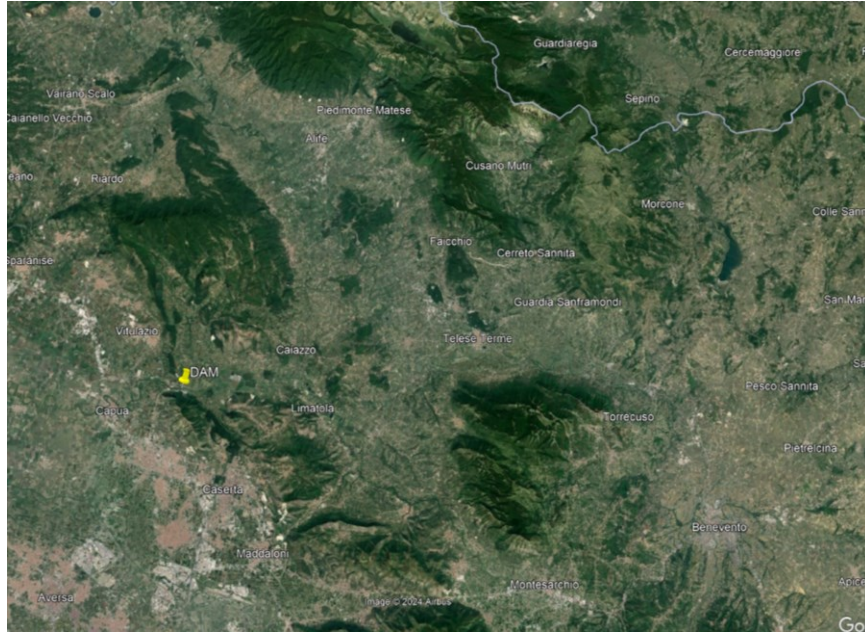


Figure 2.41 Dam of Campania.

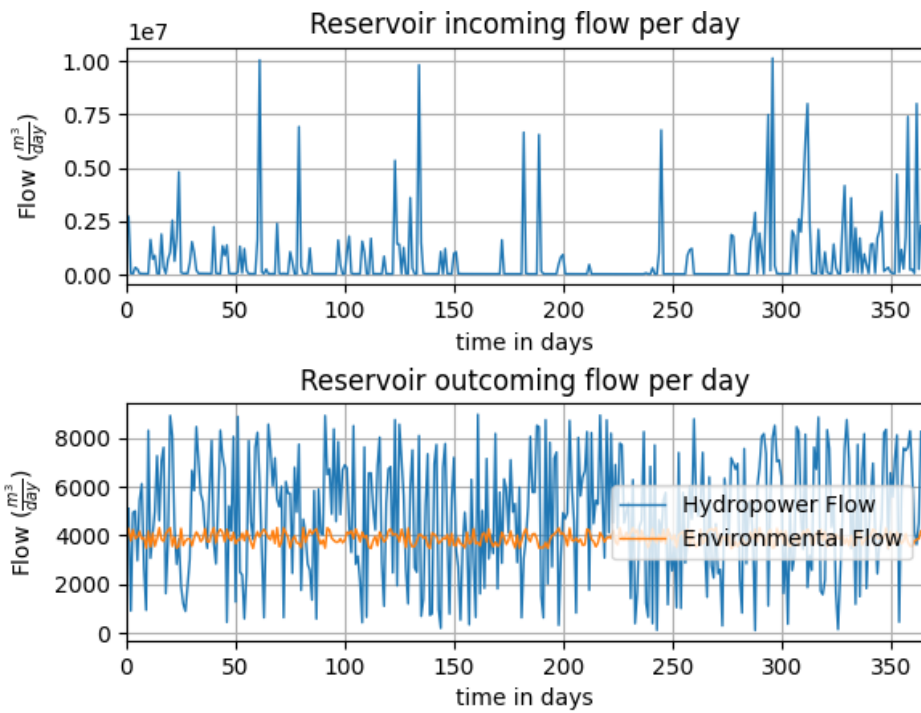


Figure 2.42 Charts of Campania Dam.

Overall, the energy production potential for the two large hydroelectric plants as well as for the rest are presented in the following figures. More specific the mean daily energy production for Marathonas and Campania is shown in Figure 2.43, while for Anthemountas and Mouriki is shown in Figure 2.44. The mean annual energy production for all dams is shown in Figure 2.45.

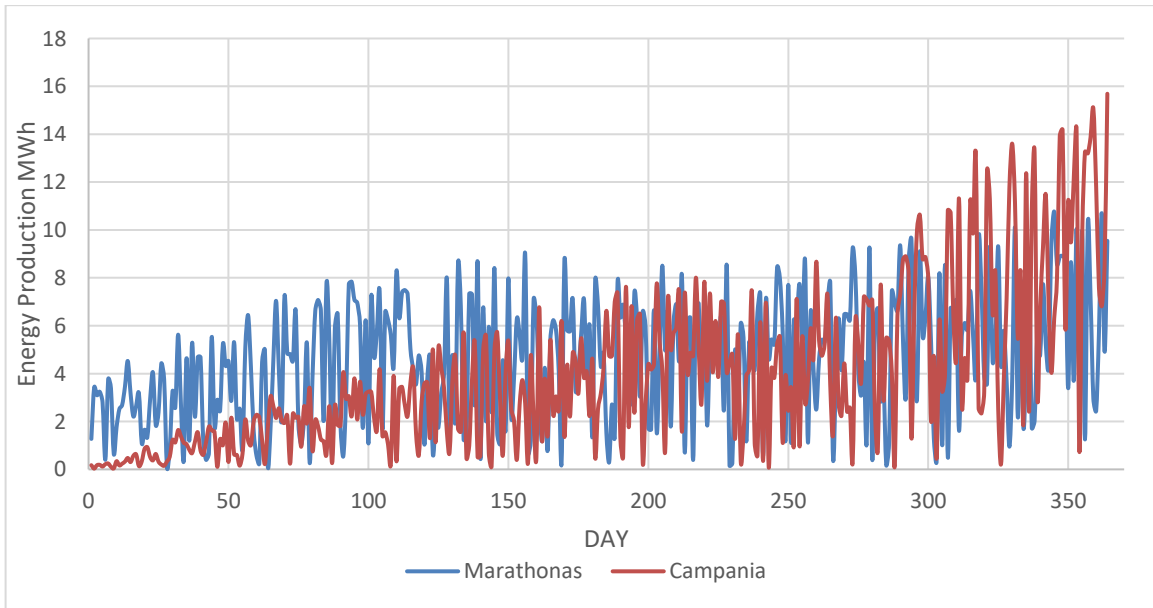


Figure 2.43 Energy Production of Marathonas and Campania.

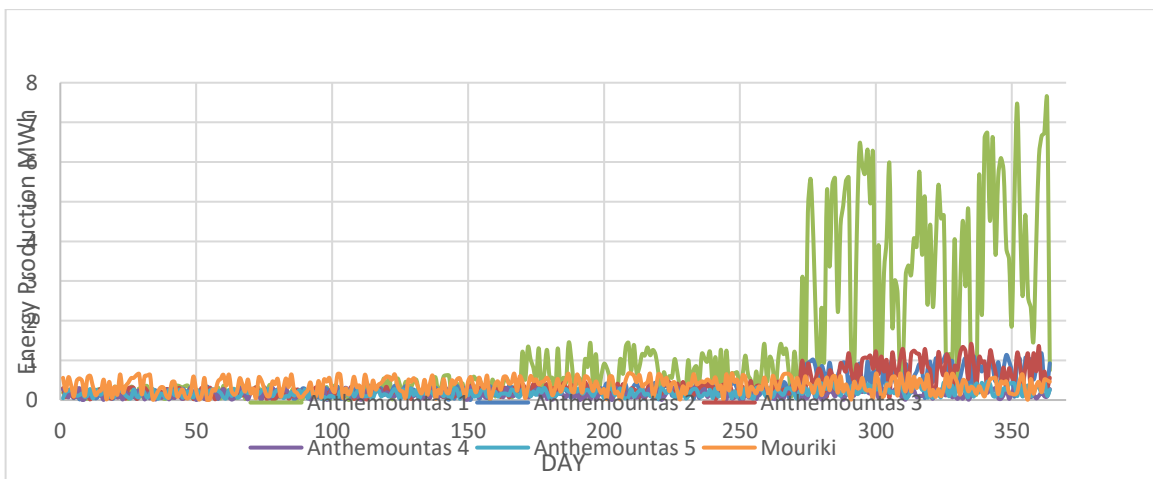


Figure 2.44 Energy Production of Anthemountas, Mouriki and Marathonas.

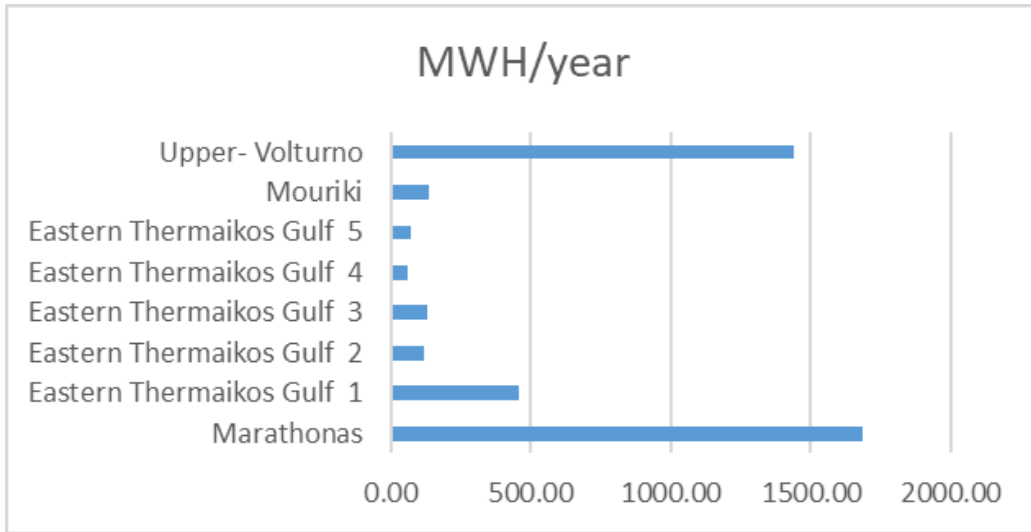


Figure 2.45 Mean annual energy production from the dams.

After the initial preparation phase, the optimization algorithm underwent two significant improvements. Firstly, a meticulous adjustment of the optimal values of the parameters within the harmony search algorithm was conducted using the K-Means clustering method. This involved a series of computational experiments designed to identify values for the Harmony Memory Consideration Rate (HMCR) and Pitch Adjustment Rate (PAR) parameters that yielded superior results. To achieve this, the solution space was categorized into three classes: "good," "average," and "bad," each representing different probabilities of algorithm convergence (80%, 50%, and 20%, respectively). Through the application of the K-Means algorithm to these results, it was observed that, for the majority of problem instances, the most effective values for both parameters fell within the range of 0.5 to 0.7. Specifically, the values of 0.5 for HMCR and 0.7 for PAR emerged as the optimal choices based on this analysis. These refined parameter values were subsequently utilized in the simulation experiments. The outcomes of the grouping process and the assessment of the parameters are graphically presented in Figure 2.46, providing a clear visual representation of the findings derived from this rigorous optimization procedure.

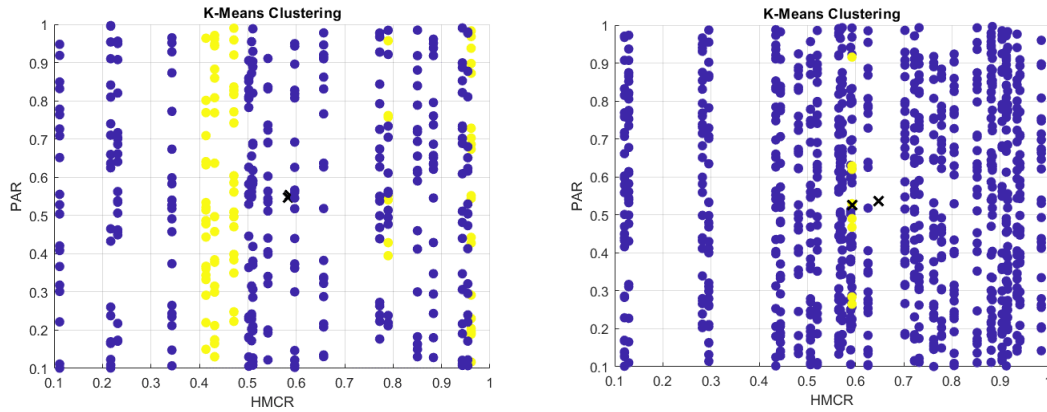


Figure 2.46 Tuning parameters for HAS.

The second improvement of the algorithm is the use of truly random numbers in its execution. As is known when using the functions of programming languages, the random numbers that are actually generated are deterministic and are characterized as pseudo-random. The generation of truly random numbers cannot be done computationally and requires the use of a suitable device. For this reason, an arduino board WeMos D1 was used, which generates random numbers by calculating the noise when connecting to a WIFI network. To extract the time series of random numbers, a suitable code is written in C language, which is presented below.

```

1 void setup()
2 {
3   Serial.begin(9600);
4 }
5 void loop()
6 {
7   Serial.println(os_random());
8   delay(200);
9 }

```

This code returns truly random numbers to the console. The arrangement is shown in the Figure 2.47, while the Figure 2.48 shows the evaluation of randomness through the probability of covering values in the interval 0 to 1.

Beyond the studied dam the code was also applied to an existing small hydroelectric plan which collects water from a local stream. The idea was to test the adaptability of the

code. We also include it within the deliverables in order to inform the readers for the capability of the code. The location of the installation of the station is at Agia Marina at an altitude of 235 m on a private area of 500 m², which is granted by the General Hospital of Pieria (owner) to TOEB Rachis, which then grants it to Ydaton Apodosa IKE for the development of the hydroelectric project .The small hydroelectric project will make use of a 140 m waterfall, from the position of Three Olives with an altitude of 375 m to the position of Agia Marina with an altitude of 235 m. The installation area is shown in Figure 2.49, while in Figure 2.50 and Figure 2.51 are show photos of the installation.

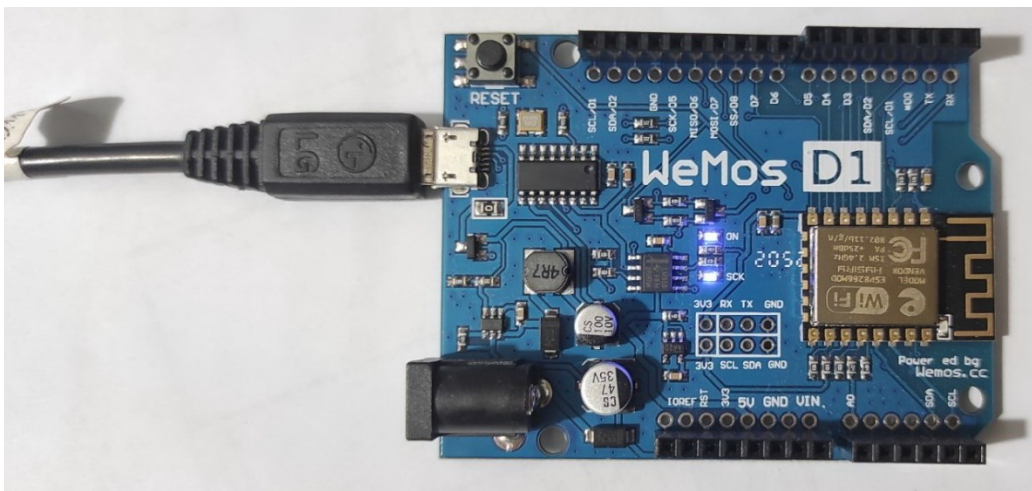


Figure 2.47 Real Random Number Generator.

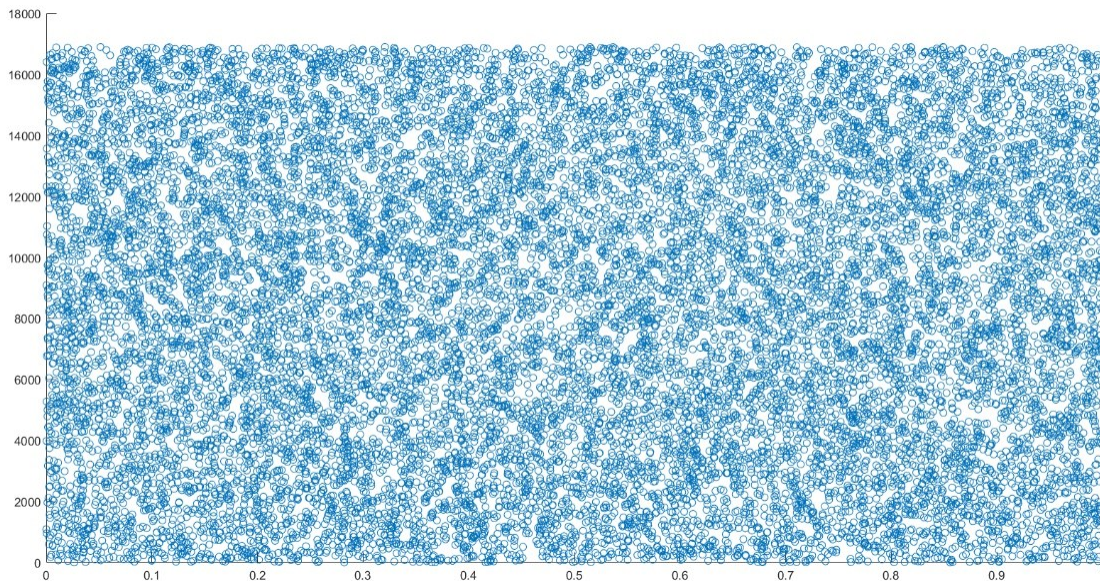


Figure 2.48 evaluation of randomness through the probability of covering values in 0 to 1.



Figure 2.49 Hagia Maria Basin.



Figure 2.50 Photo of Hydropower station.



Figure 2.51 Turbin of Hydropower.

In this particular water stream, flow measurements have been made by GRES and in combination with the correlation of the rainfall in the area, the flow curve of the Zervomylos water stream has been derived. The Figure 2.52 shows the supply curve of the water stream (Flow Duration Curve).

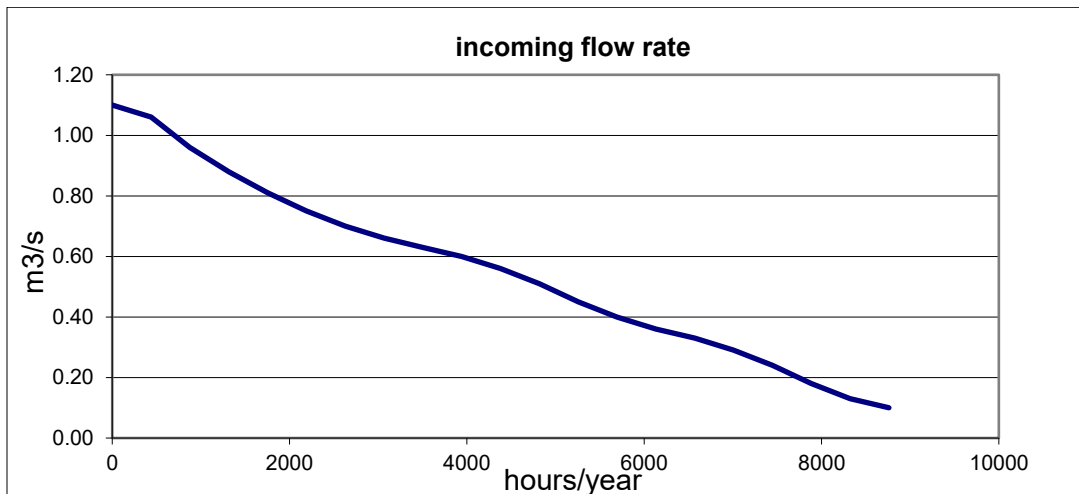


Figure 2.52 Flow Duration Curve Hagia Marina.

The results of the application of the optimization in the hydroelectric of Agia Marina are presented in Figure 2.53 and Figure 2.54. From the calculations it follows that the specific technical project can give a maximum electricity production equal to 1.5 MWh per day. This data is similar to the real production of the station and verifies the robustness of the produced code.

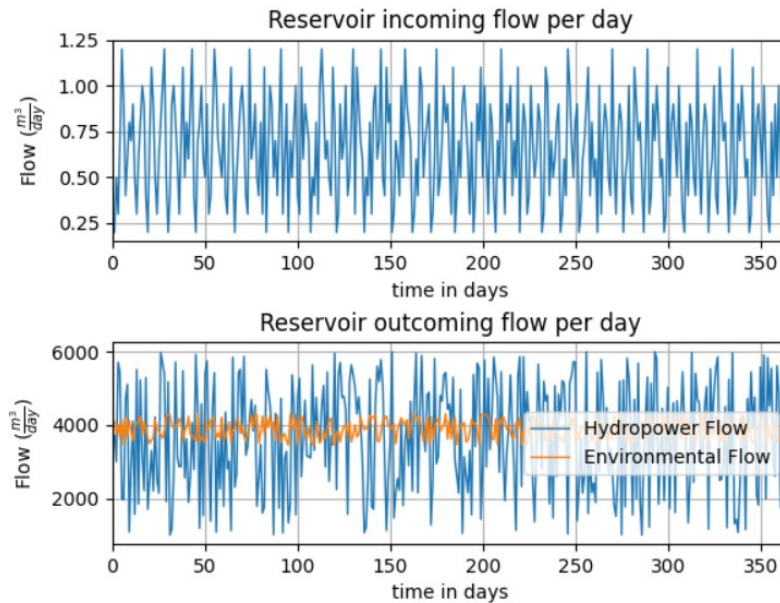


Figure 2.53 Charts of Hagia Marina Dam.

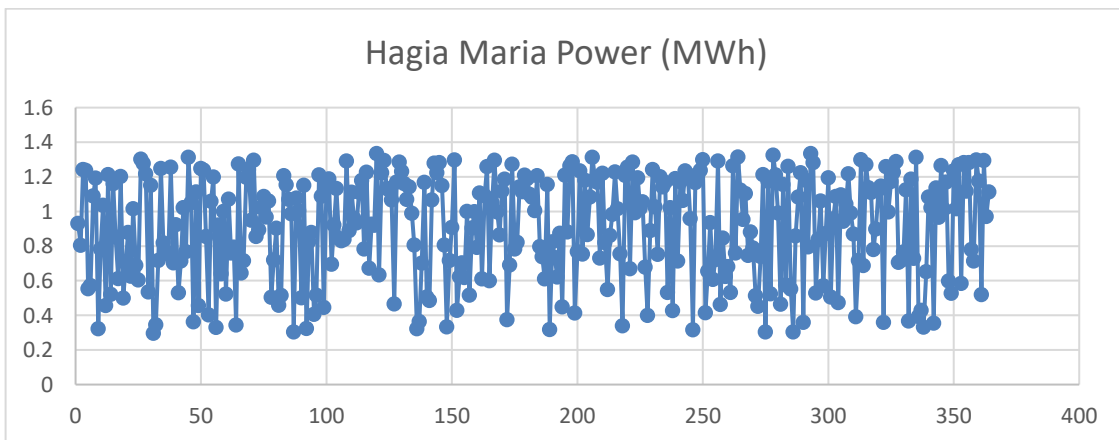


Figure 2.54 Daily energy production from Hagia Marina Dam.

A series of dams are selected for the study areas to generate energy and recharge the aquifer. For each one of these areas, a series of additional extra dams are selected in

order to examine the possibility of further expansion of the methodology. The recharge dynamics from existing and future are shown in Figure 2.55. The locations of the theoretical extra dams is shown in Figure 2.56, Figure 2.57 and Figure 2.58.

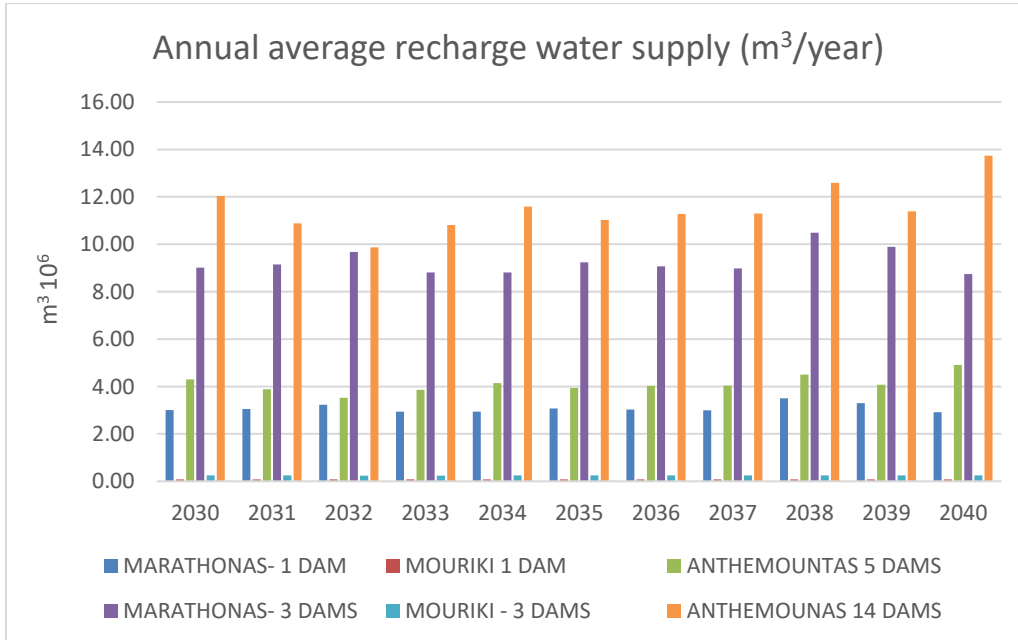


Figure 2.55 Annual average recharge water from dams.

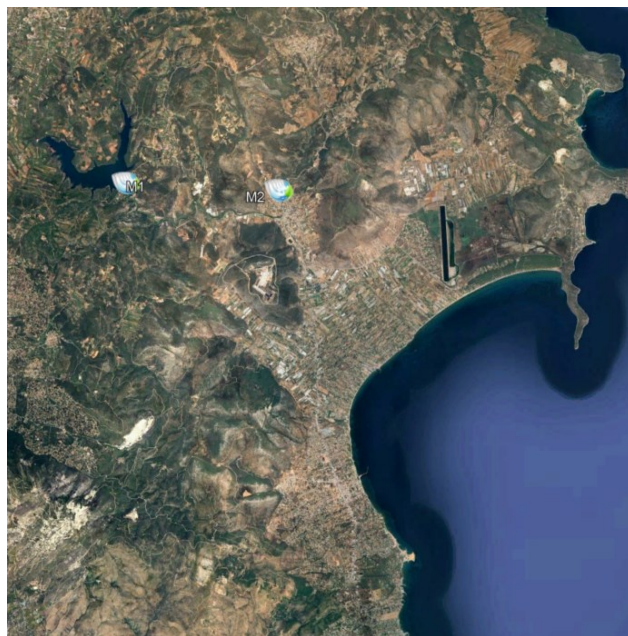


Figure 2.56 Locations of two additional dams for the Marathonas area.



Figure 2.57 Locations additional dams for the Eastern Thermaikos area.

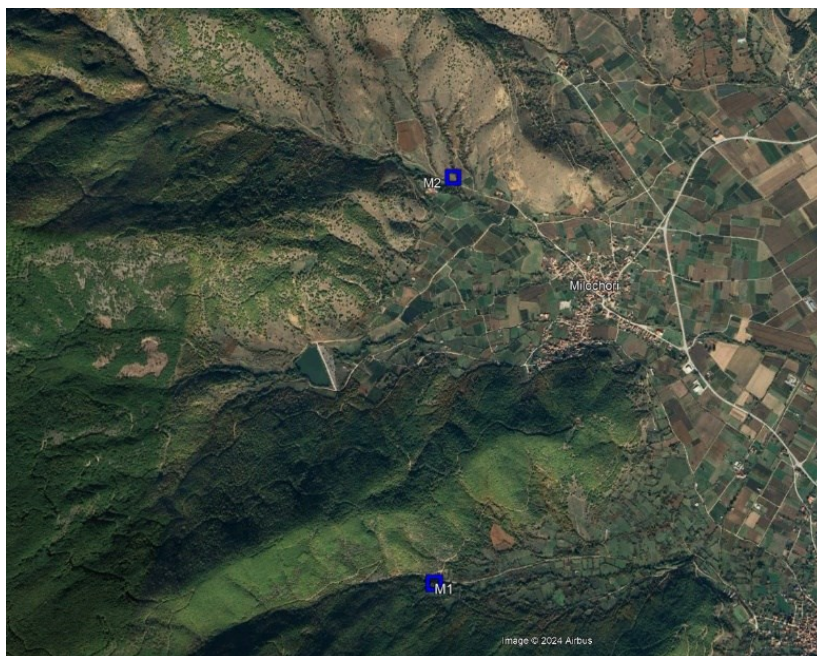


Figure 2.58 Locations additional dams for the Mouriki area.

2.4 Groundwater simulation

The Dam-Mar Model is the integrated optimization model where water after power generation is used to recharge the aquifer. The unified model gave good results for simple cases of underground aquifers but due to high computational complexity MODFLOW, through FLOPY, we tested the software FREEWAT and GMS as well as the source MODEL MUSE to be feasible to simulate the study areas. This assumption is in accordance with the form of the unified objective function as the latter is a linear combination of the two individual components (reservoir – groundwater recharge) with the same monotonicity therefore the individual optimization of the individual models is possible. We ultimately chose MODEL MUSE because of its open source to support the free software community. In the realm of optimization, particularly in multi-objective optimization, the ability to separate two objective functions is often a crucial aspect. Multi-objective optimization deals with problems where there are multiple conflicting objectives that need to be optimized simultaneously. These objectives could be maximizing profit while minimizing cost, maximizing performance while minimizing energy consumption, or any other combination of goals. The ability to separate objective functions refers to the capacity to distinctly define and analyze each objective in isolation, without undue influence from other objectives. This separation allows for a clearer understanding of each objective's contribution to the overall optimization problem. One approach to separating objective functions is through the concept of Pareto optimality. In a multi-objective optimization problem, a solution is Pareto optimal if there is no other solution that improves one objective without worsening at least one other objective. Pareto optimality provides a framework for evaluating trade-offs between conflicting objectives without explicitly combining them into a single composite objective function. This allows decision-makers to explore the trade-off space and make informed decisions based on their preferences. Another approach involves formulating the optimization problem as a weighted sum of the individual objective functions. By assigning weights to each objective, decision-makers can control the relative importance of each objective in the optimization process. However, this approach assumes linear relationships between objectives and may not capture the complexity of real-world trade-offs. In our cases we chose to optimize with equivalent weights the two objectives using modelmuse as the groundwater software. To simulate

intricate aquifers, ModelMuse was utilized alongside corresponding conceptual models of the study cases. Additionally, ArcSwat simulation data (Figure 2.15 and Figure 2.16) was utilized for the recharge package (RCH). The recharge split into two periods (wet October – March, dry May – September). This integration of different software and data sources allows for a comprehensive exploration of groundwater dynamics, facilitating informed decision-making in hydrological management and optimization efforts. In conjunction with the conceptual models, a meticulous process was undertaken to produce thematic maps delineating water load and depletion characteristics across the study regions. These maps serve as invaluable tools for visualizing the spatial distribution of groundwater dynamics and understanding the localized impacts of various factors such as extraction, recharge, and natural processes. The simulation periods were strategically designed to capture distinct phases of groundwater management and resource utilization:

- a) The initial period from 2010 to 2020 focuses on assessing the historical trend of aquifer depletion, providing a baseline understanding of groundwater dynamics over the past decade.
- b) Extending the analysis to the subsequent decade, from 2020 to 2030, enables the projection of future trends in aquifer depletion under existing management practices and anticipated changes in water demand and availability.
- c) Introducing artificial recharge strategies during the period from 2030 to 2040 represents a proactive approach to replenishing groundwater resources using available dam infrastructure. This simulation period evaluates the efficacy of such interventions in mitigating depletion and enhancing groundwater sustainability.
- d) Building upon the previous scenario, the inclusion of additional dam projects in scenario b offers insights into the potential benefits of expanding water management infrastructure and its implications for groundwater replenishment.

By systematically exploring these simulation periods, stakeholders can gain comprehensive insights into the complex dynamics of groundwater resources and assess the effectiveness of various management strategies in addressing long-term sustainability challenges. Moreover, the integration of advanced modeling techniques with geospatial analysis allows for the identification of spatially explicit patterns and trends, empowering decision-makers to formulate targeted interventions and policies for sustainable water

resource management. The data for the aquifers in the study areas are presented in Table 2.6. The conceptual model for the simulated aquifers is presented in Figure 2.59.

Table 2.6 Modeling data for the studied aquifers.

ID	Data	Eastern Thermaikos	Mouriki	Marathonas	Campania
1	Layer	1	1	1	1
2	conductivity (mean value m/d)	5	6	5	6
3	Effecitive Porocity	20	25	15	20
4	Long Disperivity	Fine sand - silt	Fine sand	Fine sand - silt	Fine sand - silt
5	Trans Dispersivity	Fine sand - silt	Fine sand	Fine sand - silt	Fine sand - silt
6	Molecular Dispersivity	Fine sand - silt	Fine sand	Fine sand - silt	Fine sand - silt
7	Terrain	DEM	DEM	DEM	DEM
8	Layer depth	100	60	80	80
9	Boundaries	GHB, CHB	GHB	GHB, CHB	GHB
11	Wells	Shape file	Shape file	Shape file	Shape file
12	Pumping (m ³ /year)	35×10 ⁶	9.5×10 ⁶	5×10 ⁶	6×10 ⁶
13	Incoming	32.5×10 ⁶	9.45 × 10 ⁶	3,5×10 ⁶	8×10 ⁶

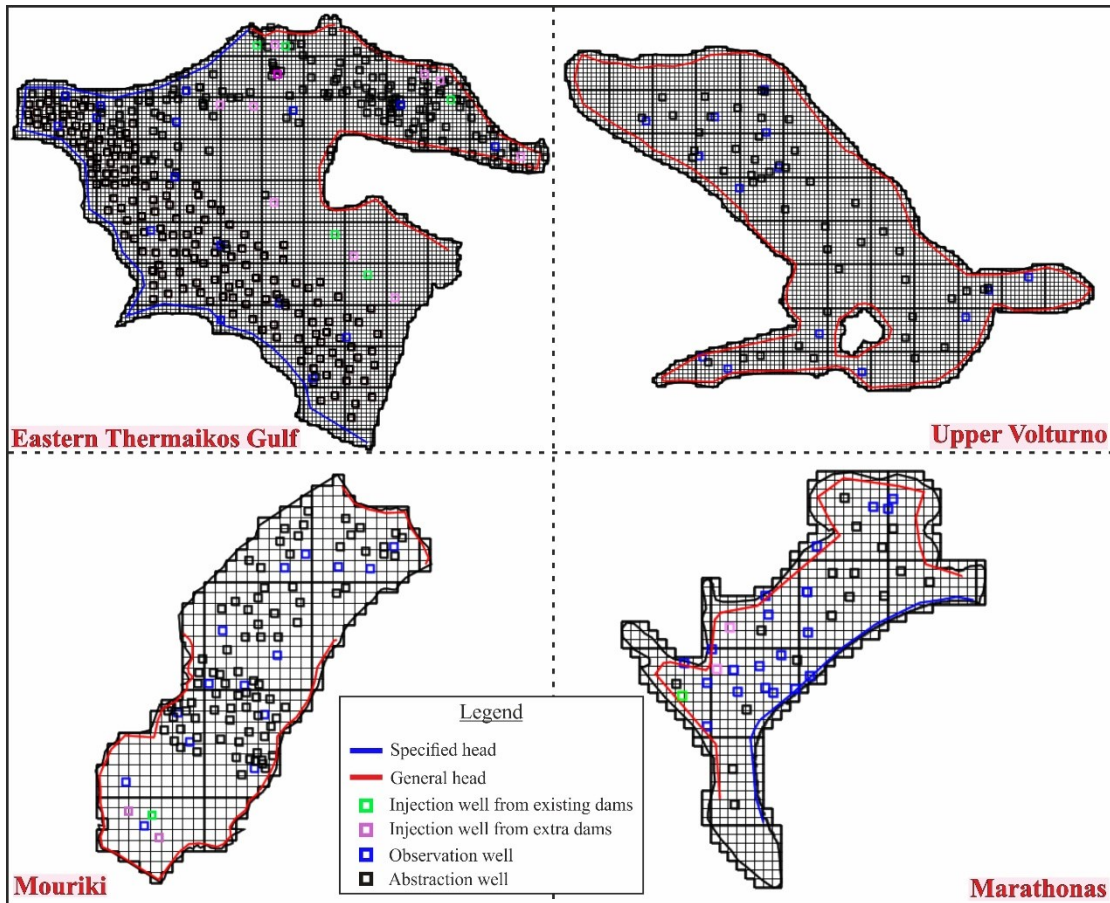


Figure 2.59 Conceptual models of the studied aquifers.

The models for the study areas are first run in a short steady state period. Then a 10-year period with transient flow is run (2010-2020) for the model validation. A second period of 10 additional years with transient flow from the year 2020 to 2030 with the same groundwater balance. It is worth to mention that groundwater balance in the Greek sites is in accordance with the official management plans of the sites. These two periods express the depletion of groundwater reserves in the last ten years, but also an additional ten-year period to forecast for future groundwater depletion. Then a period of ten years is carried out applying managed aquifer recharge using the water from the existing dams. A second scenario was applied of a ten-year period (2030-2040) managed aquifer recharge with additional dams. In Eastern Thermaikos Gulf and Anthemountas basin included nine (9) more dams with similar capacity of the nearby dams. In Mouriki and Marathonas basin used two extra dams with the same characteristics as the existing dams. The core of the MAR application after 2030 is based on the realism that the transformation of the existing

dams requires a period of time as well as the construction of new dams. In the Figure 2.60, Figure 2.61, Figure 2.62 and Figure 2.63 are presented the RMS for all simulated aquifers.

The results of the simulations are shown in Figure 2.64, Figure 2.65, Figure 2.66 and Figure 2.67. In the Campania region groundwater depletion does not occur and hence in the site we didn't simulate the scenario with the application of managed aquifer recharge.

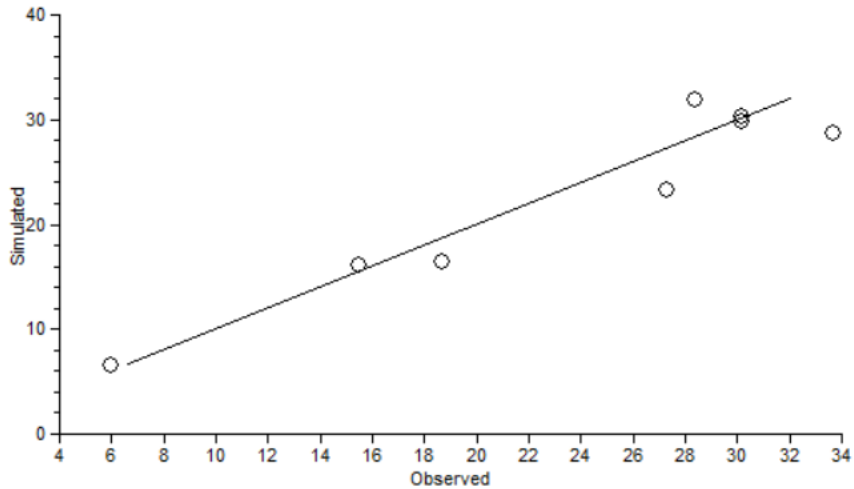


Figure 2.60 RMS Residual for Eastern Thermaikos Gulf – Anthemountas basin.

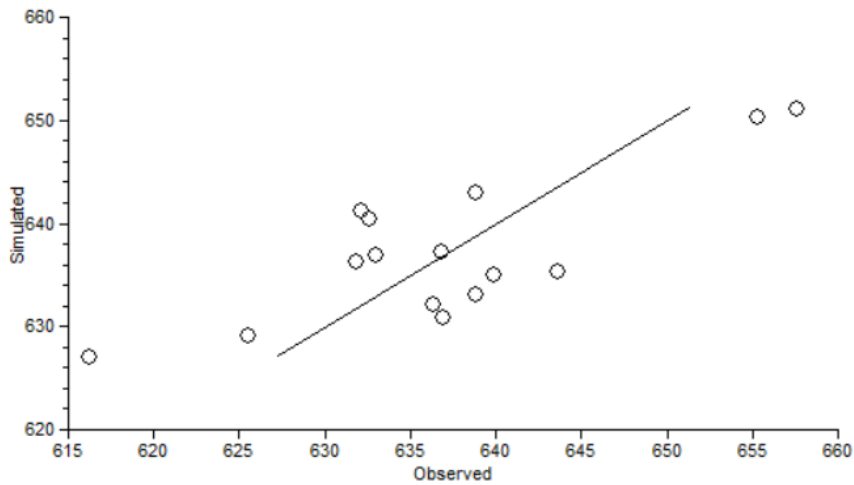


Figure 2.61 RMS Residual for Mouriki Basin.

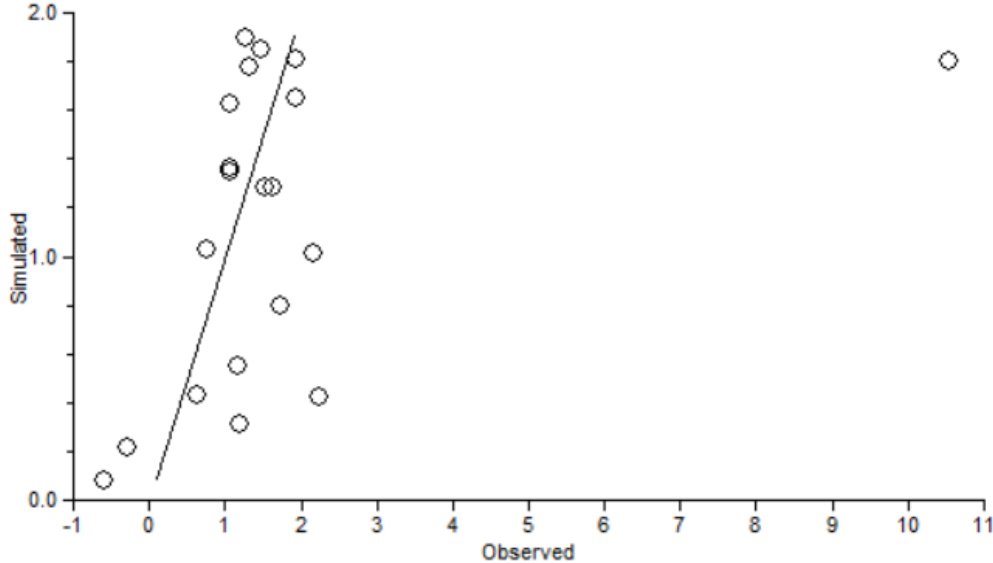


Figure 2.62 RMS Residual for Marathonas Basin.

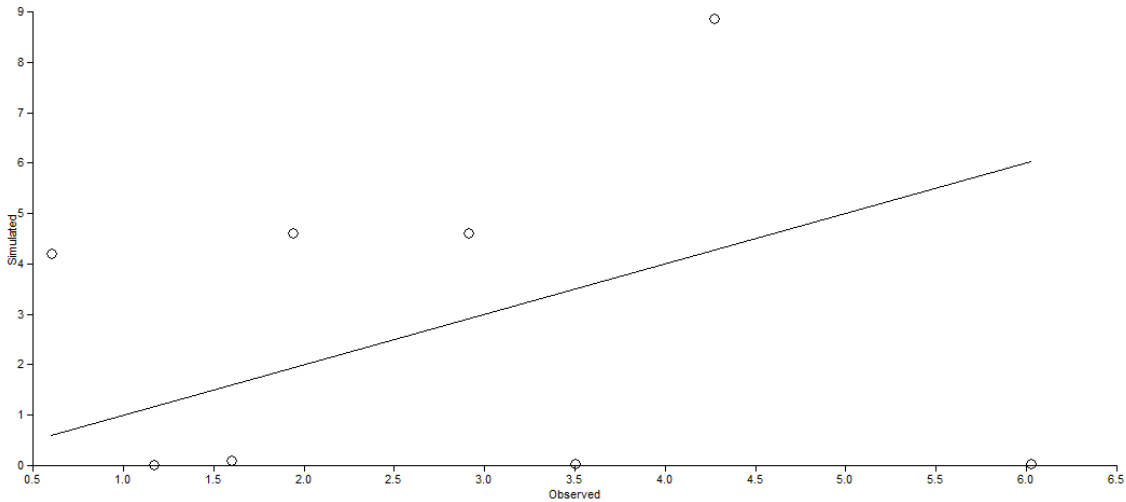


Figure 2.63 RMS Residual for Campania Basin.

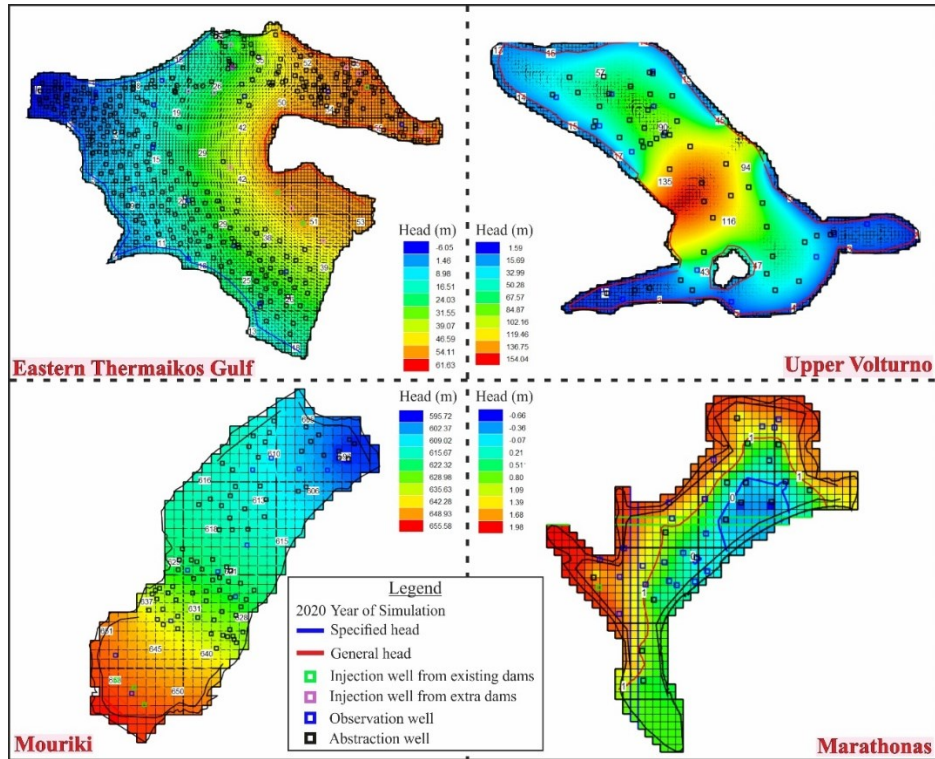


Figure 2.64 Simulation Result for the year 2020.

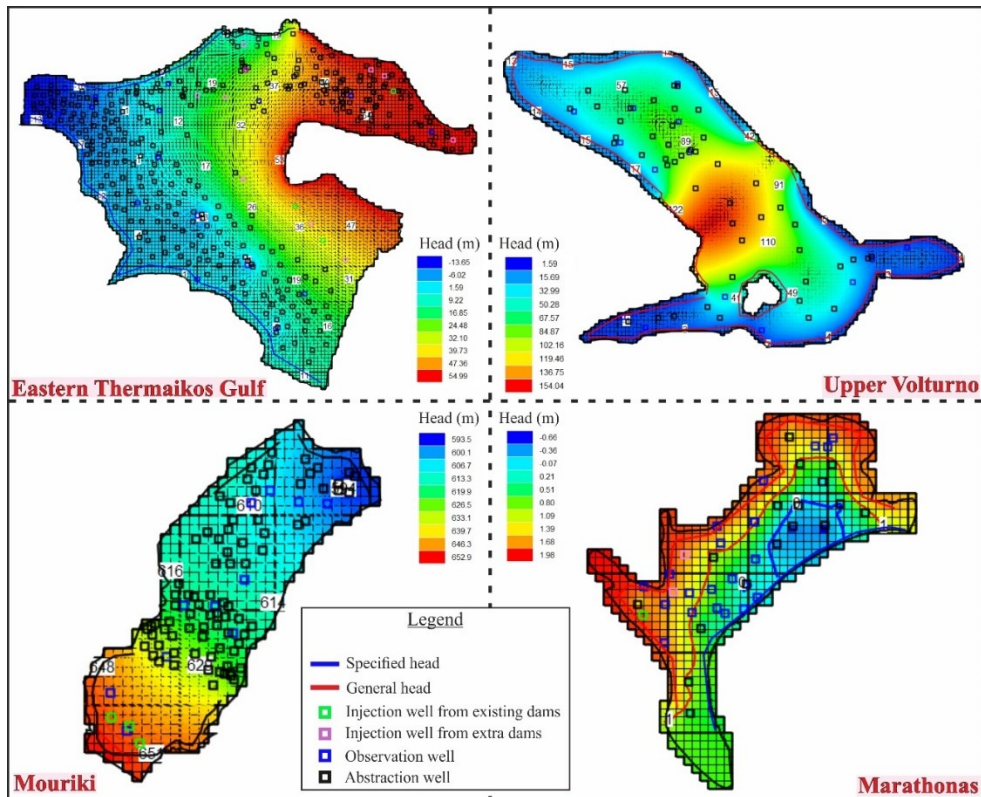


Figure 2.65 Simulation Result for the year 2030.

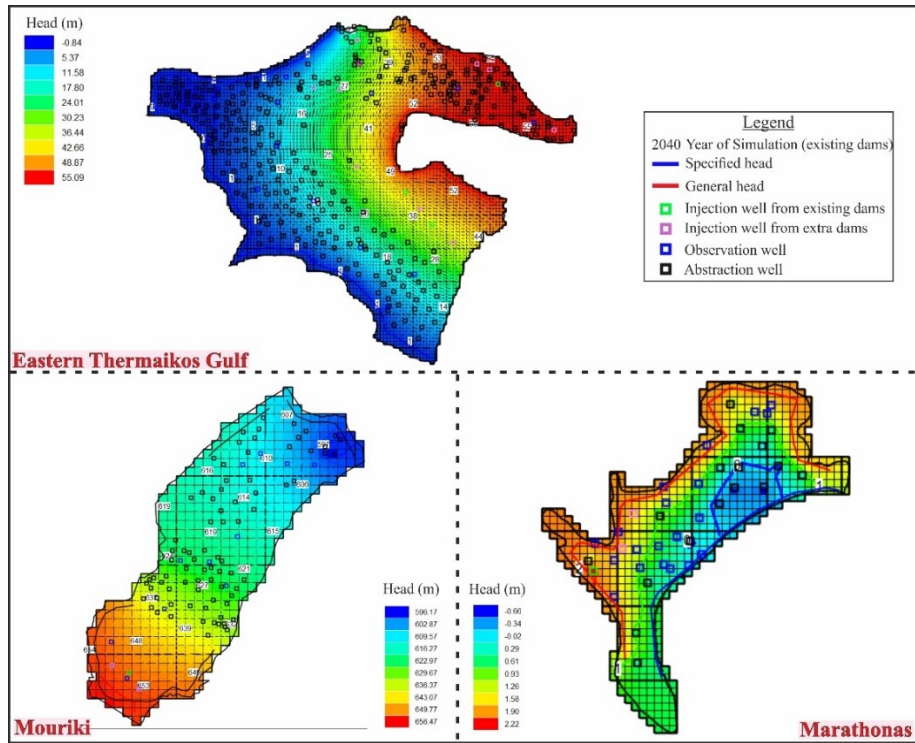


Figure 2.66 Simulation Result for the year 2040 with MAR application using the existing Dams.

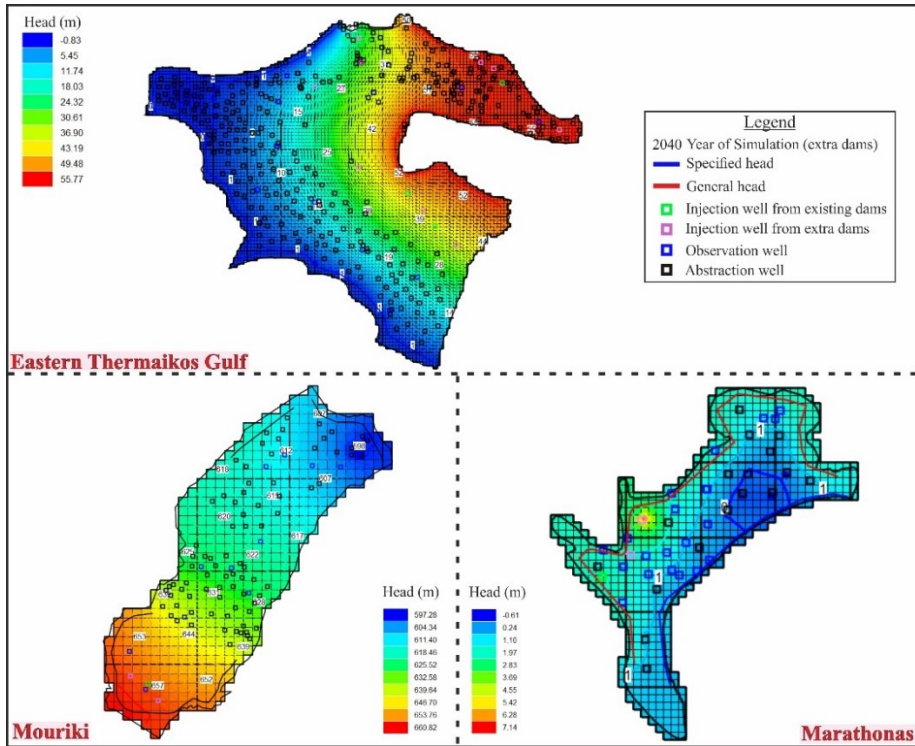


Figure 2.67 Simulation Result for the year 2040 with MAR application using the extra Dams.

According to the results of the simulation, groundwater depletion zones quantified having as reference the groundwater depth in all sites. According to literature overexploitation started since 1980, while in all sites groundwater depth varied from 0 to 1 m below the surface in the lowland. The results of the quantification are presented in Table 2.7 and Table 2.8, while the corresponding maps are shown in the deliverable 5.1 named thematic maps. The implementation and analysis of the results are presented in the final deliverable of the project and the corresponding publication.

Table 2.7 Statistics of groundwater depletion zones in studied aquifers.

Study Area	Model area		Groundwater Depletion 2020		Groundwater Depletion 2030		Groundwater Depletion 2040 after MAR application with existing Dams		Groundwater Depletion 2040 after MAR application with extra Dams	
	Km ²	%	Km ²	%	Km ²	%	Km ²	%	Km ²	%
Mouriki	30.66	100	3.4	11.09	15.3	49.90	4.48	14.61	0.15	0.49
Anthemountas	387.12	100	107.32	27.72	163.25	42.17	69.94	18.07	35.85	9.26
Marathonas	35.92	100	8.21	22.86	15.72	43.76	8.53	23.75	4.28	11.92

Table 2.8 Statistics of negative piezometric head zones in the studied aquifers.

Study Area	Model area		Negative Piezometry 2020		Negative Piezometry 2030		Negative Piezometry 2040 after MAR application with existing		Negative Piezometry 2040 after MAR application with extra Dams	
	Km ²	%	Km ²	%	Km ²	%	Km ²	%	Km ²	%
Anthemountas	387.12	100	86.32	22.30	118.05	30.49	16.44	4.25	14.96	3.86
Marathonas	35.92	100	4.01	11.16	10.68	29.73	3.59	9.99	2.63	7.32

2.4.1 SWI2 - Seawater Intrusion Package Simulation

In the context of the research, the two coastal areas were studied with SWI2 - Seawater Intrusion Package of Modelmuse in terms of the intrusion of seawater into the aquifer and to what extent this process could be reversed using the methodology described above. SWI2 (Seawater Intrusion Package 2) is a numerical modeling package designed for modeling seawater intrusion in coastal aquifers. It is part of MODFLOW, which is a widely used groundwater flow modeling software developed by the United States Geological Survey (USGS). SWI2 extends the capabilities of MODFLOW to simulate the complex processes associated with saltwater intrusion into freshwater aquifers due to factors such as groundwater pumping, sea-level rise, and other hydrological changes. The main points of a SWI2 are:

Conceptualization of the Aquifer: SWI2 requires the user to define the conceptual model of the aquifer system, including the geometry of the model domain, the distribution of aquifer properties (such as hydraulic conductivity and porosity), and the boundary conditions.

Hydraulic Conductivity and Salinity Distribution: SWI2 simulates the movement of groundwater by solving the groundwater flow equation, considering the hydraulic conductivity of the aquifer materials. Additionally, it tracks the distribution of salinity within the aquifer, accounting for factors such as initial salinity, seawater intrusion boundaries, and freshwater recharge.

Density-Dependent Flow: One of the key features of SWI2 is its ability to simulate density-dependent flow. As seawater infiltrates into the aquifer, it increases the density of the groundwater. SWI2 considers the density contrasts between freshwater and seawater to accurately model the movement of the interface between the two water types.

Boundary Conditions: SWI2 allows users to specify various boundary conditions, including pumping wells, recharge areas, and seawater intrusion boundaries. These boundary conditions influence the flow patterns and salinity distribution within the aquifer.

Simulation of Seawater Intrusion: Using the input provided by the user regarding the aquifer properties, boundary conditions, and initial conditions, SWI2 numerically solves the equations governing groundwater flow and salinity transport to simulate the process of seawater intrusion over time.

Visualization of Results: After running the simulation, SWI2 provides users with various visualization tools to analyze the results. Users can examine the spatial distribution of groundwater levels, salinity concentrations, and the movement of the freshwater-seawater interface.

The simulations for the Marathon area are presented in the following figures.

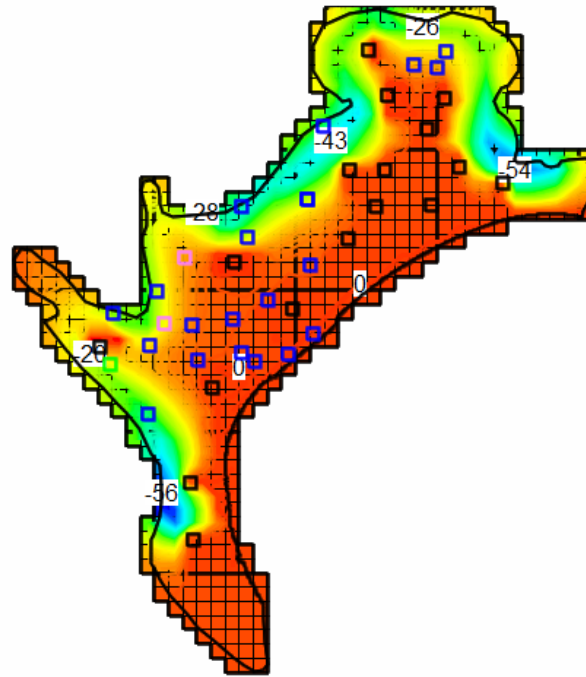


Figure 2.68 Seawater Intrusion 2020.

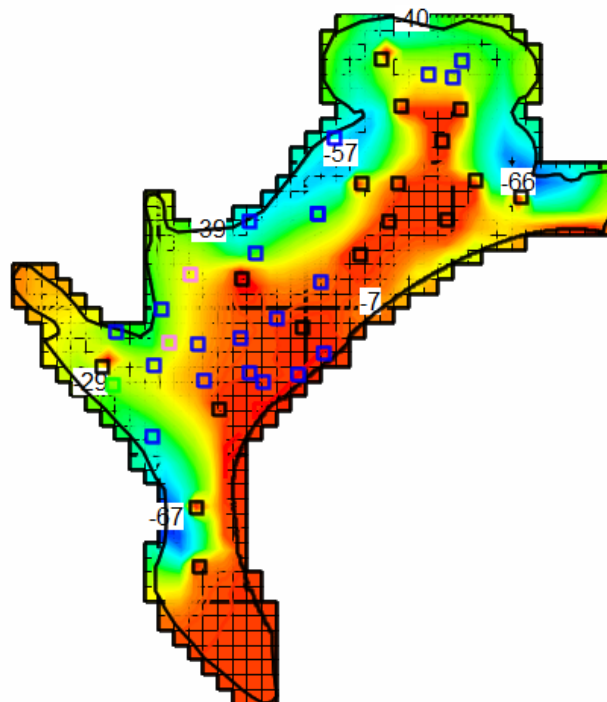


Figure 2.69 Seawater Intrusion 2030.

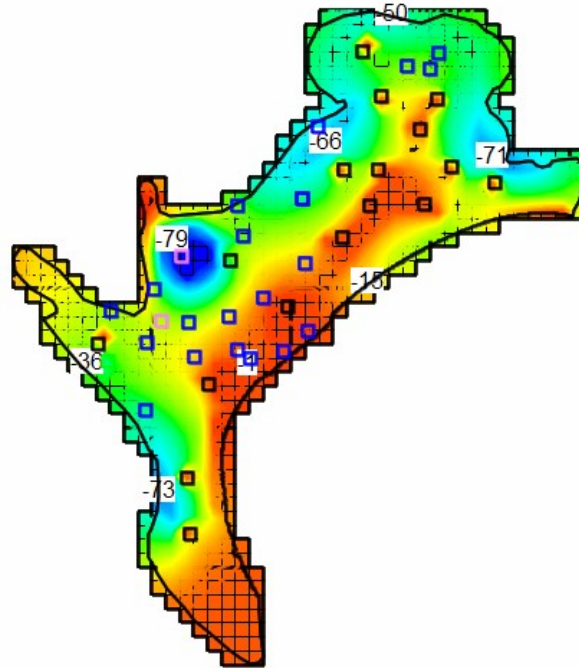


Figure 2.70 Seawater Intrusion 2040 with 1 DAM.

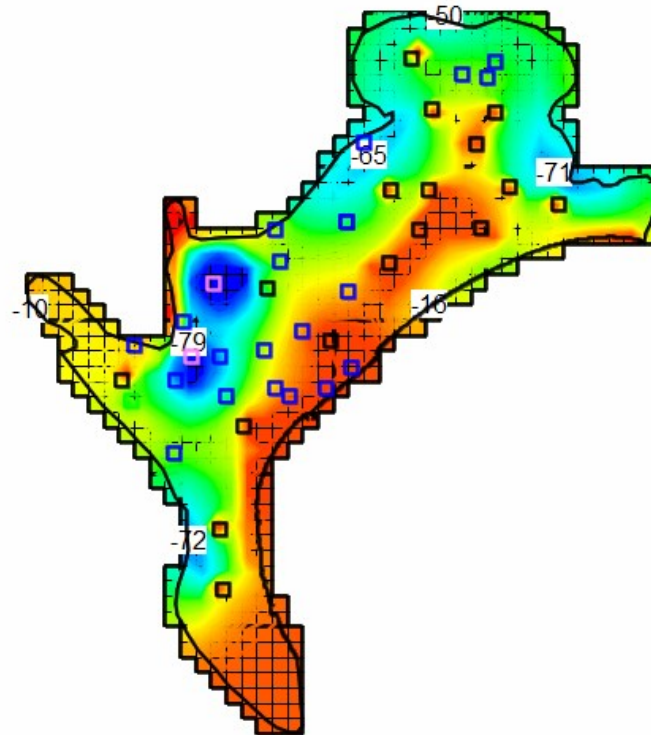


Figure 2.71 Seawater Intrusion 2040 with 3 DAM.

Similarly, for the Anthemountas area, the saline wedge intrusion model is applied. In the following figures are presented the results of the simulation.

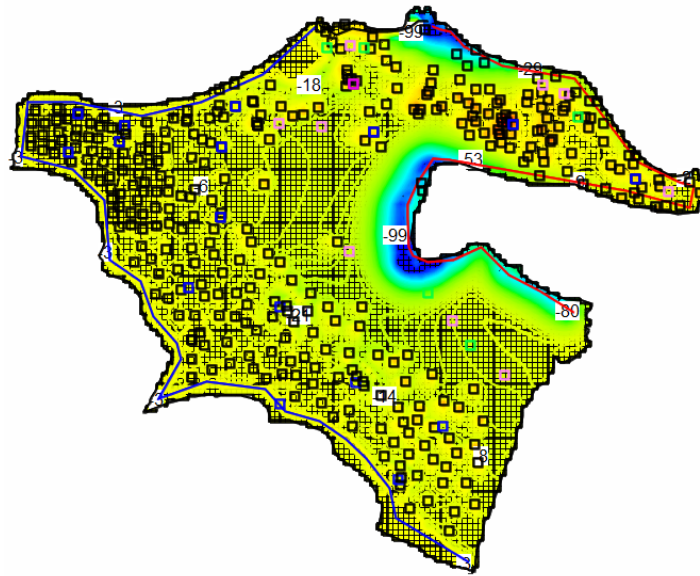


Figure 2.72 Seawater Intrusion 2020.

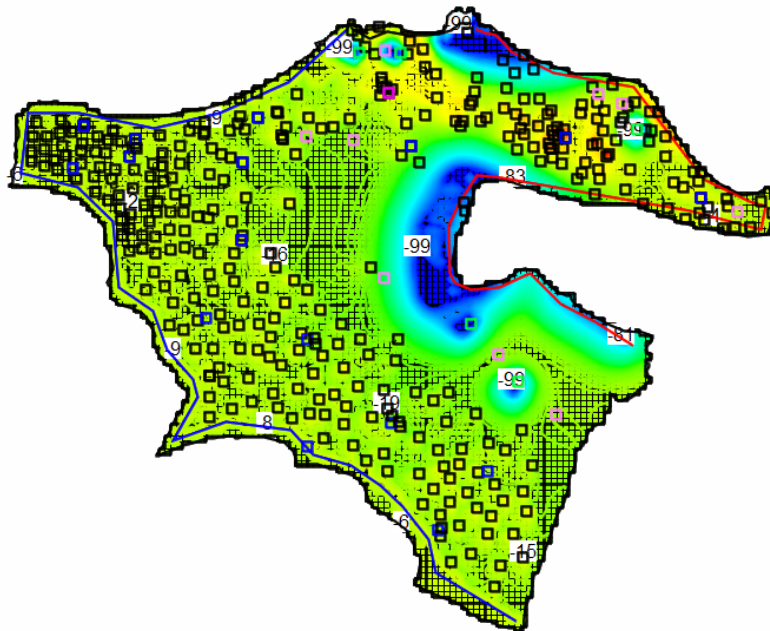


Figure 2.73 Seawater Intrusion 2030.

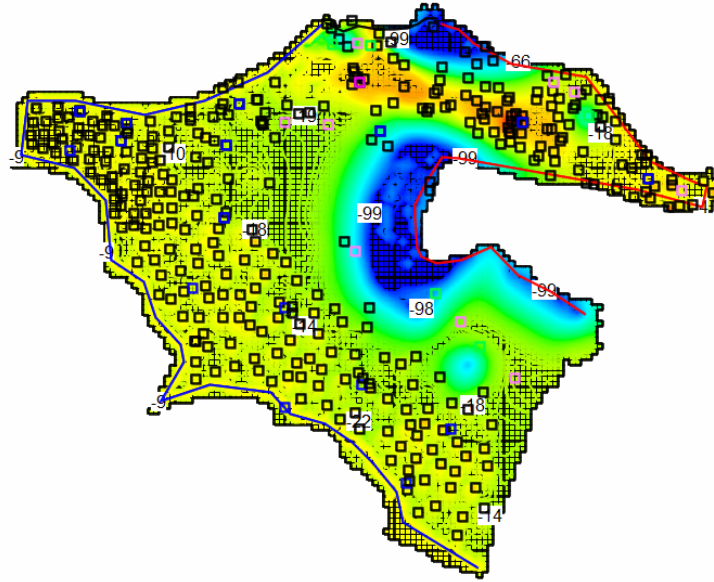


Figure 2.74 Seawater Intrusion 2040 with 5 Dams.

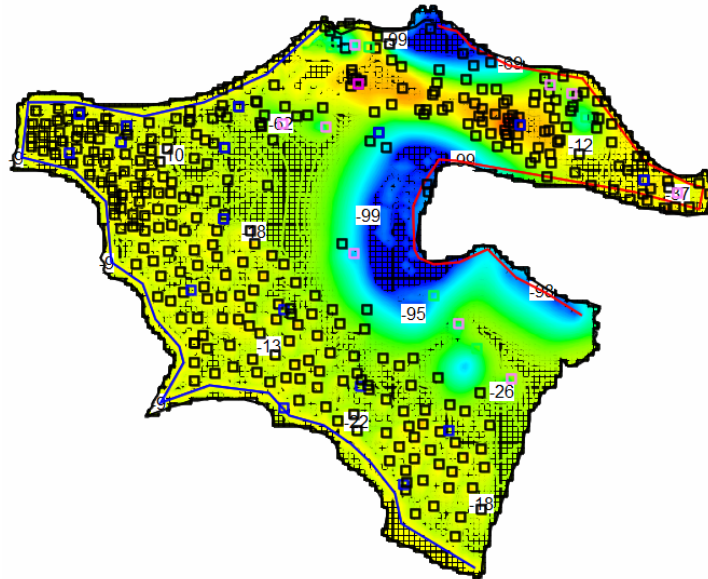


Figure 2.75 Seawater Intrusion 2040 with 14 Dams.

Observing a qualitative improvement in the penetration depth of the salty seawater wedge in aquifers typically implies that measures taken to mitigate seawater intrusion have had a positive effect.

2.4.2 Nitrate simulation

MT3DMS (Multi-species Transport Model for MODFLOW) is a numerical modeling software package designed for simulating the transport of solutes in groundwater systems. It is an extension of MODFLOW, the widely used groundwater flow modeling software developed by the United States Geological Survey (USGS). MT3DMS is specifically tailored for modeling the movement and fate of contaminants, such as pollutants or dissolved chemicals, within aquifers. The main points of a MT3DMS are:

Transport of Multiple Species: MT3DMS is capable of simulating the transport of multiple chemical species simultaneously in groundwater. This includes dissolved contaminants, such as industrial pollutants or agricultural chemicals, as well as natural solutes like salt or nutrients. **Advection, Dispersion, and Reaction Processes:** The software considers three main processes governing solute transport: advection, dispersion, and chemical reactions. Advection refers to the movement of solutes with the flow of groundwater, dispersion accounts for physical spreading of the solute plume due to heterogeneity in the aquifer properties, and chemical reactions encompass processes such as sorption, decay, and transformation of contaminants. **Interaction with Groundwater Flow:** MT3DMS integrates with MODFLOW to simulate the interaction between solute transport and groundwater flow. It utilizes the hydraulic gradient and velocity fields computed by MODFLOW to determine the advection of solutes within the aquifer. **User-defined Parameters and Boundary Conditions:** Users can specify various parameters governing solute transport, such as dispersivity coefficients, reaction rate constants, and initial concentrations. MT3DMS also allows for the definition of boundary conditions, including specified concentration boundaries, constant flux boundaries, and sources or sinks of contaminants. **Model Visualization and Analysis:** After running simulations, MT3DMS provides tools for visualizing and analyzing the results. Users can generate maps, cross-sections, and time series plots to assess the spatial and temporal distribution of solutes within the groundwater system. **Application Areas:** MT3DMS is used in a wide range of applications, including environmental impact assessments, groundwater contamination remediation studies, and groundwater resource management. It helps researchers and practitioners understand the fate and transport of contaminants in aquifers and evaluate the effectiveness of remediation strategies.

For the calculation of nitrification in the Anthemunda aquifer, 200 possible pollution sites were used. The results are presented in the figures below

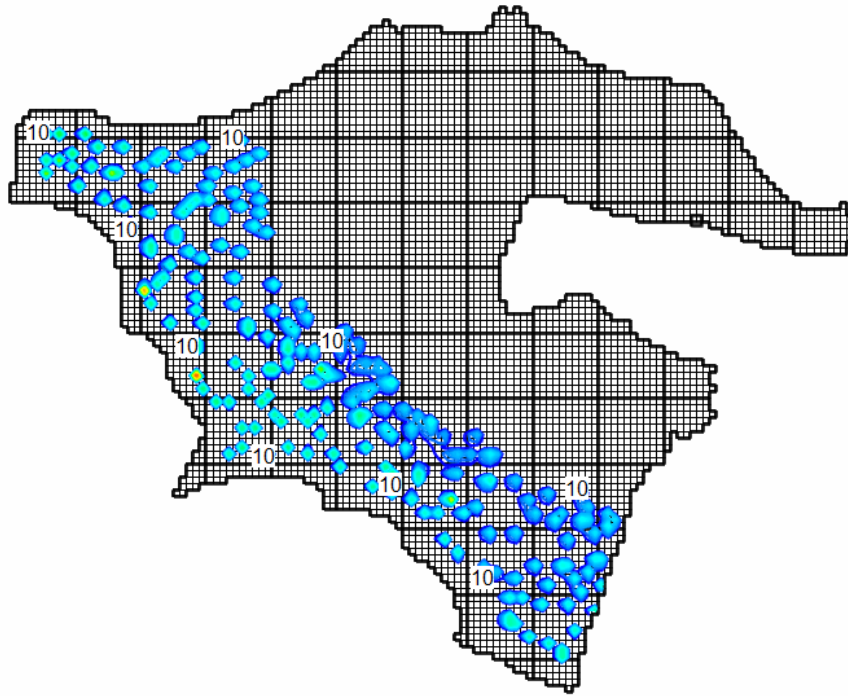


Figure 2.76 Nitrification in the Eastern Thermaikos Gulf aquifer 2020.

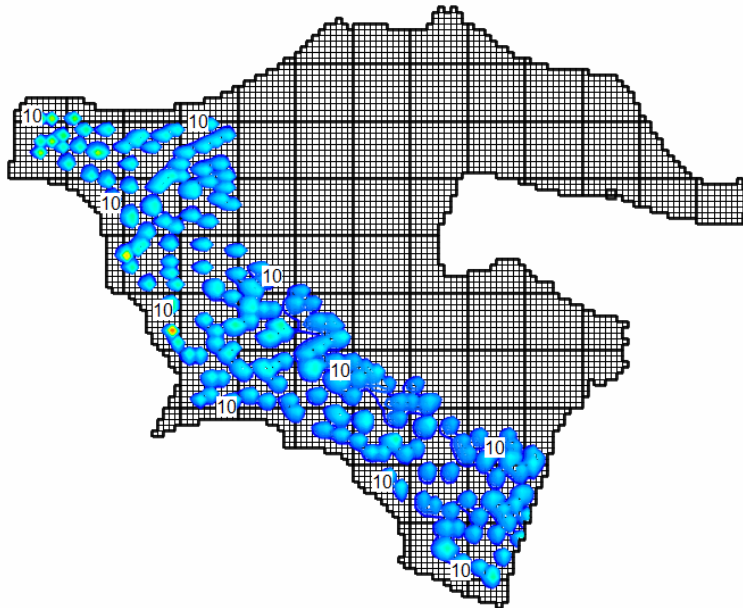


Figure 2.77 Nitrification in the Eastern Thermaikos Gulf aquifer 2030.

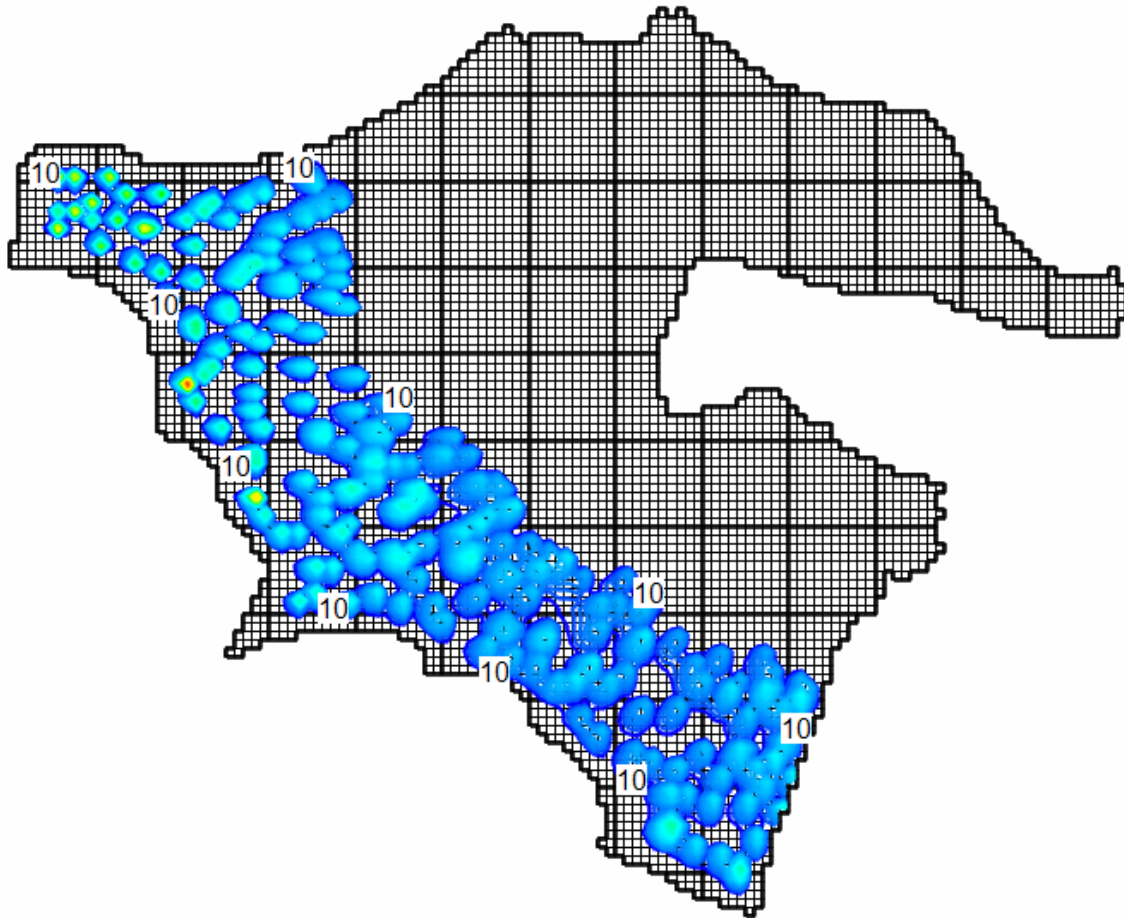


Figure 2.78 Nitrification in the Eastern Thermaikos Gulf aquifer 2040

2.5 Conclusions of simulation

Within this chapter are presented the simulation of surface water, dam operation and groundwater with application of managed aquifer recharge. The main conclusion of each application is presented in the corresponding publication. Regarding groundwater depletion the main conclusion are:

- In Campania region groundwater depletion does not occur due to the later flow and recharge of the porous aquifer from the surrounding karst aquifer system.
- In Eastern Thermaikos Gulf groundwater depletion extend in 27.7% of the porous aquifer, while in 2030 the extend will be expanded to 42% of the aquifer.
- In Marathonas groundwater depletion extends in 22.8% of the porous aquifer, while in 2030 the extend will be expanded to 43,7% of the aquifer.
- In Mouriki groundwater depletion extends in 11.1% of the porous aquifer, while in 2030 the extend will be expanded to 49,9% of the aquifer.
- The application of managed aquifer recharge with injection wells can support to the inversion of the phenomenon and simultaneous generate hydropower.
- The existing small dam dynamic cannot eliminate the phenomenon if the application is obtained for 10 years. However, the construction of extra dams and the application of MAR can eliminate in some cases the phenomenon.
- Seawater intrusion and nitrification modeling require future improvements. It is essential monthly measurements of water quality in order to validate the models and obtain more detailed and accurate results. Nevertheless, the simulation within this project, constitute an important step in order to stimulate local authorities and authors to work on this topic.

3 Thematic maps

In this section are presented the thematic maps of groundwater depletion distribution which obtained from the modeling process. In the two coastal areas was mapped also the zones with negative piezometric head. It is worth to mention that in the Campania basin groundwater depletion do not occur.

3.1 Anthemountas basin

In the following figures are presented the thematic maps of Eastern Thermaikos Gulf and Anthemountas basin.



Figure 3.1 Groundwater depletion zones in Eastern Thermaikos Gulf and Anthemountas basin for the year 2020.

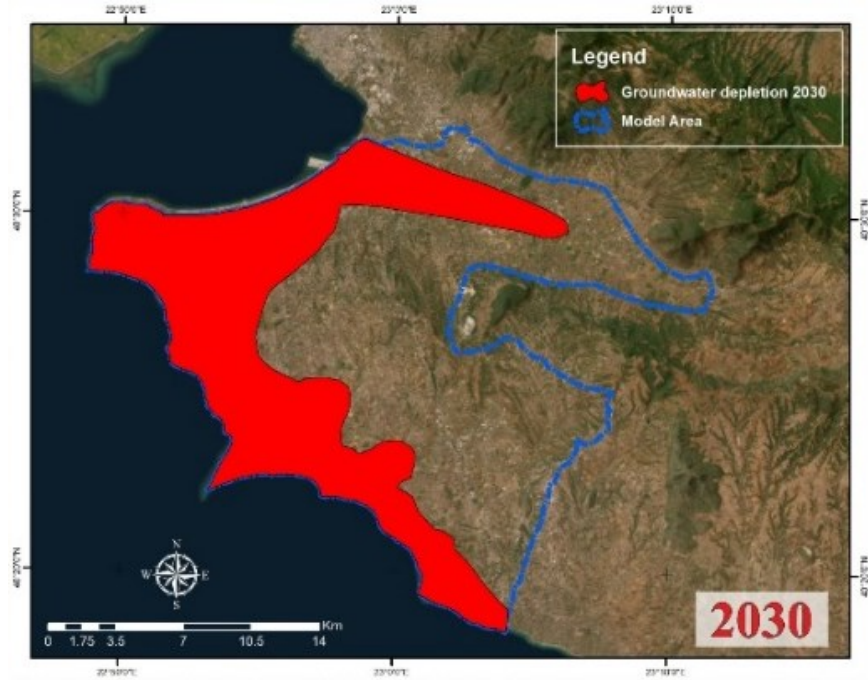


Figure 3.2 Groundwater depletion zones in Eastern Thermaikos Gulf and Anthemountas basin for the year 2030.



Figure 3.3 Groundwater depletion zones in Eastern Thermaikos Gulf and Anthemountas basin for the year 2040 applying scenario A (MAR application with existing dams).



Figure 3.4 Groundwater depletion zones in Eastern Thermaikos Gulf and Anthemountas basin for the year 2040 applying scenario B (MAR application with extra dams).



Figure 3.5 Zones with negative piezometric head in Eastern Thermaikos Gulf and Anthemountas basin for the year 2020.

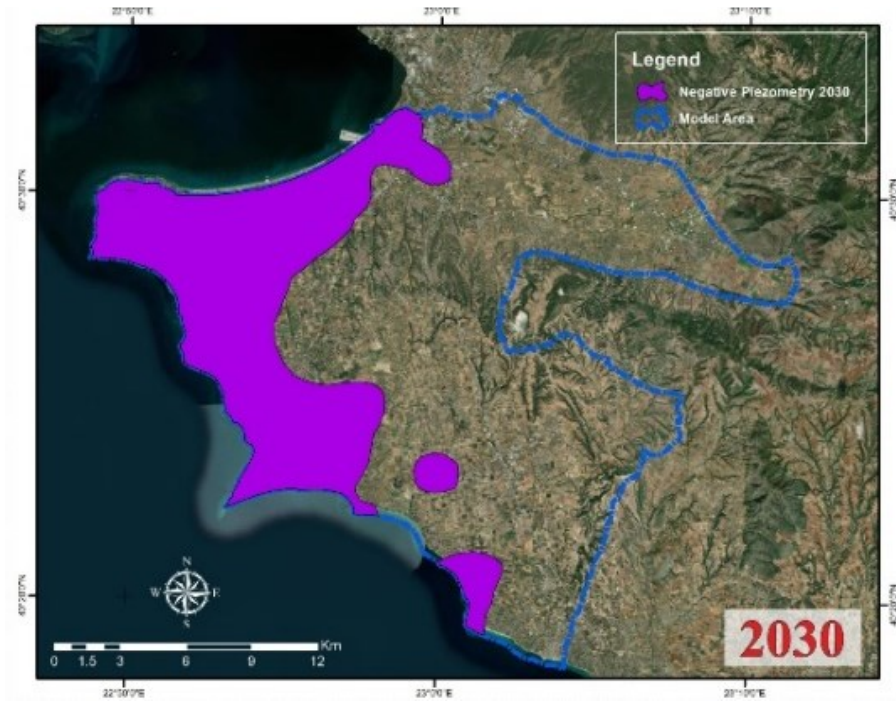


Figure 3.6 Zones with negative piezometric head in Eastern Thermaikos Gulf and Anthemountas basin for the year 2030.



Figure 3.7 Zones with negative piezometric head in Eastern Thermaikos Gulf and Anthemountas basin for the year 2040 applying scenario A (MAR application with existing dams).



Figure 3.8 Zones with negative piezometric head in Eastern Thermaikos Gulf and Anthemountas basin for the year 2040 applying scenario B (MAR application with extra dams).

3.2 Mouriki basin

In the following figures are presented the thematic maps of Mouriki basin.

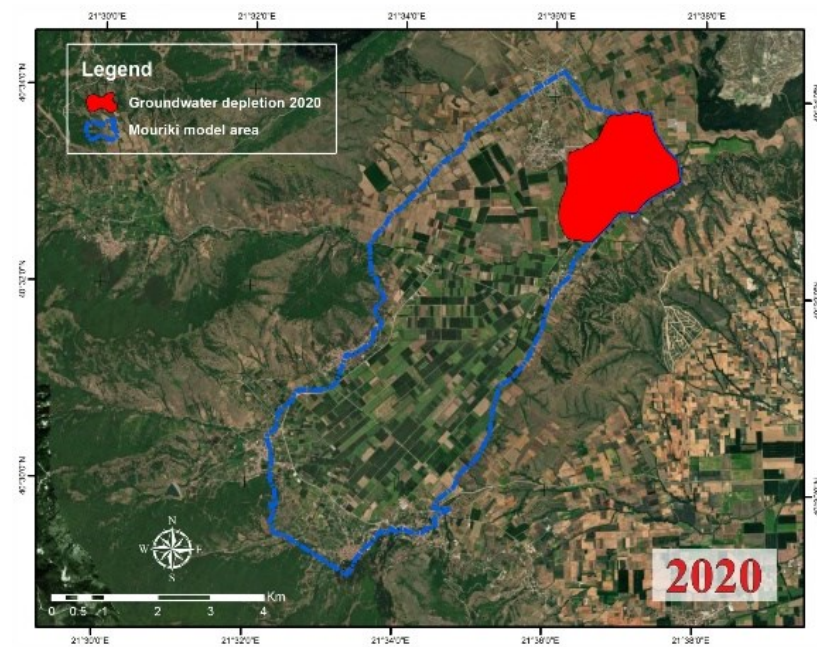


Figure 3.9 Groundwater depletion zones in Mouriki basin for the year 2020.

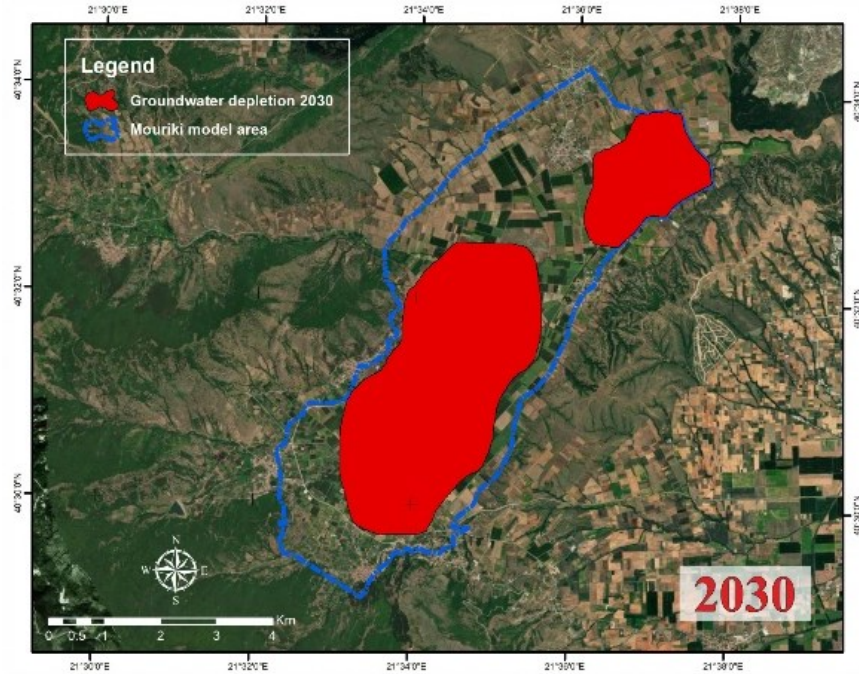


Figure 3.10 Groundwater depletion zones in Mouriki basin for the year 2030.

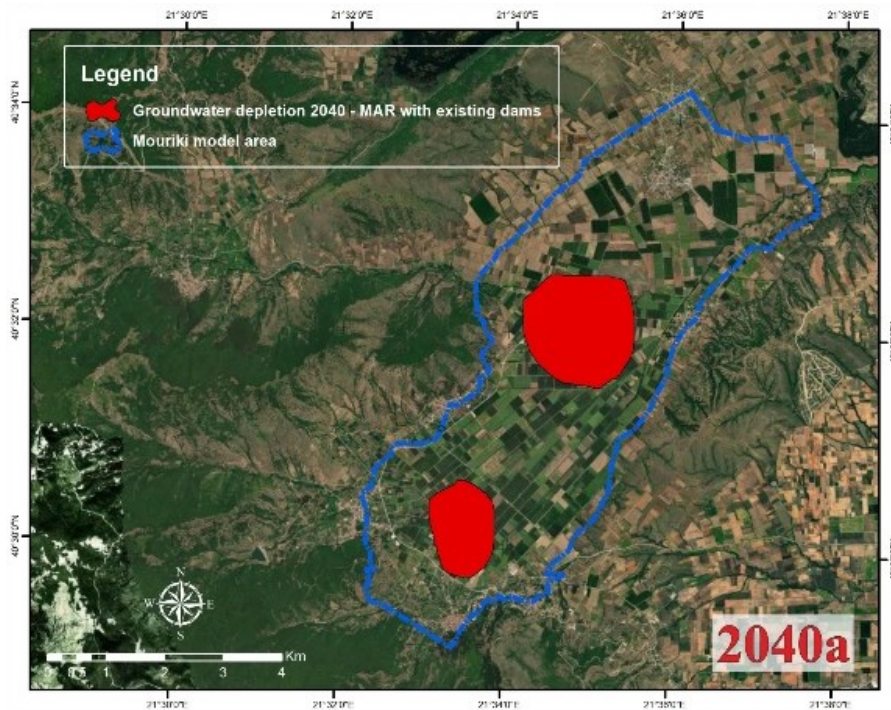


Figure 3.11 Groundwater depletion zones in Mouriki basin for the year 2040 applying scenario A (MAR application with existing dams).

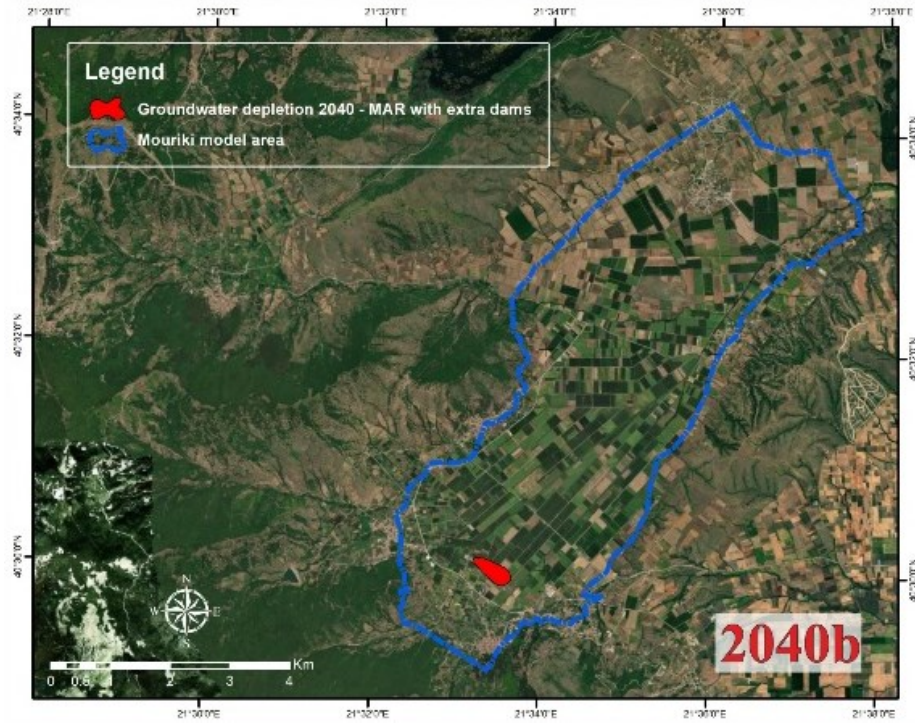


Figure 3.12 Groundwater depletion zones in Mouriki basin for the year 2040 applying scenario B (MAR application with extra dams).

3.3 Marathonas basin

In the following figures are presented the thematic maps of Marathonas basin.



Figure 3.13 Groundwater depletion zones in Marathonas basin for the year 2020.

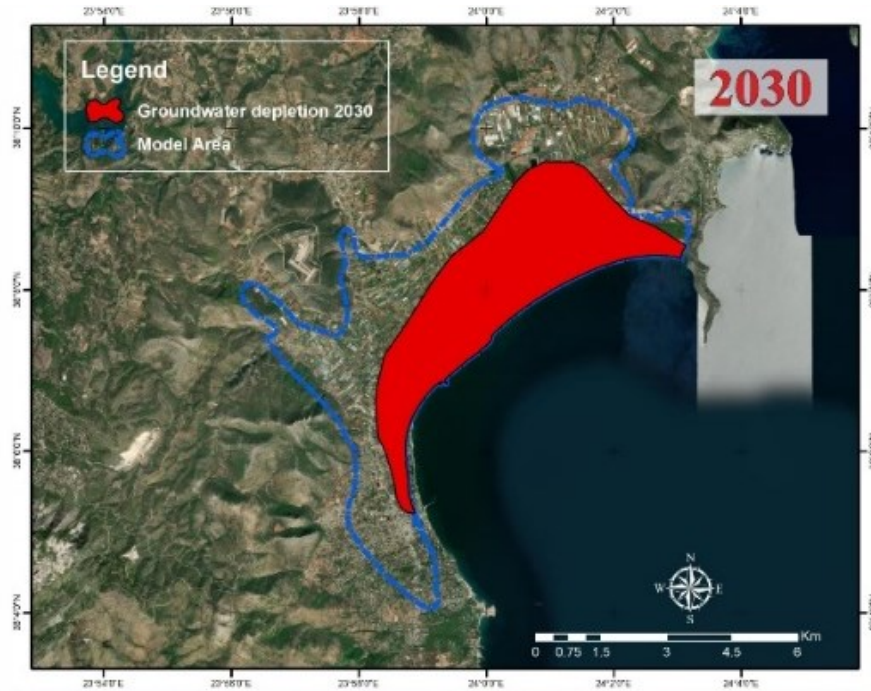


Figure 3.14 Groundwater depletion zones in Marathonas basin for the year 2030.

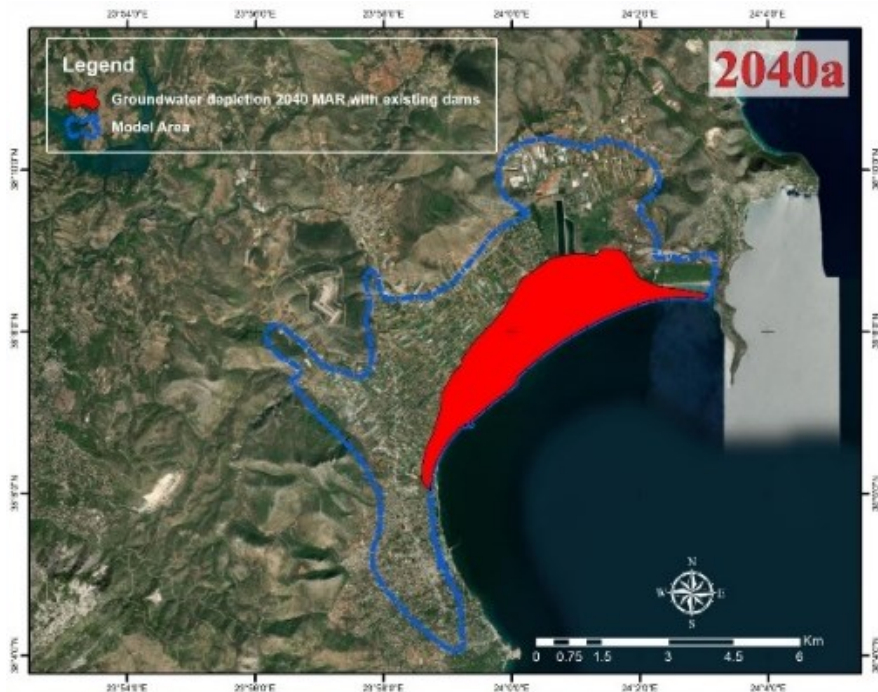


Figure 3.15 Groundwater depletion zones in Marathonas basin for the year 2040 applying scenario A (MAR application with existing dams).

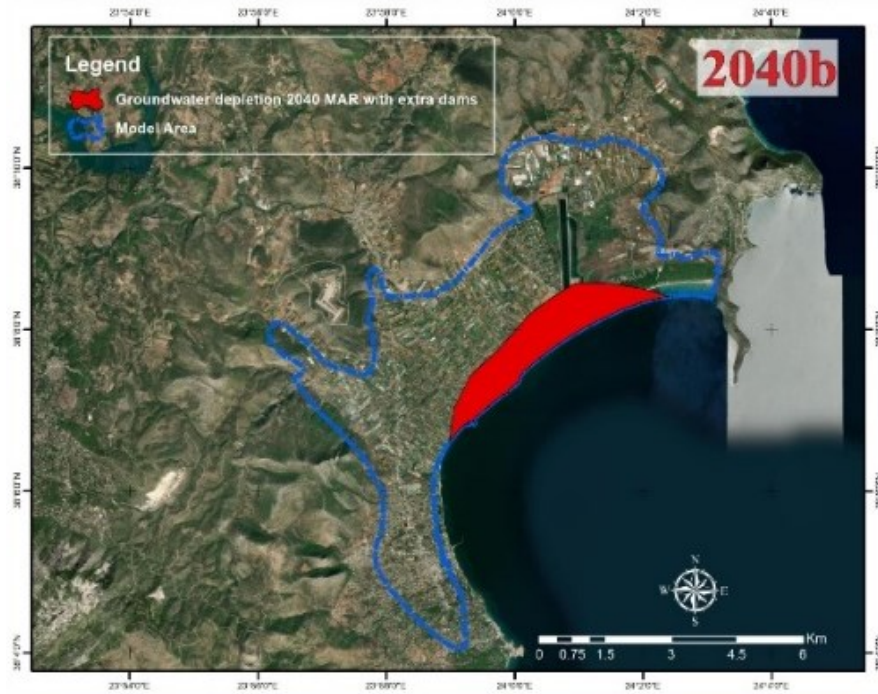


Figure 3.16 Groundwater depletion zones in Marathonas basin for the year 2040 applying scenario B (MAR application with extra dams).

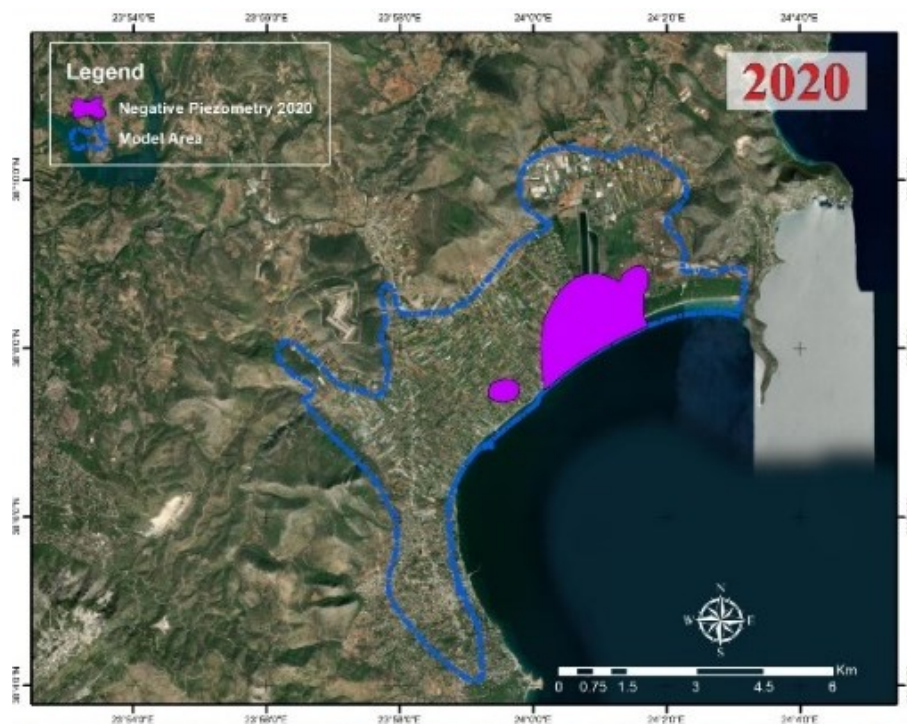


Figure 3.17 Zones with negative piezometric head in Marathonas basin for the year 2020.

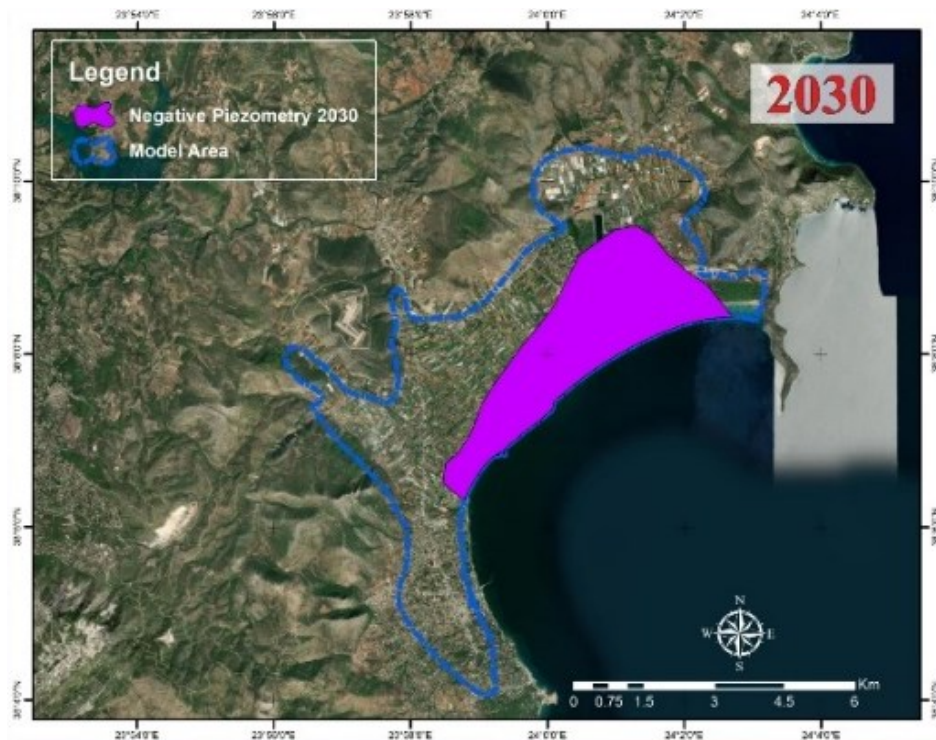


Figure 3.18 Zones with negative piezometric head in Marathonas basin for the year 2030.

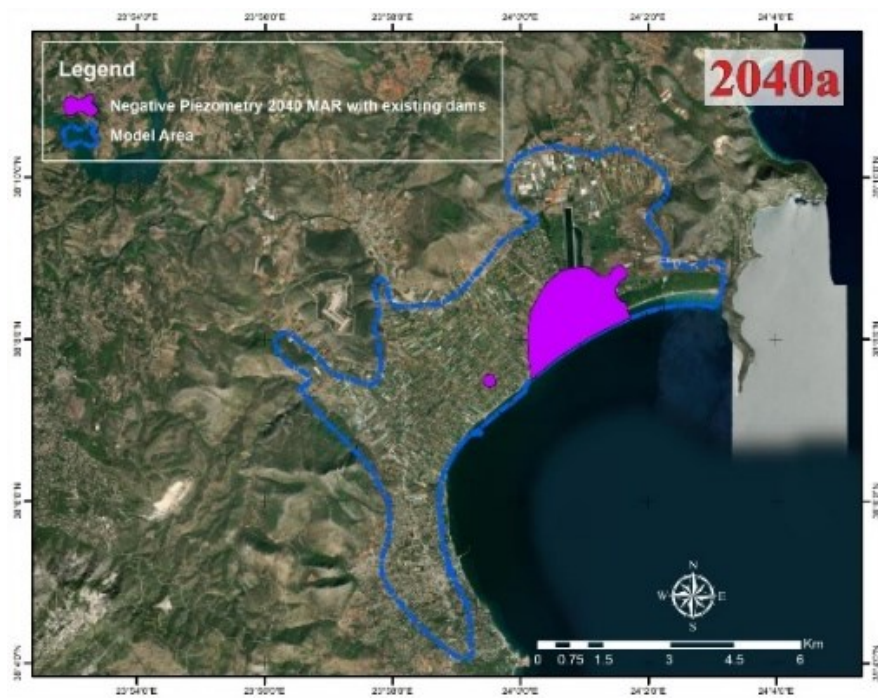


Figure 3.19 Zones with negative piezometric head in Marathonas basin for the year 2040 applying scenario A (MAR application with existing dams).

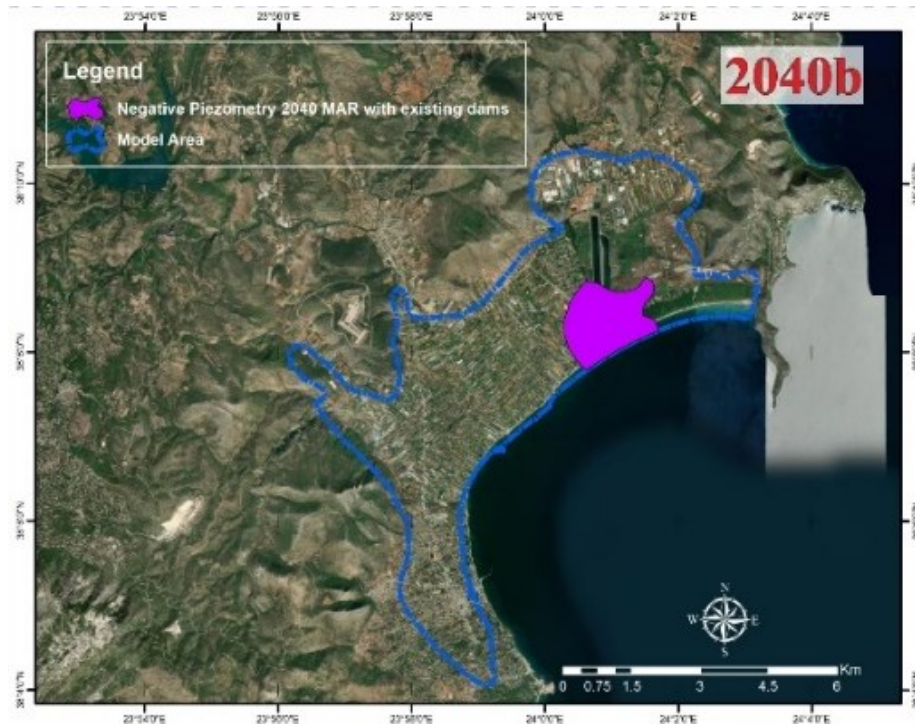


Figure 3.20 Zones with negative piezometric head in Marathonas basin for the year 2040 applying scenario B (MAR application with extra dams).

4 Publications

Within this section are presented the publication until the February 2024. It worth to mention that one chapter and one article are under review.

4.1 Conferences

The research team have been participated in four (4) conferences and published four (4) articles from March 2022 to February 2024. The conferences and the article titles are presented below, while the full publications are included in the appendix of the deliverable.

4.1.1 Online Youth Water Congress: “Emerging water challenges since COVID-19”

- Kazakis N. (2022) Strategies to mitigate the phenomenon of groundwater depletion in the Mediterranean region. Youth” in the forefront: before and after World Water Forum. Online Youth Water Congress: “Emerging water challenges since COVID-19”. pp. 79-80, 6-8 April 2022.

4.1.2 16th International Congress of the Geological Society of Greece

- Ntona M.M., Busico G., Mastrociccio M., Kazakis N. (2022) The impacts of drought on groundwater resources in the Upper Volturno basin, Southern Italy. 16th International Congress of the Geological Society of Greece. Patra, 17-19 October.

4.1.3 6th Edition of FLOWPATH

- Ntona M.M., Busico G., Kalaitzidou K., Mitrakas M., Kazakis N., Mastrociccio M. (2023). Identification of major sources controlling groundwater quality under different hydrogeological regimes in Mediterranean catchments. 6th Edition of FLOWPATH, Malta, 14-16 June 2023.

4.1.4 12th World Congress on Water Resources and Environment (EWRA 2023)

- Ntona M.M., Kalaitzidou K., Mitrakas M., Busico G., Mastrociccio M., Kazakis N., (2023). Anthropogenic sources and hydrogeochemical characteristics of groundwater in Mediterranean regions. 12th World Congress on Water Resources and Environment

(EWRA 2023), “Managing Water-Energy-Land-Food under Climatic, Environmental and Social Instability”, Thessaloniki, Greece, 27 June - 1 July 2023.

4.2 Book Chapter

The research team submitted one (1) article in a Book chapter from March 2022 to February 2024. The article accepted after minor revisions and currently is under revision. The Book names is presented below, while the full article is included in the appendix of the deliverable.

4.2.1 Handbook of Hydrosystem Restoration

- Voudouris K., Kazakis N., Kolokytha E. (2024) Classification Methods for Ranking the Appropriate Locations for Groundwater Artificial Recharge with Conventional Water. Handbook of Hydrosystem Restoration (resubmitted after minor revisions - under revision)

4.3 International Journals

The research team have been published six (6) article and submitted one (1) in scientific journals from March 2022 to February 2024. The article titles and journal names are presented below, while the full publications are included in the appendix of the deliverable.

4.3.1 Science of the Total Environment

- Ntona M.M. Busico G., Mastrocicco M., Kazakis N. (2022) Modeling groundwater and surface water interaction: an overview of current status and future challenges. Science of the Total Environment. 846:157355. <https://doi.org/10.1016/j.scitotenv.2022.157355>
- Kazakis et al. (2024) Groundwater depletion. Are Eco-friendly energy recharge dams a solution? (under review)

4.3.2 Remote Sensing

- Voudouri K.A., Ntona, M.M., Kazakis, N. (2023) Snowfall Variation in Eastern Mediterranean Catchments. Remote Sens., 15, 1596. <https://doi.org/10.3390/rs15061596>

4.3.3 Journal of Environmental Management

- Ntona M.M., Busico G., Mastrocicco M., Kazakis N. (2023) Coupling SWAT and DPSIR models for groundwater management in Mediterranean catchments. Journal of Environmental Management 344, 118543. <https://doi.org/10.1016/j.jenvman.2023.118543>

4.3.4 Water

- Karakatsanis, D., Patsialis, Th., Kalaitzidou, K., Kougias, I., Ntona, M.M., Theodossiou, N., Kazakis, N. (2023) Optimization of dam operation and interaction with groundwater. An overview focusing on Greece. Water, 15, 3852. <https://doi.org/10.3390/w15213852>
- Ntona, M.M., Chalikakis, K., Busico, G., Mastrocicco, M., Kalaitzidou, K., Kazakis, N. (2023) Application of judgmental sampling approach for the monitoring of groundwater quality and quantity evolution in Mediterranean catchments. Water, 15, 4018. <https://doi.org/10.3390/w15224018>
- Kalaitzidou, K., Ntona, M.M., Zavridou, E., Tzelatas, S., Patsialis, Th., Kallioras, A., Zouboulis, A., Virgiliou, Ch., Mitrakas, M., Kazakis N. (2023) Water quality evaluation of groundwater and Dam reservoir water. Application of water quality indices in study sites of Greece. Water. 15, 4170. <https://doi.org/10.3390/w15234170>

5 Conclusions

Within work package 5 elaborated all data from previous work packages fulfilling the simulation process of dams and groundwater. Groundwater depletion zones was mapped, while two simulation scenarios obtained in order to test the efficiency of MAR application using the dam water after the energy production. The results are promising, however more steps should be done in order to reverse the phenomenon. The simulation of seawater intrusion and nitrate pollution obtained with available data. The main suggestion is that monthly monitoring should be obtained in order to provide results with higher accuracy. Due to the low concentrations of trace elements the simulation process focused on the hydrodynamics of the systems. Elevated concentrations of trace elements have geothermal origin, while such process might be future research in the Eastern Thermaikos Gulf aquifer. The results and summary of the project are included within the final report and the corresponding publication.

Within work package 5 fulfilled the 9th and 10th milestones of the project which are the **Groundwater Modeling (M5.1)** and **Dam software (M5.2)**.

6 References

- Abbaspour, K.C., Vaghefi, S.A., Yang, H., Srinivasan, R., 2019. Global soil, landuse, evapotranspiration, historical and future weather databases for SWAT Applications. *Sci. Data* 6, 26. <https://doi.org/10.1038/s41597-019-0282-4>
- Aeschbach-Hertig, W., Gleeson T., 2012. Regional strategies for the accelerating global problem of groundwater depletion. *Nat. Geosci.* 5, 853–861.
- Anderson, M.P., Woessner, W.W., Hunt, R.J., 2015. *Applied groundwater modeling: simulation of flow and advective transport*, 2nd edn. Academic, San Diego.
- Bates, B. C., Kundzewicz, Z. W., Wu, S., Palutikof, J.P. (eds), 2008. *Climate Change and Water* (IPCC Secretariat).
- Busico, G., Kazakis N., Colombani, N., Mastrocicco, M., Voudouris, K., Tedesco, D., 2017. A modified SINTACS method for groundwater vulnerability and pollution risk assessment in highly anthropized regions based on NO₃⁻ and SO₄²⁻ concentrations. *Sci Total Environ*, 609, 1512-1523.
- Busico, G., Ntona, M.M., Carvalho, S.C.P., Patrikaki, O., Voudouris, K., Kazakis, N., 2021. Simulating future groundwater recharge in coastal and inland catchments. *Water Resource Management* 35(11), 3617-3632. <https://doi.org/10.1007/s11269-021-02907-2>
- Busico, G., Ntona, M.M., Carvalho, S.C.P., Patrikaki, O., Voudouris, K., Kazakis, N., 2021. Simulating future groundwater recharge in coastal and inland catchments. *Water Resour. Manag.* 35, 3617–3632. <https://doi.org/10.1007/s11269-021-02907-2>
- Costantini, E.A.C., Dazzi, C., 2013. *The soils of Italy*, World soils Book Series. New York, NY: Springer. <https://doi.org/978-94-007-5642-7>
- Crosbie, R.S., Dawes, W.R., Charles, S.P., Mpelasoka, F.S., Aryal, S., Barron, O., Summerell, G.K., 2011. Differences in future recharge estimates due to GCMs, downscaling methods and hydrological models. *Geophys. Res. Lett.* 38(11), 1–5.
- Dee, D.P., Balmaseda, M., Engelen, R., Simmons, A.J., Thépaut, J.M., 2013. Toward a consistent reanalysis of the climate system. *Bull. Am. Meteorol. Soc.* 95, 1235–1248.
- Di Baldassarre, G., Wanders, N., AghaKouchak, A., Kuil, L., Rangelcroft, S., Veldkamp, T.I.E., Garcia, M., van Oel, P.R., Breinl, K., and Van Loon A.F. 2018. Water shortages worsened by reservoir effects. *Nature Sustainability* 1(11), 617-622
- Doll, P., Muller Schmied, H., Schuh, C., Portmann, F.T., Eicker, A., 2014. Global-scale assessment of groundwater depletion and related groundwater abstractions: Combining hydrological modeling with information from well observations and GRACE satellites, *Water Resour. Res.* 50, 5698–5720.
- Sifang Feng, Zengchao Hao, Yitong Zhang, Xuan Zhang, Fanghua Hao, 2023. Amplified future risk of compound droughts and hot events from a hydrological perspective, *Journal of Hydrology*, 617, C, <https://doi.org/10.1016/j.jhydrol.2023.129143>.

- Foster, S., Garduno, H., Evans, R., Olson, D., Tian, Y., Zhang, W., Han, Z., 2004. Quaternary aquifer of the North China plain—assessing & achieving groundwater resource sustainability. *Hydrogeol. J.* 12, 81–93.
- Gemitzi, A., Lakshmi, V., 2018. Evaluating Renewable Groundwater Stress with GRACE Data in Greece. *Groundwater*, 56(3), pp. 501-514.
- Gleeson, T., Befus, K.M., Jasechko, S., Luijendijk, E., Cardenas, M.B., 2015. The global volume and distribution of modern groundwater. *Nat. Geosci.* 9, 161–167.
- Gleeson, T., Vander Steen, J., Sophocleous, M.A., Taniguchi, M., Alley, W.M., Allen, D.M., Zhou, Y., 2010. Groundwater sustainability strategies. *Nature Geosci.* 3, 378–379.
- Gleeson, T., Wada, Y., Bierkens, M.F., van Beek, L.P., 2012. Water balance of global aquifers revealed by groundwater footprint. *Nature*, 488 (7410), 197–200.
- Hutchison, W.R., 2010. The use of groundwater availability models in Texas in the establishment of desired future conditions. GSA Annual Meeting 2010 (Geological Society of America).
- Jacob, D., Elizalde, A., Haensler, A., Hagemann, S., Kumar, P., Podzun, R., et al., 2012. Assessing the Transferability of the Regional Climate Model REMO to Different COordinated Regional Climate Downscaling EXperiment (CORDEX) Regions. *Atmosphere*, 3(1), 181–199. <https://doi.org/10.3390/atmos3010181>
- Kalaitzidou, K., Ntona, M.M., Zavridou, E., Tzelatas, S., Patsialis, Th., Kallioras, A., Zouboulis, A., Virgiliou, Ch., Mitrakas, M., Kazakis N., 2023. Water quality evaluation of groundwater and Dam reservoir water. Application of water quality indices in study sites of Greece. *Water* 15, 4170. <https://doi.org/10.3390/w15234170>.
- Kaldelis, J., 2007. The contribution of small hydropower stations to the electricity generation in Greece: technical and economic considerations. *Energy Policy* 35, 2187-2196.
- Karakatsanis, D., Patsialis, Th., Kalaitzidou, K., Kougiyas, I., Ntona, M.M., Theodossiou, N., Kazakis, N., 2023. Optimization of dam operation and interaction with groundwater. An overview focusing on Greece. *Water* 15, 3852. <https://doi.org/10.3390/w15213852>.
- Kazakis, N., Pavlou, A., Vargemezis, G., Voudouris, K., Soulios, G., Pliakas, F., Tsokas, G., 2016. Seawater intrusion mapping using electrical resistivity tomography and hydrochemical data. An application in the coastal area of eastern Thermaikos Gulf, Greece. *Sci Total Environ*, 543: 373-387
- Kendy, E., 2003. The false promise of sustainable pumping rates. *Ground Water* 41, 2–4.
- Kendy, E., Zhang, Y. Q., Liu, C. M., Wang, J. X. & Steenhuis, T., 2004. Groundwater recharge from irrigated cropland in the North China Plain: Case study of Luancheng County, Hebei Province, 1949–2000. *Hydrol. Processes* 18, 2289–2302.
- Konikow, L.F., Kendy, E., 2005. Groundwater depletion: A global problem. *Hydrogeol. J.* 13, 317–320.

- Kundzewicz, Z. W. et al. 2007. Freshwater resources and their management. in IPCC Climate Change 2007: Impacts, Adaptation and Vulnerability (eds Parry, M. L. et al.) 173–210 (Cambridge Univ. Press.).
- MacDonald, A., Bonsor, H., Ahmed, K., Burgess, W., Basharat, M., Calow, R., Dixit, A., Foster, S., Krishan, G., Lapworth, D., Lark, M., Moench, M., Mukherjee, A., Rao, M.S., Shamsudduha, M., Smith, L., Taylor, R., Tucker, J., van Steenberg, F., Yadav, S., 2016. Groundwater depletion and quality in the Indo-Gangetic basin mapped from in situ observations. *Nat. Geosci.* 9, 762–766.
- Mavromatis, T., 2009. Use of drought indices in climate change impact assessment studies: an application to Greece. *International Journal of Climatology* 30 (9), 1336–1348.
- McKee, T.B., Doesken, N.J., Kleist, J., 1993. The relationship of drought frequency and duration of time scales. Eighth Conference on Applied Climatology, American Meteorological Society, Jan17-23, 1993, Anaheim CA, pp.179-186.
- Mu Q. Zhao M. Running SW. (2011). Improvements to a MODIS global terrestrial evapotranspiration algorithm. *Remote Sens. Environ.* 115(8), 1781-1800. <https://doi.org/10.1016/j.rse.2011.02.019>.
- Neitsch, S., Arnold, J., Kiniry, J., Williams, J., 2000. Soil and Water Assessment Tool Theoretical Documentation 2000. Grassland, Soil and Water Research Laboratory, Agricultural Research Service, 808 East Blackland Road, Temple, Texas, 76502:506.
- Ntona, M.M., Busico, G., Mastrocicco, M., Kazakis, N., 2022. Modeling groundwater and surface water interaction: an overview of current status and future challenges. *Sci. Total Environ.* 846, 157355. <https://doi.org/10.1016/j.scitotenv.2022.157355>
- Ntona, M.M., Busico, G., Mastrocicco, M., Kazakis, N., 2023. Coupling SWAT and DPSIR models for groundwater management in Mediterranean catchments. *Journal of Environmental Management* 344, 118543. <https://doi.org/10.1016/j.jenvman.2023.118543>
- Ntona, M.M., Chalikakis, K., Busico, G., Mastrocicco, M., Kalaitzidou, K., Kazakis, N. (2023) Application of judgmental sampling approach for the monitoring of groundwater quality and quantity evolution in Mediterranean catchments. *Water*, 15, 4018. <https://doi.org/10.3390/w15224018>
- Papageorgakis and Koumantakis 1978. Hydrogeological research of Anthemountas basin and the coastal area of Chalkidiki. Ministry of Agriculture (unpublished technical report).
- Patrikaki, O., Kazakis, N., Voudouris, K., 2012. Vulnerability map: A useful tool for groundwater protection: An example from Mouriki basin, North Greece. *Fresenius Environmental Bulletin*, vol. 21, No 8c:2516-2521.
- Patsialis, T., Kougiaris, I., Kazakis, N., Theodossiou, N., Droege, P., 2017. Supporting renewables' penetration in remote areas through the transformation of non-powered dams. *Energies*, 9 – 1054.

- Pliakas, F., Petalas, C., Diamantis, I., Kallioras, A., 2005. Modeling of groundwater artificial recharge by reactivating on old stream bed. *Water Resources Management*, 19(3), 279–294.
- Running, S., Mu, Q., Zhao, M., Moreno, A., 2019. MOD16A2GF MODIS/Terra Net Evapotranspiration Gap-Filled 8-Day L4 Global 500 m SIN Grid V006. NASA EOSDIS Land Processes DAAC. <https://doi.org/10.5067/MODIS/MOD16A2GF.006>
- Schismenos, S., Emmanoulidis, D., Stevens, G.J., Katopodes, N.D., Melesse, A.M., 2022. Soil governance in Greece: A snapshot. *Soil Security*, 6, 100035.
- Schneider, D., Molotch N.P., 2016. Real-time estimation of snow water equivalent in the Upper Colorado River Basin using MODIS-based SWE Reconstructions and SNOTEL data. *Water Resour. Res.*, 52, 7892–7910.
- Sophocleous, M., 2000. From safe yield to sustainable development of water resources — the Kansas experience. *J. Hydrol.* 235, 27–43.
- UNESCO, 2009. World Water Assessment Programme. The United Nations World Water Development Report 3: Water in a Changing World. Report No. 978-92-3-104235-5, 407.
- USGS, 2022. ModelMuse: A Graphical User Interface for Groundwater Models.
- Vicente-Serrano, S.M., Beguería, S., López-Moreno, J.I., 2010. A Multi-scalar drought index sensitive to global warming: The Standardized Precipitation Evapotranspiration Index – SPEI. *Journal of Climate*, 23, 1696-1718.
- Voudouri, K.A., Ntona, M.M., Kazakis, N., 2023. Snowfall Variation in Eastern Mediterranean Catchments. *Remote Sens.*, 15, 1596. <https://doi.org/10.3390/rs15061596>
- Voudouris K., Sotiriadis M., Pavlou A., Hatziliontos C. (2006). Groundwater quality in the coastal aquifer system of eastern Thermaikos Gulf, North Greece. *Journal of Environmental Protection and Ecology*, vol. 7, No 2, 269-279.
- Wada, Y., van Beek, L.P.H., Sperna, Weiland, F.C., Chao, B.F., Wu, Y.H., Bierkens, M.F.P., 2012. Past and future contribution of global groundwater depletion to sea-level rise. *Geophys Res Lett* 39: L09402.
- Weider, K., Boutt, D.F., 2010. Heterogeneous water table response to climate revealed by 60 years of ground water data. *Geophys. Res. Lett.* 37, L24405.
- Zavridou, E., Markantonis, K., Argyrokastritis, I., Voudouris, K., Kallioras, A., 2018. Preliminary results from unsaturated zone studies in unconfined unconsolidated coastal aquifers. *MDPI Proceedings* 2(11), 642. doi.org/10.3390/proceedings2110642